NAVAL POSTGRADUATE SCHOOL

MONTEREY, CALIFORNIA

THESIS

WIND FLOW THROUGH SHROUDED WIND TURBINES

by

Jonathan P. Scheuermann

March 2017

Thesis Advisor: Muguru Chandrasekhara
Second Reader: Kevin Jones

Approved for public release. Distribution is unlimited.

THIS PAGE INTENTIONALLY LEFT BLANK

REPORT DOCUMENTATION PAGE			Form Approved OMB No. 0704-0188
Public reporting burden for this collection of information is estimated to average 1 hour per response, including the time for reviewing instruction, searching existing data sources, gathering and maintaining the data needed, and completing and reviewing the collection of information. Send comments regarding this burden estimate or any other aspect of this collection of information, including suggestions for reducing this burden, to Washington headquarters Services, Directorate for Information Operations and Reports, 1215 Jefferson Davis Highway, Suite 1204, Arlington, VA 22202-4302, and to the Office of Management and Budget, Paperwork Reduction Project (0704-0188) Washington, DC 20503.			
1. AGENCY USE ONLY ***(Leave blank)***	**2. REPORT DATE** March 2017	**3. REPORT TYPE AND DATES COVERED** Master's thesis	
4. TITLE AND SUBTITLE WIND FLOW THROUGH SHROUDED WIND TURBINES			**5. FUNDING NUMBERS**
6. AUTHOR(S) Jonathan P. Scheuermann			
7. PERFORMING ORGANIZATION NAME(S) AND ADDRESS(ES) Naval Postgraduate School Monterey, CA 93943-5000			**8. PERFORMING ORGANIZATION REPORT NUMBER**
9. SPONSORING /MONITORING AGENCY NAME(S) AND ADDRESS(ES) N/A			**10. SPONSORING / MONITORING AGENCY REPORT NUMBER**
11. SUPPLEMENTARY NOTES The views expressed in this thesis are those of the author and do not reflect the official policy or position of the Department of Defense or the U.S. Government. IRB Protocol number ____N/A____.			
12a. DISTRIBUTION / AVAILABILITY STATEMENT Approved for public release. Distribution is unlimited.			**12b. DISTRIBUTION CODE**

13. ABSTRACT (maximum 200 words)

Wall pressure distributions and cross section flow distribution on wind turbine shroud designs, determined through static pressure measurements, were quantified in order to determine the most ideal design that could increase power output and reduce the radar cross section.

Engineering and Expeditionary Warfare Center (EXWC) Port Hueneme provided four shroud designs in a 1:160 scale for analysis, including a model with a free-spinning wind turbine incorporated. These models were studied in the Naval Postgraduate School MAE wind tunnel. Tunnel velocity and model angle were varied. Additionally, static wall pressures and cross section flow were studied with the addition of a screen. The pressure measurements were collected by a Scanivalve pressure scanner from up to 90 taps drilled into the models at various locations as well as through an Aeroflow 5-hole probe, which took various measurements at multiple planes of each model.

Flow visualization tests, including oil and tufts, were also conducted to help determine the aerodynamic efficiency of each model and identify any sign of flow separation. These studies provided a good evaluation of the efficiency of these models from a fluid flow perspective.

While none of the models proved ideal, certain attributes, most importantly the geometry of a wind lens or flange on the shroud and a gradually diverging shape, proved to accelerate the flow through the duct.

14. SUBJECT TERMS wind turbine, wind lens, shroud, screen, wind tunnel			**15. NUMBER OF PAGES** 111
			16. PRICE CODE
17. SECURITY CLASSIFICATION OF REPORT Unclassified	**18. SECURITY CLASSIFICATION OF THIS PAGE** Unclassified	**19. SECURITY CLASSIFICATION OF ABSTRACT** Unclassified	**20. LIMITATION OF ABSTRACT** UU

NSN 7540-01-280-5500 Standard Form 298 (Rev. 2-89)
Prescribed by ANSI Std. 239-18

THIS PAGE INTENTIONALLY LEFT BLANK

Approved for public release. Distribution is unlimited.

WIND FLOW THROUGH SHROUDED WIND TURBINES

Jonathan P. Scheuermann
Lieutenant, United States Navy
B.S.C.E., Old Dominion University, 2009

Submitted in partial fulfillment of the
requirements for the degree of

MASTER OF SCIENCE IN MECHANICAL ENGINEERING

from the

NAVAL POSTGRADUATE SCHOOL
March 2017

Approved by: Muguru Chandrasekhara, Ph.D.
Thesis Advisor

Kevin Jones, Ph.D.
Second Reader

Garth Hobson, Ph.D.
Chair, Department of Mechanical and Aerospace Engineering

THIS PAGE INTENTIONALLY LEFT BLANK

ABSTRACT

Wall pressure distributions and cross section flow distribution on wind turbine shroud designs, determined through static pressure measurements, were quantified in order to determine the most ideal design that could increase power output and reduce the radar cross section.

Engineering and Expeditionary Warfare Center (EXWC) Port Hueneme provided four shroud designs in a 1:160 scale for analysis, including a model with a free-spinning wind turbine incorporated. These models were studied in the Naval Postgraduate School MAE wind tunnel. Tunnel velocity and model angle were varied. Additionally, static wall pressures and cross section flow were studied with the addition of a screen. The pressure measurements were collected by a Scanivalve pressure scanner from up to 90 taps drilled into the models at various locations as well as through an Aeroflow 5-hole probe, which took various measurements at multiple planes of each model.

Flow visualization tests, including oil and tufts, were also conducted to help determine the aerodynamic efficiency of each model and identify any sign of flow separation. These studies provided a good evaluation of the efficiency of these models from a fluid flow perspective.

While none of the models proved ideal, certain attributes, most importantly the geometry of a wind lens or flange on the shroud and a gradually diverging shape, proved to accelerate the flow through the duct.

THIS PAGE INTENTIONALLY LEFT BLANK

TABLE OF CONTENTS

LIST OF FIGURES

THIS PAGE INTENTIONALLY LEFT BLANK

LIST OF TABLES

ACKNOWLEDGMENTS

I would like to give a very heartfelt thanks to my incredibly patient thesis advisor, Professor Muguru Chandrasekhara, for his guidance and help. His knowledge of fluid mechanics and willingness to help were invaluable. While his courses were sometimes difficult, his mentoring during my thesis experience was second to none. I would also like to thank Professor Kevin Jones for taking on the role of the second reader. His willingness to assist me despite his extremely busy schedule is much appreciated. Thanks also go to Ben Wilcox from EXWC for building the models that were studied. I would like to acknowledge John Mobley and Stefan Kohlgrueber from the NPS Machine Shop who, despite a huge demand from many faculty and other students, were able to assist me in performing all the modifications to my models. Sameera Gunathilaka from U.S. Army AFDD/AMRDEC at NASA Ames Research Center was instrumental in developing and amending the software that I needed to allow the pressure sensor suite to communicate with the computer. Most importantly, I want to thank Ethan, Meagan and Tristan. My children were so patient with me during this process, sometimes spending hours in the wind tunnel room with me while I performed what seemed like endless runs. I love you guys.

THIS PAGE INTENTIONALLY LEFT BLANK

I. INTRODUCTION

The United States only accounts for 4.4% of the world's population, but Americans consume nearly 20% of the world's energy [1]. The Department of Defense (DOD) is the largest consumer of energy in the United States, and the majority of that comes from fossil fuels. The DOD has requisitioned the deployment of 3 GW of renewable energy to power military facilities by 2025. This meets a larger DOD mandate, Title 10 USC § 2911, which directs at least 25 percent of any DOD facility's energy consumption come from renewable energy sources [1].

Along with troops and equipment, energy concerns are at the forefront of the Navy's ability to ensure it maintains the global presence necessary to ensure freedom of the seas, and maintain strategic deterrence for our enemies. In light of the DOD mandate, the Navy has set its own goals, which are more ambitious. In 2009, the Secretary of the Navy detailed the renewable energy expectations for the Department of the Navy (DON) in a five-part plan.

1. Increase total energy use from alternative sources to 50 percent by 2020 DON wide.
2. Increase shore-based energy use from alternative sources by 50 percent by 2020 and have a net-zero energy use from 50 percent of installations.
3. Deploy a Green Strike Group by 2016.
4. Reduce petroleum use in the non-tactical fleet by 50 percent.
5. Energy considerations will be mandatory for all DON facility contract awards. [1]

Plans are in place to accomplish these goals by employing a range of measures to include wind, solar and geothermal energy sources.

A. GREEN POWER GENERATION AT NAVAL INSTALLATIONS

To date, the wind generation for the Department of the Navy is near 6 MW, with the largest sources coming from wind turbines in Guantanamo Bay (shown in Figure 1), San Clemente Island, and Marine Corps Logistics Base Barstow. The latter is the most recent where a wind turbine was deployed to

power 1,000 homes and generate approximately 3,000 MWH of energy each year [2].

Figure 1. Wind Turbines Servicing Guantanamo Bay Naval Station. Source: [3].

Wind energy is a very efficient and cost effective renewable energy source. It is also labor intensive, and so it creates many jobs. With most of the Navy's bases and facilities located in coastal areas, wind energy is a desirable source as these areas are more prone to higher winds.

B. WIND TURBINE RADAR INTERFERENCE

One problem that arises with wind power is the disorderly wind velocities that result from the rotating turbine blades. In 2011, a study conducted by the White House Office of Science and Technology determined that wind turbines within line of sight of radar interfere by "creating clutter, reducing detection sensitivity, obscuring potential targets, and scattering target returns" [4]. Furthermore, the shadowing effects from spinning wind turbine blades can adversely impact air-traffic control radar's ability to detect aircraft, resulting in a

potential risk to aviation safety [5]. These effects are not filtered out by the algorithms associated with radars, which were implemented to eliminate returns on non-moving structures such as tall buildings and towers.

While buildings and stationary structures also create problems for radar, these problems are minimal. In Figure 2, only the area directly behind the structure will be blocked from radar, while detection is still possible in the area of "partial shadow."

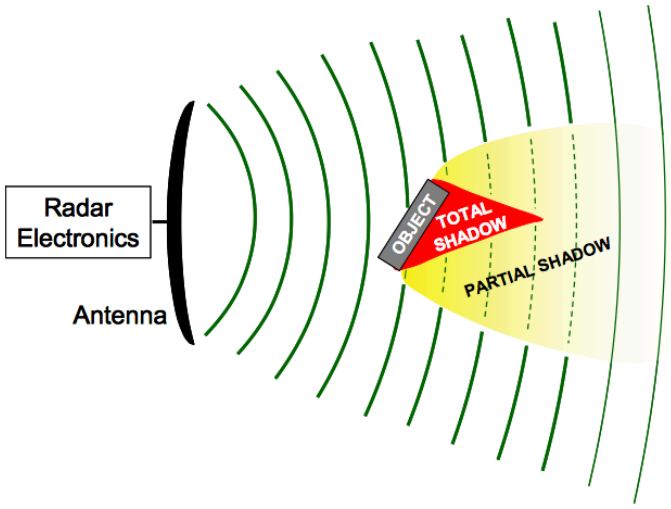

Figure 2. Regions of Partial and Complete Blockage of Radar Illumination. Source: [6].

Wind turbines present another form of radar interference. Figure 3 illustrates a phenomenon known as diffraction.

> Diffraction can be illustrated as propagation of spherical waves from each of the [wind turbines.] These waves will combine constructively and destructively on the far side of the [turbines.] In the zone of the disrupted waves, the reflection of the radar signal is significantly different from the areas where it has not been disturbed. [6]

For military and civilian radar operators, detecting targets in this region will be compromised.

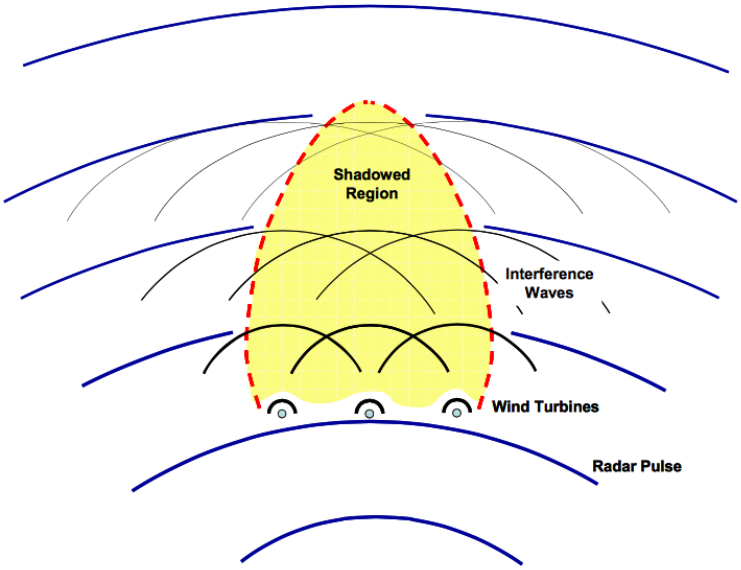

Figure 3. Effect of a Diffraction Grating on a Propagating Wave.
Source: [6].

A study conducted at the University of Oklahoma collected time-series data and used spectral analysis to observe the effects of wind turbine farms on radar performance. Figure 4 illustrates an example of the findings. “The false echo region (circled in red) behind the wind farm (circled in black) is thought to be the result of multipath scatter between turbines, the ground and/or the radar dish itself” [7].

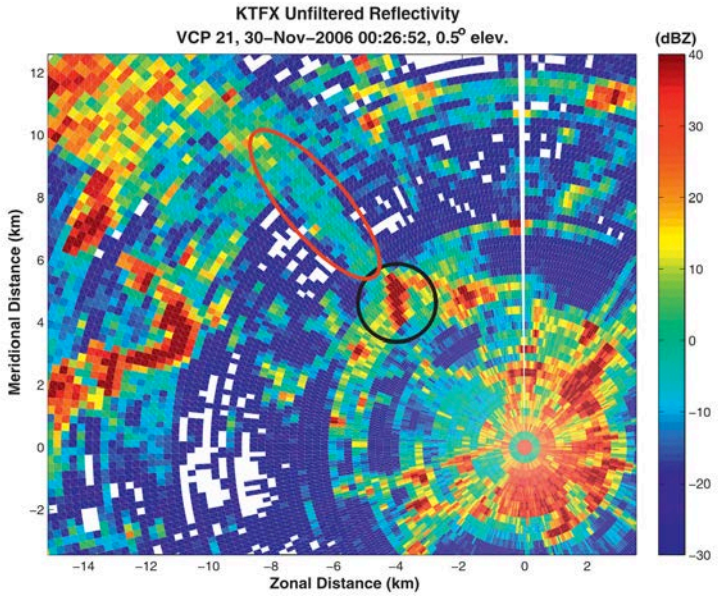

Figure 4. An Unfiltered Reflexivity PPI Plot of Multipath Scattering Effects Taken from KTFX (Doppler Radar Site in Great Falls, Montana). Source [7].

Wind turbines present new and unaccounted for issues with radar. To address this problem, most efforts have been concentrated on improving radar hardware and software to reduce clutter.

C. RADAR CROSS-SECTION (RCS) SUPPRESSION

The severity of this issue led the U.S. Congress to establish the Interagency Field Test and Evaluation (IFT&E) Program to study the problem and explore possible mitigation techniques. Sandia National Laboratories (SNL) was funded by the program to study and develop mitigation techniques. The lab's study focused on six avenues of mitigation:

1. Reduced radar cross section turbines
2. Wind farm design
3. Radar replacement
4. Augmentation radar
5. Radar upgrades
6. Automation upgrades

After testing eight separate mitigation strategies covering these six avenues, the conclusion reached was “the technologies tested did not significantly improve the surveillance capability over wind farm,” and therefore “were not considered an effective mitigation” [4].

Despite this and other studies being conducted to address the issue, the Department of Defense has not approved any mitigation strategy. As such, no wind turbines are currently allowed to be built within radar’s line of sight (LOS).

D. SHROUD WITH RF MESH

A separate approach to this problem is to modify the wind turbines themselves by shrouding them, as opposed to the radar equipment. The Navy Engineering Expeditionary Warfare Center (EXWC), Port Hueneme, CA, through the Office of Naval Research Energy Systems Technology and Evaluation Program (ONR ESTEP) support has initiated a program to design a shroud with Radio Frequency Mesh to suppress RCS of wind turbine rotors. Shrouded wind turbines have already been developed to help increase mass flow through the turbine, thus increasing the total turbine power output. This is because the power output of a turbine is proportional to the cube of the velocity through it. Since increased velocity is a consequence of shrouding, net power increase appears possible.

The concept consists of an enclosure around the wind turbine (the shroud), which would serve to shield the moving blades from the radar. Figure 5 shows a preliminary concept. The shroud itself can be coated with radar absorbing material and thus improve the situation.

The proposal also includes the use of screens or mesh at the inlet, outlet or both, of the shroud to ensure RCS reduction at all viewing angles.

Figure 5. Wind Turbine with Shroud: Preliminary Design. Source: [8].

As can be expected, a shroud would add considerable costs both with the manufacturing and installation as well as additional structural support issues. Consequently, the design should be such that it would ideally pay for itself. The goal of ONR is to expand on that concept and develop a shroud that accomplishes both objectives with the expectation that the "shroud design [is] affordable, maintainable, and [does] not degrade WT efficiency" [8].

E. ROLE OF FLUID MECHANICS IN SHROUD DESIGN

The development of a wind turbine shroud must incorporate the study of fluid flow. Air flow over wind turbine blades can be studied as 2-D flow over an airfoil. This is due to the normal component of velocity being much larger than the perpendicular or spanwise component. Airflow over a wind turbine blade, creates a pressure differential similar to an airplane wing and the resulting lift force is what creates blade rotation and subsequent turbine power. This is important to keep in mind because this same concept can be applied to the shroud design. Modeling the shroud geometry appropriately could accomplish this same concept by generating a lift force through a diffusing shroud. The lift generated effectively creates ring vortices, which induce a velocity through the

shroud. This will theoretically increase the mass flow through the turbine cross section and thus increase turbine power.

Basic fluid mechanics principles must be duly considered in the design. If the diffusing geometry is such that the exit area is far greater than the turbine cross sectional area, the pressure differential may become too large causing the boundary layer along the shroud to separate. This is undesirable as a flow stall within the shroud would lead to a decrease in mass flow rate through the turbine and a subsequent degraded turbine power output.

F. WIND LENS

As stated earlier, the maximum power that can be generated by a wind turbine is proportional to the cube of the upstream wind velocity. This simple fact has led researchers to develop a means of increasing the wind speed through a turbine as even a small increase in velocity can have great returns in the form of power. Ohya et al [9]. have developed a shroud design which consists of a diffusing shroud and brim, as shown in Figure 6, designed to achieve this goal.

Figure 6. 3 kW “Wind Lens” Turbine Located in Fukuoka City, Japan. Source: [9].

While still in the testing phase, early testing results are promising. By adopting these concepts in the development of the “reduced RCS shroud” a potential solution to optimize both power optimization and RCS reduction may be achievable.

THIS PAGE INTENTIONALLY LEFT BLANK

II. REVIEW OF LITERATURE

Renewable energy continues to grow each year as environmental and economic concerns with petroleum-based fuels grow. Wind energy is one of the leading forms of renewable energy. In this century alone, wind power has grown in the United States from 2.53 GW in the year 2000, to 73.99 GW in 2015 and is projected to grow to approximately 400 GW by the year 2050 [10].

Along with that growth, comes advances in technology. Just as research has been conducted to increase the efficiency of petroleum based fuels, so, too, have many studies been conducted to maximize the amount of power that can be harnessed from the wind.

The applications of these studies are very limited; however, this thesis aims to address it. Many have set out to improve wind turbine performance, while still others have aimed at modifying wind farm designs, which could limit radar interference. Attempting to solve both problems at once is a relatively new idea. Literature in both areas will be reviewed in order to introduce and identify approaches that have been attempted thus far and the applicable data will be incorporated into the recommendations being put forth in this thesis.

A. BASIC WIND TURBINE CONCEPTS

A wind turbine is simply a mechanism by which kinetic energy is extracted from the wind and converted into mechanical energy. This has been used for a variety of applications throughout history to include windmills for grinding grain or pumping water, for propelling ships, and most recently, for powering electric generators.

1. Actuator Disc Theory

The energy extraction process for wind turbines can be described in its most basic form with the use of an actuator disc [11]. This theoretical disc takes the place of a turbine in order to set a baseline for turbine efficiencies. This

model presumes no frictional drag, incompressible flow, an infinite number of turbine blades and homogenous, steady state flow with a pressure drop across the disc. Using this model, wind turbine power and thrust can be calculated by Equations 1 and 2 [11].

$$Power = \frac{1}{2}\rho U_t A_t (U_u^2 - U_d^2) \tag{1}$$

$$T = \frac{1}{2}\rho A_t (U_u^2 - U_d^2) \tag{2}$$

As shown in Figure 7, A_t and U_t represent the area and velocity at the disc. Using conservation laws along with Bernoulli's equation, we can determine the turbine efficiency by equation 2.

$$\eta = \frac{Power}{\frac{1}{2}\rho A_t U_u^3} \tag{3}$$

The denominator represents the maximum theoretical energy available which would be achieved if the wind speed was reduced to zero downstream of the turbine. This efficiency is commonly referred to as the power coefficient (C_p) and will be referenced as such for the remainder of this thesis

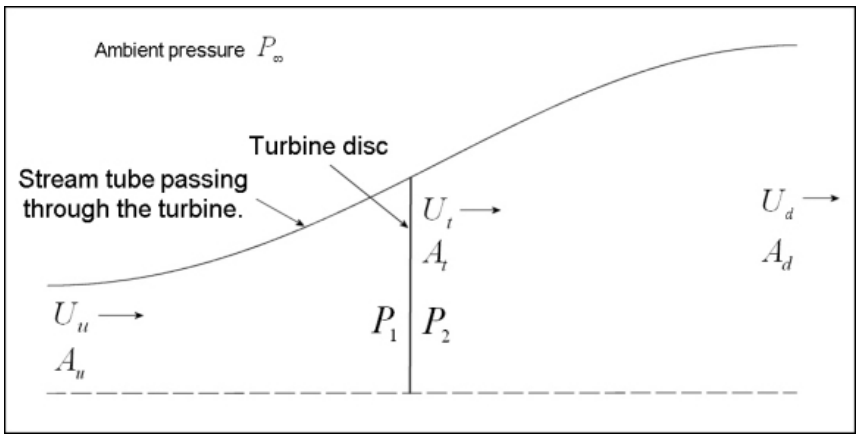

Figure 7. Actuator Disc Model. Source: [11].

Similarly, the thrust coefficient can be defined as

$$C_T = \frac{T}{\frac{1}{2}\rho A_t U_u^2} \tag{4}$$

2. Betz Limit

The ideal turbine would achieve the maximum theoretical power and 100% of the wind's energy would be converted to turbine power. This is, of course, not possible due to the requirement to exhaust the flow through the turbine. The C_p for a wind turbine is defined as the ratio between the actual power output of the turbine with the total available power, as shown in Equation 2. In 1920, Betz published a study of power coefficient and found that the maximum C_p for a wind turbine to be 0.59, as illustrated in Figure 8, which is achieved when the downstream velocity U_d is 1/3 of the upstream velocity U_u.

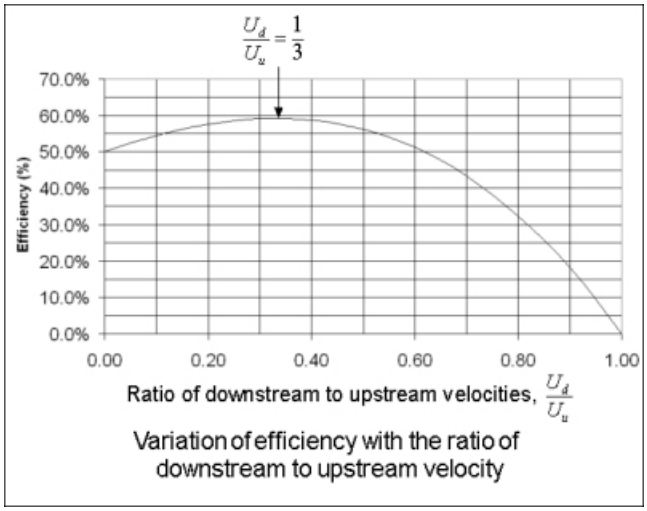

Figure 8. Betz Limit. Source: [11].

3. Tip Speed Ratio

Although the prevailing factor in the design of wind turbines is cost of energy (COE), which is a ratio of the money spent to the electricity produced, many wind turbines in use today have been able to come very close to the Betz

limit. One of the key parameters used to achieve this is the Tip Speed Ratio (TSR). This is the ratio of the turbine blade tip speed to the free stream wind speed [12].

The basic idea follows logic. Should the blades move too slowly, a large portion of air could pass through undisturbed, while moving too fast could produce excessive drag. This parameter is optimized by manufactures by altering the number of blades as well as the blade profile.

B. WIND TURBINE POWER MAXIMIZATION

When Betz performed his derivation and determined the maximum theoretical C_p for wind turbines, there were certain parameters that did not vary. The wind speed at the turbine (U_t) was simply the result of the conservation of mass where $A_u U_u = A_t U_t$. Clearly, the wind velocity U_u and the turbine area A_t cannot be varied. However, if the stream tube incident on the rotor (A_u) could somehow be increased, the mass flow through the turbine could be increased. Remembering that turbine power is proportional to wind speed cubed, any method that could accomplish this could succeed in greatly increasing the power output of the turbine for the same wind speed.

Hansen [13] showed computationally through CFD analysis that by placing the wind turbine in an airfoil-shaped diffusing shroud, as shown in Figure 9, the mass flow through the turbine could be considerably increased.

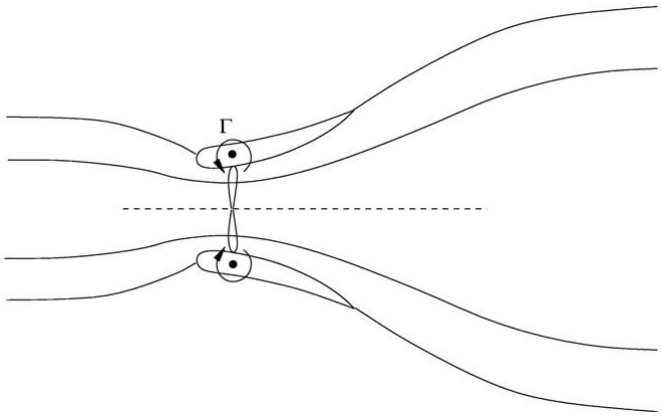

Figure 9. Ideal Flow through a Wind Turbine in a Diffuser. Source: [13].

The simple geometry seen in Figure 9 was modeled in CFD with 266,240 grid points and choosing a turbulence model, which was sensitive to adverse pressure gradients, he was able to achieve C_p values far exceeding the Betz limit [13, Ch. 5]. Figure 10 demonstrates the results. With computed values of C_p exceeding 0.9, it stands to reason that if real life results can compare, this is a technology that would transform the wind industry.

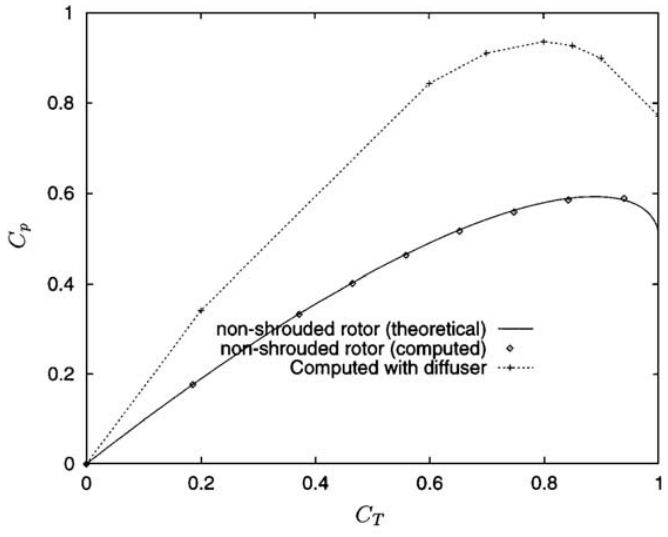

Figure 10. Comparison of Rotor with and without Diffusing Shroud. Source: [13].

It also follows, that in addition to the benefit of increased power output, this technology would allow smaller wind turbines to be utilized to generate the same power as larger unshrouded turbines. This concept has already been realized through multiple designs.

1. Mixer-Ejector Wind Turbine

Engineers at Ogin Energy in Massachusetts have designed a wind turbine that utilizes a shroud consisting of two parts. As seen in Figure 11, a mixer shroud in the front acts to accelerate the wind and transfer more energy to the turbine blades. In the rear is an ejector shroud, which acts to reduce the pressure downstream of the turbine, further aiding to accelerate the airflow through the turbine [14].

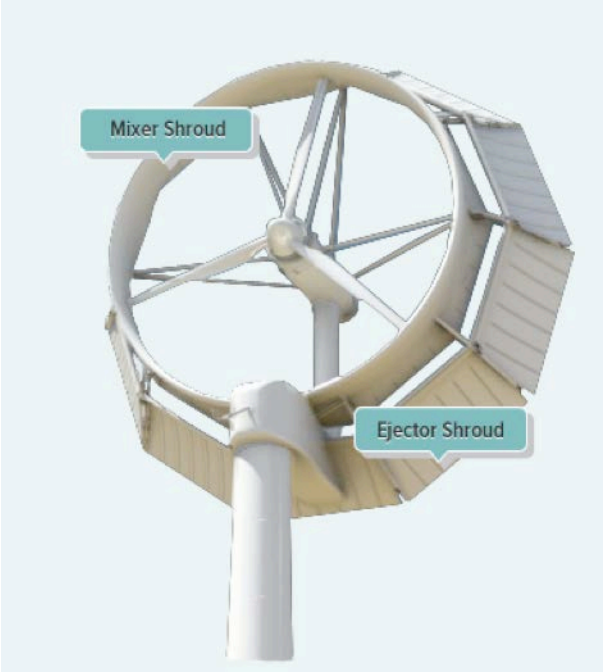

Figure 11. Ogin Mixer-Ejector Wind Turbine. Source: [14].

The company claims that the shroud also acts to return ambient wind speed back to normal more quickly by reducing the downstream turbulence, which would allow additional turbines to be placed closer together.

2. Wind Lens

Similar to the mixer ejector is the idea of a wind lens. This is a single shroud with three sections consisting of an inlet shroud, diffusing section and brim, as seen in Figure 12. The inlet shroud acts to direct airflow to the turbine. The diffuser and the brim both act to create vortices on the outlet side of the shroud, which act to draw more air through the turbine.

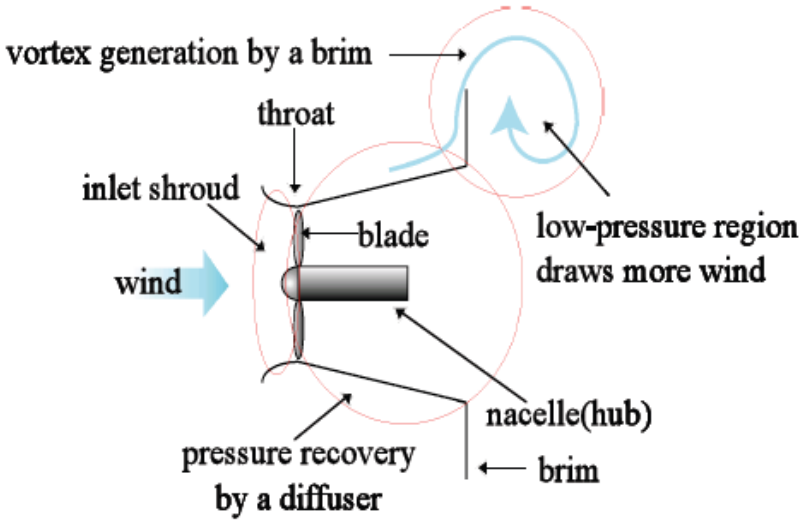

Figure 12. Wind-Lens Concept. Source: [15].

Ohya et al. [16] have performed many field experiments on this design with promising results. The initial concept was tested on a small 500 W turbine and the results, as seen in Figure 13, showed a fourfold increase in power output compared to a non-shrouded turbine.

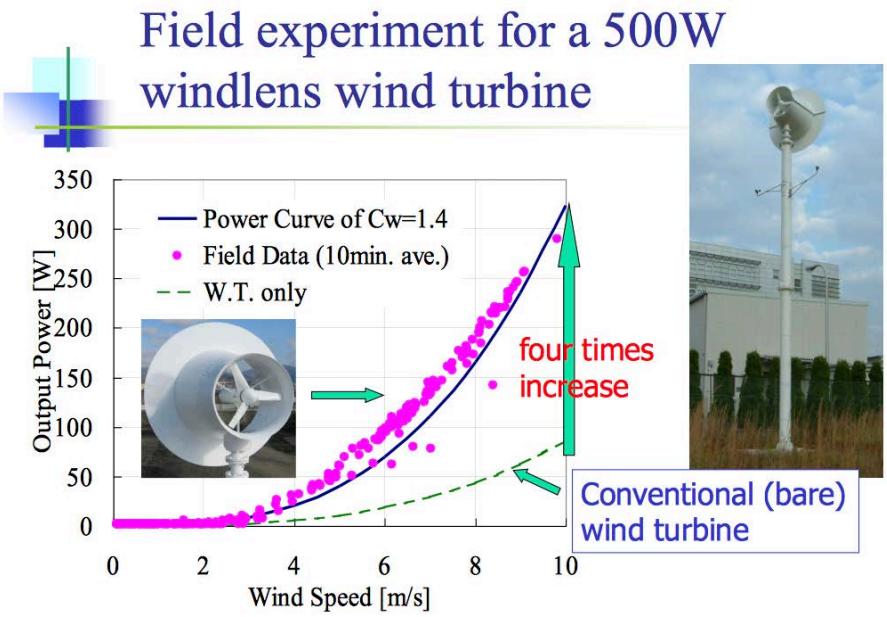

Figure 13. Results of Field Experiment for a 50W Windlens Wind Turbine. Source: [9].

Additionally, variations have been tested in an attempt to optimize the wind lens performance. The original concept, while very effective, was very large scale, which greatly increased the structural weight of the turbine. The brim was very wide as welll which led to high wind loads. Several variations were tested with varying shroud length and diffuser shape. As seen in Figure 14, these results also demonstrated great success. While the turbine efficiency decreased with decreasing shroud length, Betz limit was still far exceeded in all cases.

An important point to note is that all studies done thus far involve small to midsize wind turbines. The increased structural loading resulting from the shroud weight and increased susceptibility to wind loads has thus far prohibited this concept from being employed on large wind turbines, which typically have rotor diameters in excess of 100 meters [16].

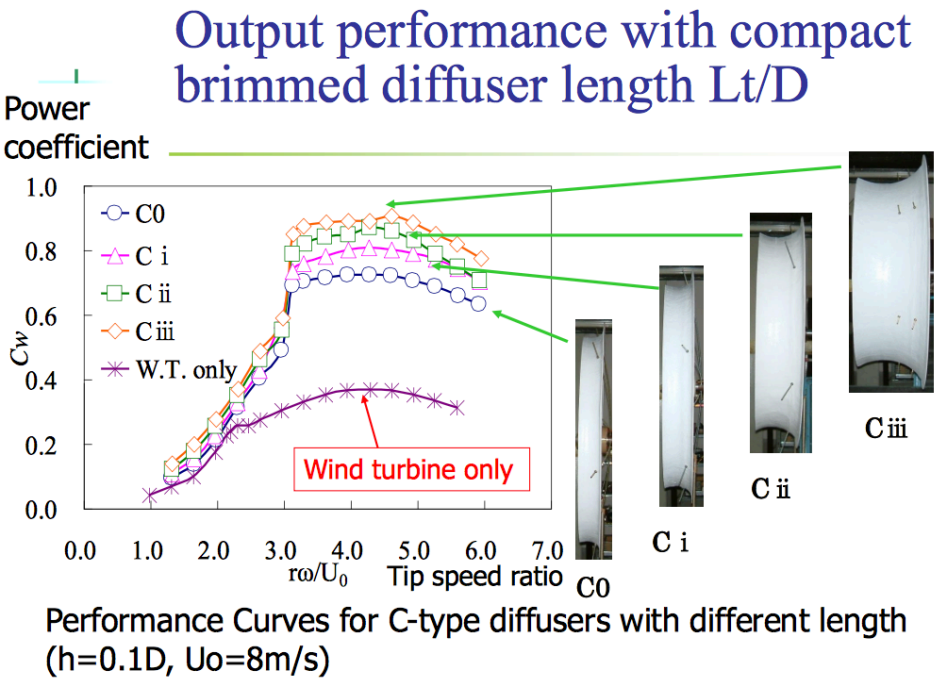

Figure 14. Wind Lens Variations Performance Curves. Source: [9].

C. RCS REDUCTION

With radar interference becoming such a hindrance to new wind farms being built and limiting the locations, Balleri et al. performed an analysis of the wind lens turbine radar signature. The experiment, performed in the UK, saw a marked decrease in RCS for the wind lens when compared to conventional turbines. Additionally, the inclusion of a metallic mesh around the shroud obscured the turbine blades and reduced the RCS by 15dB [17].

Jenn (NPS) has performed similar studies of RCS measurements of mesh. Using simple window screen obtained from a local hardware store, preliminary tests showed Doppler suppression of 8dB. These tests are currently in progress and formal results have not yet been published [18].

D. PRESENT STUDY

This thesis aims to continue with the shrouded wind turbine concept. Four separate 1:160 scale shroud models with varying geometry were developed by EXWC and provided to NPS in order to perform small scale wind tunnel studies to document the aerodynamic properties. Tests were performed with varying wind speeds and angles to determine pressure and velocity distribution with additional flow visualization around the shrouds.

III. DESCRIPTION OF CURRENT WORK

To address this problem, multiple aspects must be studied in parallel. Designing a shrouded wind turbine that simply decreases the radar cross section alone is not practical. The design must also be able to affect the power output of the turbine so that the added turbine power obtained from the shroud can offset the cost of the shroud itself. Additionally, the use of screens must be studied. These studies must include both RCS reduction capabilities as well as optimizing the geometry and open area ratio (OAR) to limit the adverse effects the screen could have on the flow through the turbine. Structural studies will also need to be performed in order to determine the addition geotechnical requirements resulting from the added weight and wind loads associated with the shroud.

The aspect this thesis will address is to study the aerodynamic properties of four shroud models of varying geometry. The four models engineered and provided by EXWC incorporate many features that have already shown promise in the field.

A. WIND TURBINE SHROUDS

The engineers at EXWC have taken on the challenge of producing a shroud, which can be used on wind turbines in the vicinity of coastal military facilities. As previously discussed, DOD currently prohibits the construction of new wind turbine farms in these areas. Building on concepts that have been previously attempted, four separate designs were decided upon with the objective that these designs would be tested in the NPS wind tunnel on small scale models. Once sufficient data was obtained, two designs would be chosen for larger scale testing in the 2.13 m (7 foot) wind tunnel at NASA AMES. These large scale tests would aim to provide the final shroud concept to be field tested.

All shrouds were 3-D printed from clear acrylic. The shrouds were then drilled to accommodate the installation of 1.651 mm (0.065 inch) stainless steel tubing to be used as pressure taps. The tubing was cut in one inch sections and

inserted into the predrilled holes of the shroud making sure not to extend beyond the shroud interior so that the interior surface remained true. To ensure there was no leakage and that the tubing would stay in place, each tube was secured with Loctite super glue.

1. Model 1

The first shroud that was provided was a 15.24 cm (6 inch) long shroud, shown in Figure 15. The shroud consisted of a 10.16 cm (4 inch) long cylindrical section with a 15.24 cm (6 inch) inside diameter followed by a 5.08 cm (2 inch) section that flared out at an angle of 36.9 degrees. The inside diameter of the flared section increased from 15.24 cm (6 inches) to 22.84 cm (9 inches).

Model one was drilled to accommodate 54 pressure taps. These pressure taps were distributed around the model at every 45 degrees. The top of the model, or 90-degree position contained 12 pressure taps along its length while the remaining positions contained 6. The pressure taps along the top correspond to station numbers 1–12 for which data was taken. Station 0 and 13 correspond to the inlet and outlet of the model, respectively.

This model was tested in both orientations to assess the aerodynamic properties of both a converging and diverging shroud.

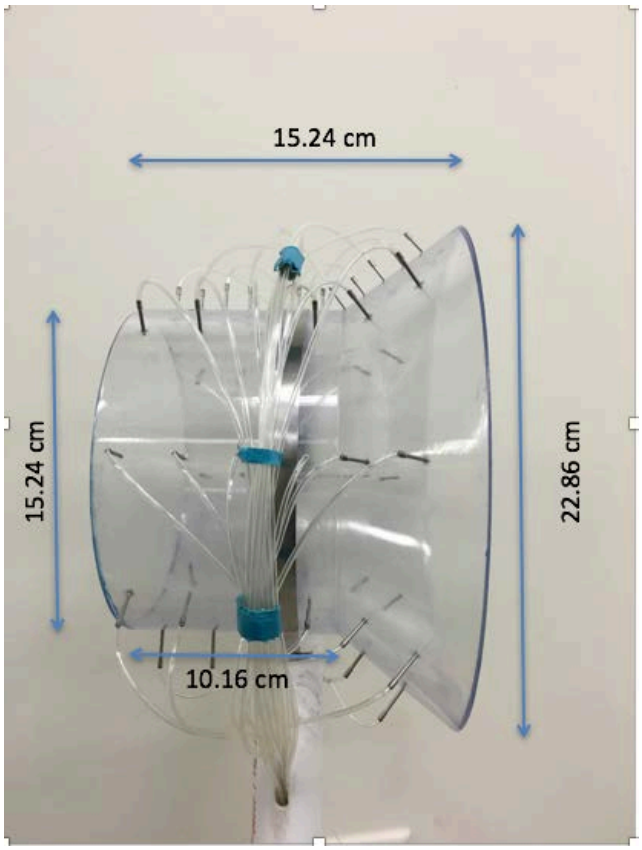

Figure 15. Model One Dimensions.

2. Model 2

The second shroud that was provided was a 15.24 cm (6 inch) long shroud shown in Figure 16. The shroud was a constant diameter cylinder with an inside diameter of 14.605 cm (5.75 in.). The outlet side of the shroud featured a flange with an outside diameter of 24.765 cm (9.75 inches).

Model two was drilled to accommodate 48 pressure taps. These pressure taps were distributed around the model at every 45 degrees. The 90-degree position contained 11 pressure taps along its length while the remaining positions contained 5. The pressure taps along the top correspond to station numbers 1–11 for which data was taken. Station 0 and 12 correspond to the inlet and outlet of the model, respectively.

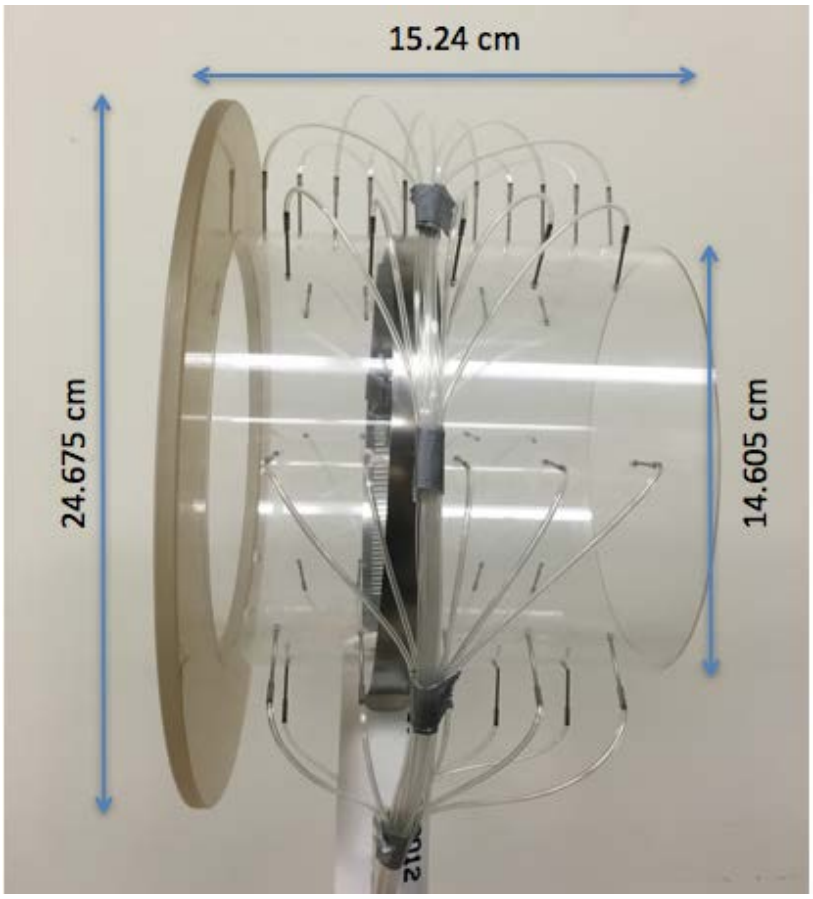

Figure 16. Model Two Dimensions.

3. Model 3

The third shroud that was provided was a 25.4 cm (10 inch) long shroud shown in Figure 17. The shroud consisted of a converging diverging hyperbolic profile. The inside diameter varied from 24.765 cm (9.75 inches) at the inlet to 21.59 cm (8.5 inches) at the outlet with a 15.24 cm (6 inch) center section.

Model three was drilled to accommodate 91 pressure taps. These pressure taps were distributed around the model at every 45 degrees. The 90-degree position contained 21 pressure taps along its length while the remaining positions contained 10. The pressure taps along the top correspond to station numbers 1–21 for which data was taken. Station 0 and 22 correspond to the inlet and outlet of the model, respectively.

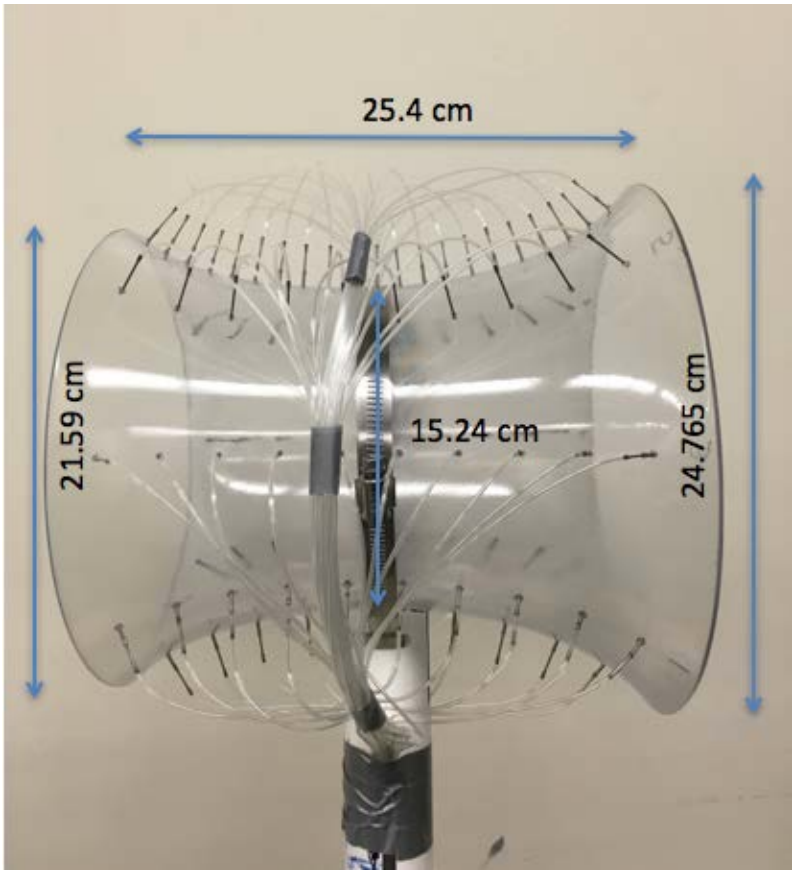

Figure 17. Model Three Dimensions.

4. Model 4

The fourth shroud that was provided was adapted from journal articles detailing the Wind Lens concept developed by researchers at Kyushu University in Japan. The profile of this model was based on academic work on the properties of an annulus to increase flow. This model, as shown in Figure 18, is a 5.08 cm (2 inch) long shroud. The inlet features a 15.24 cm (6 inch) inside diameter which diverges to a 20.32 cm (8 inch) outlet. The outlet also features a brim which measures 25.4 cm (10 inches).

Model 4 also featured a small-scale wind turbine, which consisted of three blades, and was designed to spin freely with a screw that acts as a friction brake. No pressure taps were drilled in this model.

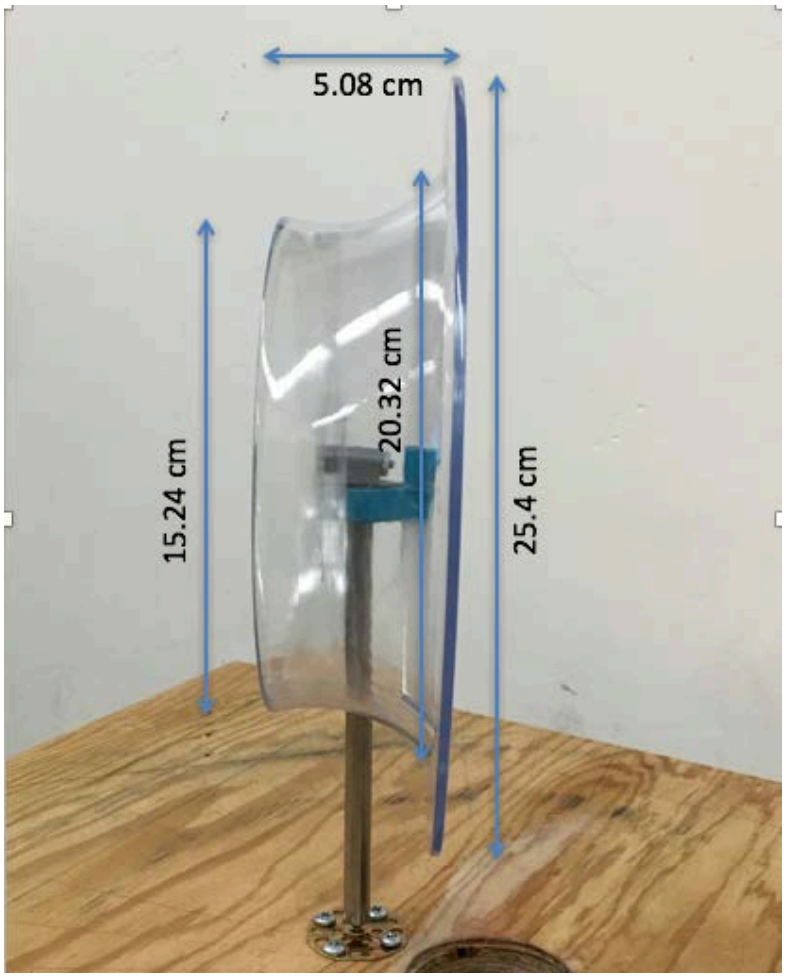

Figure 18. Model Four Dimensions.

5. Model Mounting

In order to mount models 1–3 in the wind tunnel for testing, PVC tubing was cut to length. A 25.4 cm (6 inch) hose clamp was fitted through a milled slot in the PVC and wrapped around the model. A 1.6 mm (0.063 inch) diameter urethane tubing was then attached to each pressure tap and routed through slots in the PVC as demonstrated with model one in Figure 19. The tubes then were run through the PVC and out the bottom of the wind tunnel.

Model Four came supplied with a steel rod which was connected to the turbine. This rod was then threaded into a baseplate and secured with screws to a wooden base mounted in the tunnel test section.

Figure 19. Pressure Tap Routing.

B. NAVAL POSTGRADUATE SCHOOL WIND TUNNEL AND INSTRUMENTATION

To perform this analysis, a low-speed wind tunnel operated by the mechanical engineering department at NPS was used. As seen in Figure 20, this wind tunnel, produced by Plint and Partners Ltd., includes a test section of .457 meter by .457 meter by 1.22 meters. It is driven by a horizontally mounted, variable speed, 11kW motor, with a maximum wind speed of approximately 40 m/s.

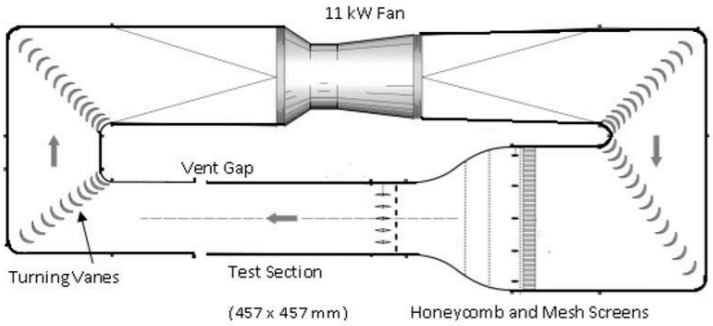

Figure 20. NPS Wind Tunnel. Source: [19].

1. Pressure Instrumentation

The urethane tubes from the model were connected to a Scanivalve pressure measuring system. Each tube was first connected to a 1.60 mm-1.016 mm (0.063 inch-0.040 inch) reducer as the Scanivalve equipment accommodates this size tubing. The 1.016 mm (0.040 inch) urethane tubes were then connected to female Scanivalve 31 pin connectors to facilitate swapping models during testing. Male connectors were used for the Scanivalve pressure scanner. To ensure proper connection, the tubes must be attached to the connectors in the orientation, shown in Figure 21, and the red dots must align when connected.

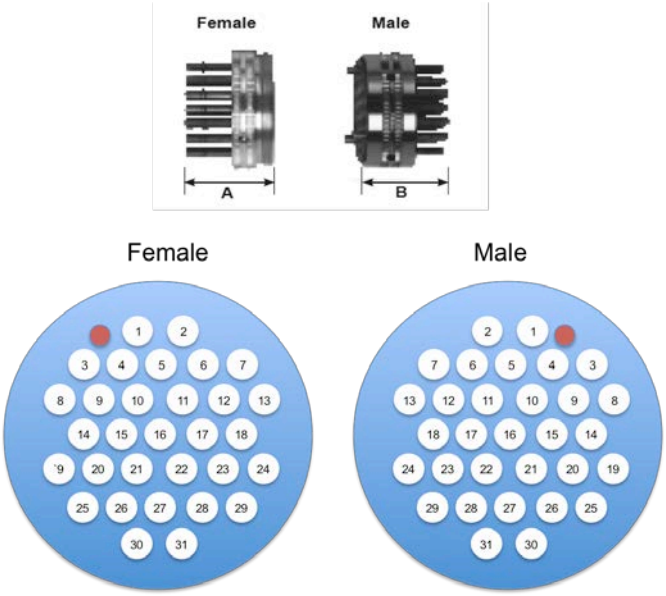

Figure 21. Scanivalve 31 Pin Pneumatic Connectors.

To collect pressures, a Scanivalve ZOC 33 Duplex system was used, as illustrated in Figure 22. All of the tubes fed through the connectors to 1 of 2 ZOC 33 pressure scanners. Each one of these scanners accommodated 128 pressure inputs. These inputs are divided into banks A and B, each of which includes 64 inputs. Additionally, the scanners were fed by a model PAA-8-KL Pitot-static tube, mounted in the wind tunnel, to provide reference pressure for the system. All pressures reported by this system are with respect to tunnel static pressure.

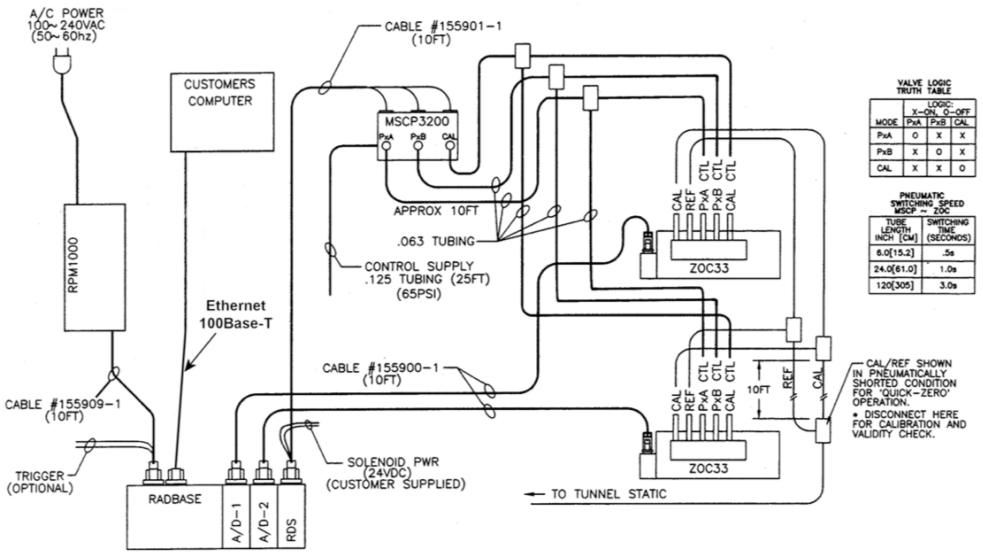

Figure 22. Scanivalve ZOC 33 Duplex Pressure Acquisition Suite. Source: [20].

The pressure scanner is connected to a Scanivalve ERAD4000 Ethernet Remote analog to digital system. This system, while able to accommodate up to eight ZOC 33 scanners with 128 pressure inputs each, can only read 1 bank at a time.

A Scanivalve MSCP miniature solenoid pack was used to control which bank was being monitored. This pack was powered by 24 VDC power supply. The solenoid valve inside was operated using nitrogen gas supplied through a regulator at 65 psi. The position of this valve determined whether bank A or bank B was being monitored. The valve also had a third position, which provided for calibration of the system.

A RPM4000 power module, as shown in Figure 23, powers the entire system. The ERAD 4000 connected via Ethernet to a host computer with LabVIEW software.

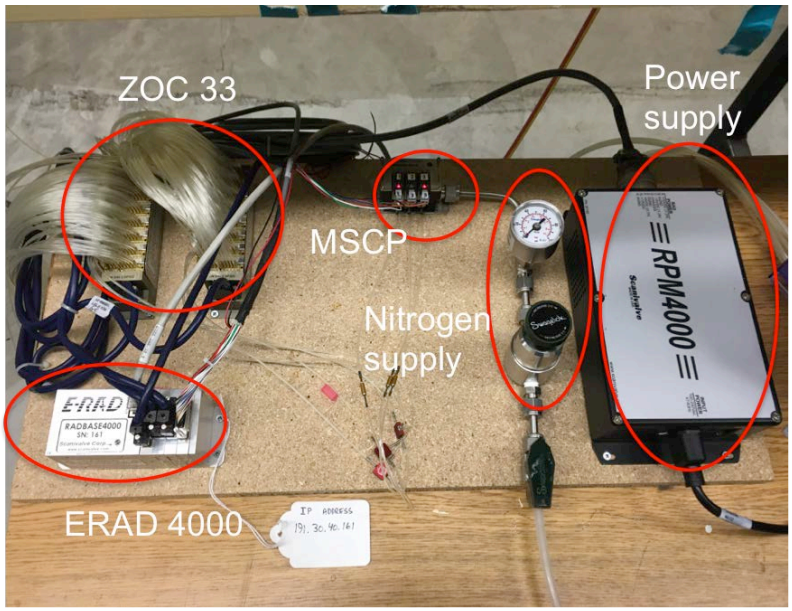

Figure 23. Scanivalve Lab Arrangement.

In addition to surface pressures, an Aeroflow 5-hole probe was utilized to measure pressure and velocity vertical profiles at various stations throughout the models. This probe, depicted in Figure 24, consists of 5 separate pressure ports. These ports enable the software provided with the probe to measure the wind speed and pressure as well as the pitch and yaw angles of the flow. This information is critical to determining the effect the shroud geometry has on the flow.

The probe was mounted on a Velmex BiSlide traversing assembly. With the model base fixed, the use of the traverse was necessary to position the 5-hole probe appropriately. The probe was mounted through a hole in the traverse guide arm and secured in place by a clamping screw. With this mounting method, the position of the probe was able to be modified in both the x and z directions, as depicted in Figure 24.

Movements in the x direction were measured with a machinist's scale. Movements in the z direction were measured by the VP9000 Stepper motor controller. Each step on the controller equates to 0.00508 mm (0.0002 inches)

per step. All measurements were taken at 2500 step increments, which equates to 1.27 cm (0.5 inches).

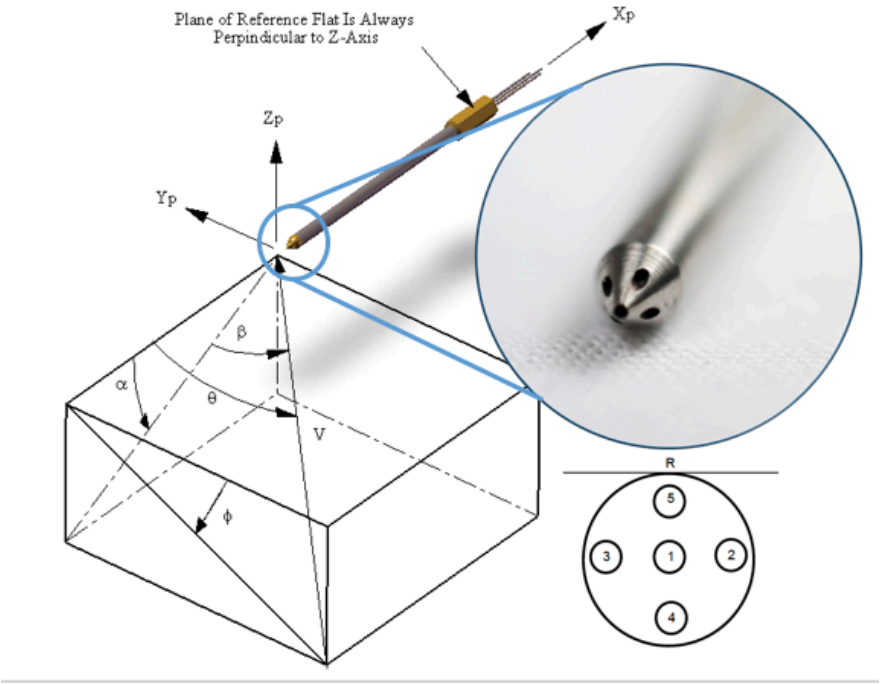

Figure 24. Aeroprobe 5-hole Probe. Source: [21]

2. Data Acquisition

In order to read and compile all of the pressure measurements taken by the Scanivalve suite, software was developed by engineers at NASA Ames. This software was run through a LabVIEW interface and was able to collect data and provide it in a text format.

a. Test Setup

Everything needed to perform this test is located in the Scanivalve_old folder on the desktop, as seen in Figure 25. The system is already set up to measure pressures. To start the program, open the ScaniTest_Two Banks template in the folder.

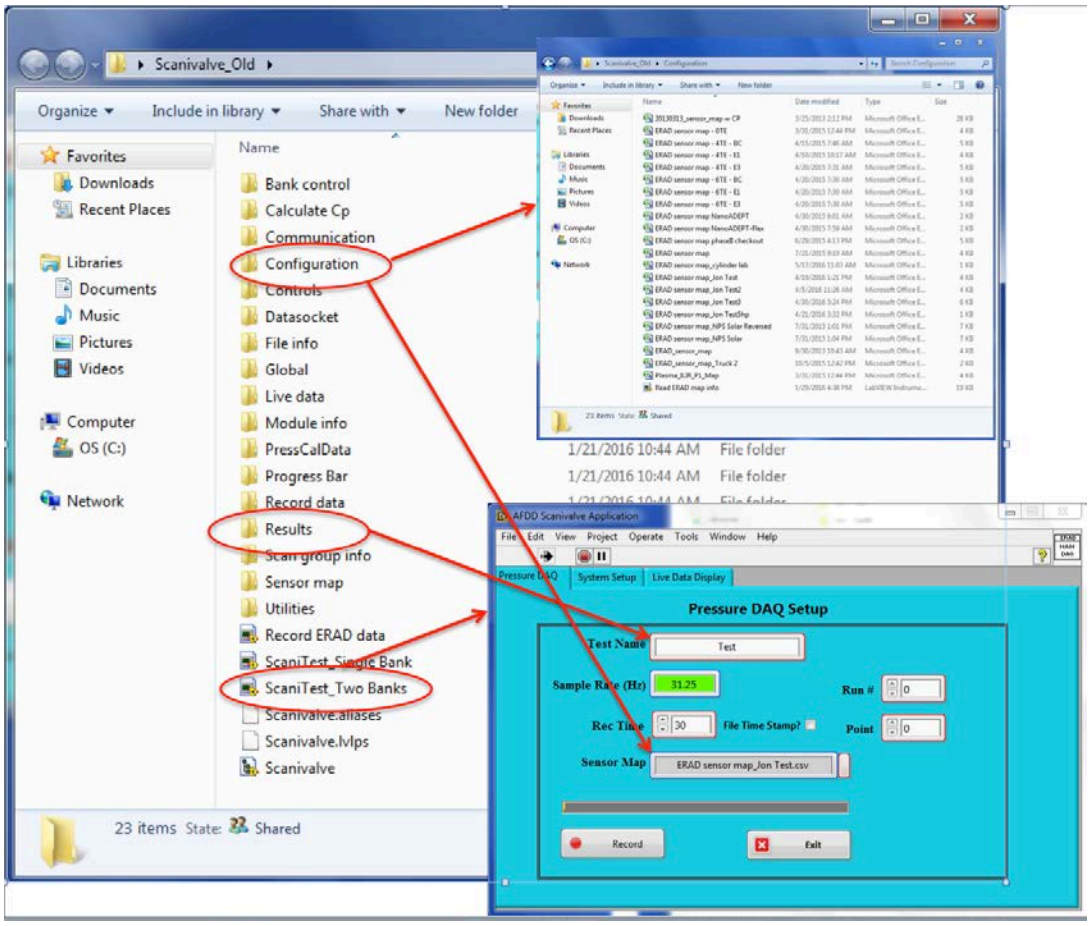

Figure 25. Scanivalve_Old Folder.

The program, as seen in the bottom right corner of Figure 25, will open. It is ready to record immediately. To properly perform the test, however, the output must be customized by performing the following steps.

1. A map must be created and saved in the “Configuration” folder. Select his map under the “Sensor Map” dropdown menu.

i) This map, an example of which is shown in Figure 26, tells the program which tubes need to be recorded and what those tubes correspond to.

ii) The system will measure the pressures from all tubes in both banks each time the record button is pushed, but will only record the tubes listed in the selected Sensor Map.

iii) The title and coordinate location of the tube can be customized on this map.

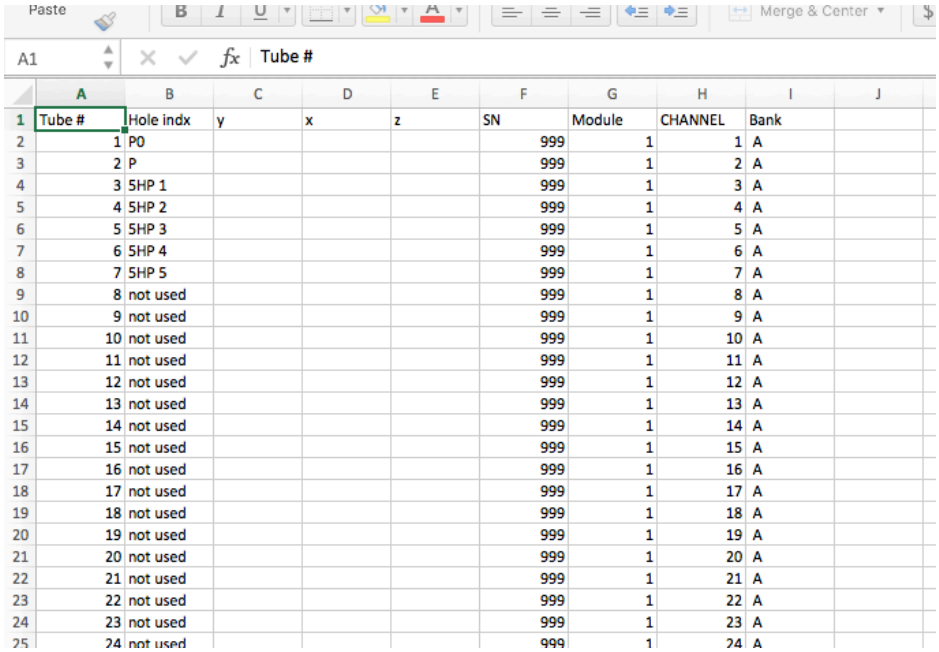

	A	B	C	D	E	F	G	H	I	J
1	Tube #	Hole indx	y	x	z	SN	Module	CHANNEL	Bank	
2	1	P0				999	1	1	A	
3	2	P				999	1	2	A	
4	3	5HP 1				999	1	3	A	
5	4	5HP 2				999	1	4	A	
6	5	5HP 3				999	1	5	A	
7	6	5HP 4				999	1	6	A	
8	7	5HP 5				999	1	7	A	
9	8	not used				999	1	8	A	
10	9	not used				999	1	9	A	
11	10	not used				999	1	10	A	
12	11	not used				999	1	11	A	
13	12	not used				999	1	12	A	
14	13	not used				999	1	13	A	
15	14	not used				999	1	14	A	
16	15	not used				999	1	15	A	
17	16	not used				999	1	16	A	
18	17	not used				999	1	17	A	
19	18	not used				999	1	18	A	
20	19	not used				999	1	19	A	
21	20	not used				999	1	20	A	
22	21	not used				999	1	21	A	
23	22	not used				999	1	22	A	
24	23	not used				999	1	23	A	
25	24	not used				999	1	24	A	

Figure 26. Configuration Map.

2. Type a customized title into “Test name” box. This will create a subfolder under “Results” where the recorded data can be accessed.

   i) The data recorded will be labeled according to the “Run” and “Point” number selected. If the “File Time Stamp” box is checked, time information will also be included in the results file name.

3. Select the desired sample time by filling in the “Rec Time” box.

   i) This will determine the amount of time that recorded pressures will be averaged. Each bank will be monitored for half of the time selected.

4. Under the “System Setup” tab, verify that the ZOC modules are connected by checking the “ERAD Module Information” box. As seen in Figure 27.

5. From the “Bank Control” dropdown menu, select “CalZero” to calibrate the ERAD 4000.

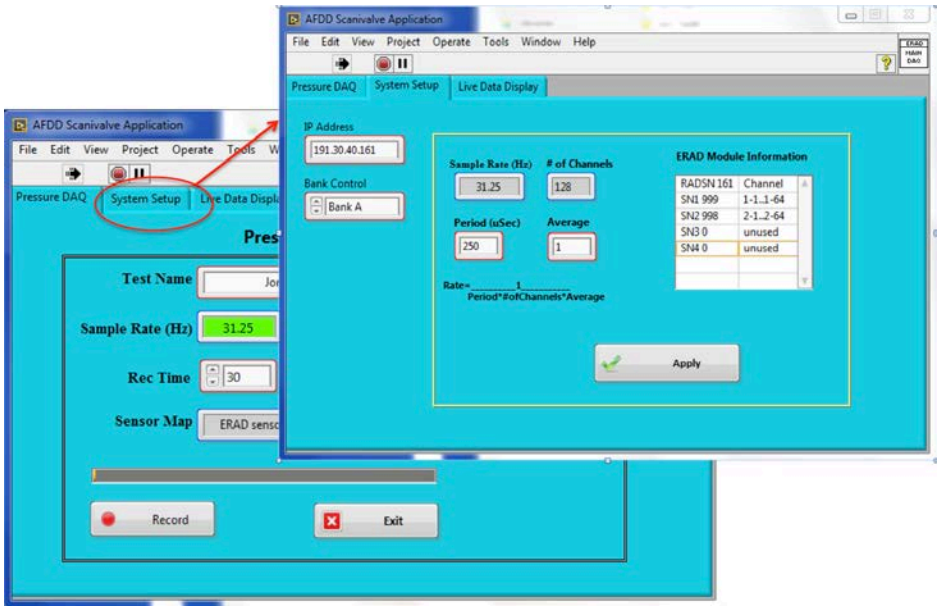

Figure 27. System Setup.

6. Under the “Live Data Display” tab, manipulate the Module and Bank to verify that all tubes are connected properly by observing real time pressure data, as seen in Figure 28.

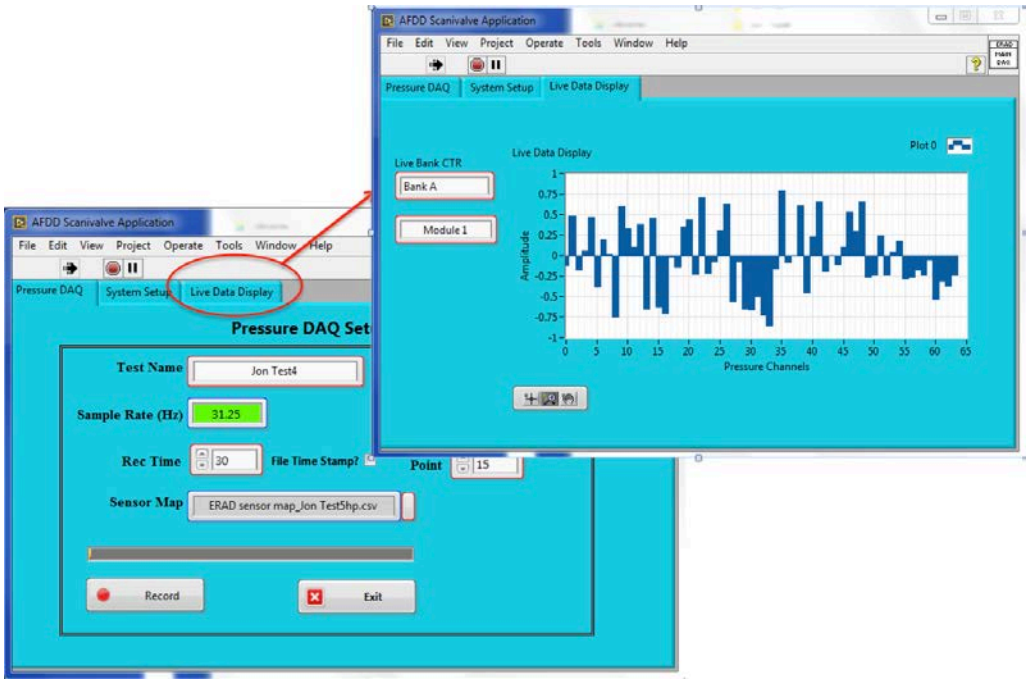

Figure 28. Live Data Display.

The Software is now ready to take measurements. Under the “Pressure DAQ” tab, depress the “Record” button.

C. FLOW VISUALIZATION

Pressure measurement alone is not sufficient to determine flow characteristics. By employing flow visualization techniques, Flow orientation can be studied visually. This information, when combined with measured pressure distributions, creates a more complete picture of the flow. Both oil and tuft flow visualization techniques were utilized in this study for models 1 and 3.

The oil used in this study consisted of dry pigment mixed with oleic acid. This solution was applied in a spray pattern to the interior of the shrouds. When exposed to the wind the air flowing over the droplets it is carried along with the flow direction leaving streaks behind for observation. Additionally, the use of oil flow is also very useful in determining any areas of flow separation, which is especially important in this study.

Tufts were also used on model one in the diverging orientation. By attaching short lengths of string to the model surface, wind direction and magnitude could be qualitatively studied. In this study, string was cut to one half inch lengths and taped to the model interior along the bottom at one inch intervals. As the wind speed was increased, the tufts were visually observed to determine the surface flow properties along the length of the duct.

D. SCREENS

Prior studies have shown that screens have great RCS reduction properties. In consideration of this, the models in this study were also tested with screens attached at both the inlet and outlet of the shrouds. This data, when compared to the data with the same test conditions without screens, is necessary to determine any benefit or detriment to flow that screens have on the shroud.

Two types of screens were utilized in this study. Window screens were obtained from a local hardware store and wind tunnel screens were also used.

Each screen had a similar Open Area Ratio (OAR), however the geometry of the wire on wind tunnel screens is more aerodynamic. Both of these screens were cut to shape and attached with tape to the models. The data obtained from both screens was virtually identical and accordingly only one set will be provided for comparison.

E. TEST CONDITIONS

The methods previously described were used to compile data and provide a clear picture of the aerodynamic properties of each model. A test matrix found in appendix a, was developed to capture the full fluid dynamic properties of each model.

Surface pressure measurements were first taken on each model at various wind speeds ranging from 5 to 15 m/s in order to determine if flow characteristics varied with speed.

Subsequent tests were all performed at a constant speed of approximately 14 m/s. With the speed constant, the other test conditions were varied. The model angle was varied with respect to the direction of flow from 5 to 15 degrees. The models were also tested with screens at the inlet only and at the inlet and outlet. Figure 29 shows an example of these varied test conditions. Model one is mounted in the test section at an angle of 5 degrees to the flow. The model has screens attached at both the inlet and outlet of the shroud.

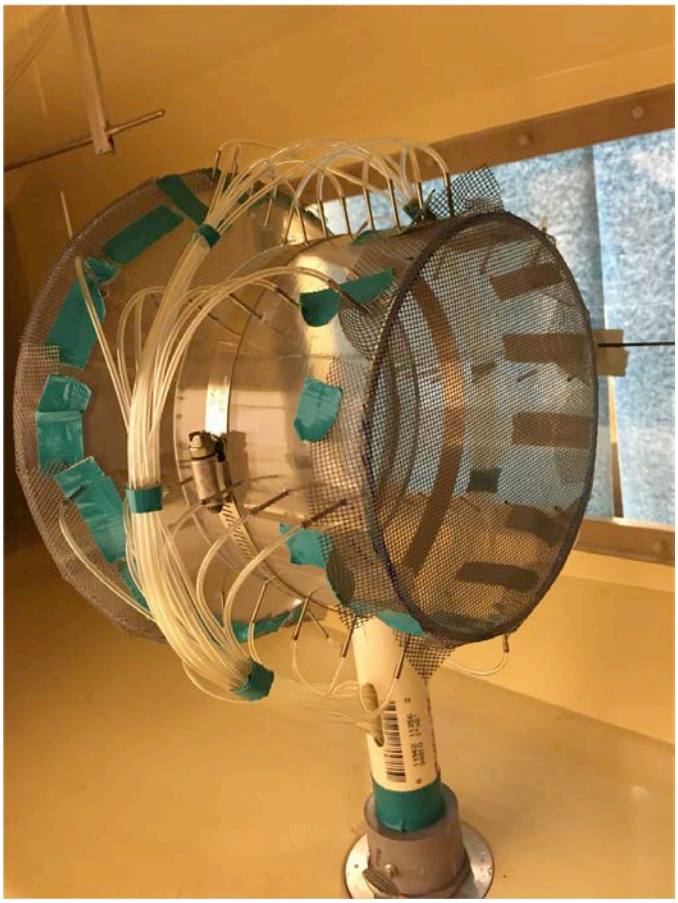

Figure 29. Example Test Position.

THIS PAGE INTENTIONALLY LEFT BLANK

IV. RESULTS AND DISCUSSION

In this section, test results from each model will be presented and analyzed with reference to the possible benefits or impairments to wind turbine performance. The raw data obtained from the pressure instrumentation will be compiled and explained. As discussed, flow visualization results will be presented to augment pressure data obtained.

A. WIND TUNNEL CONDITIONS

Prior to analyzing the models, the wind tunnel was first studied to determine flow quality and uniformity. The 5-hole probe was used to traverse the wind tunnel centerline and take pressure measurements at half inch intervals in order to evaluate tunnel uniformity in both wind velocity and angle. Tunnel velocity, as seen in Figure 30, was found to be uniform with a 3% margin of variation. The variation increases to 5% in the lower 6 cm of the tunnel, however this region is outside the dimensions of the models studied.

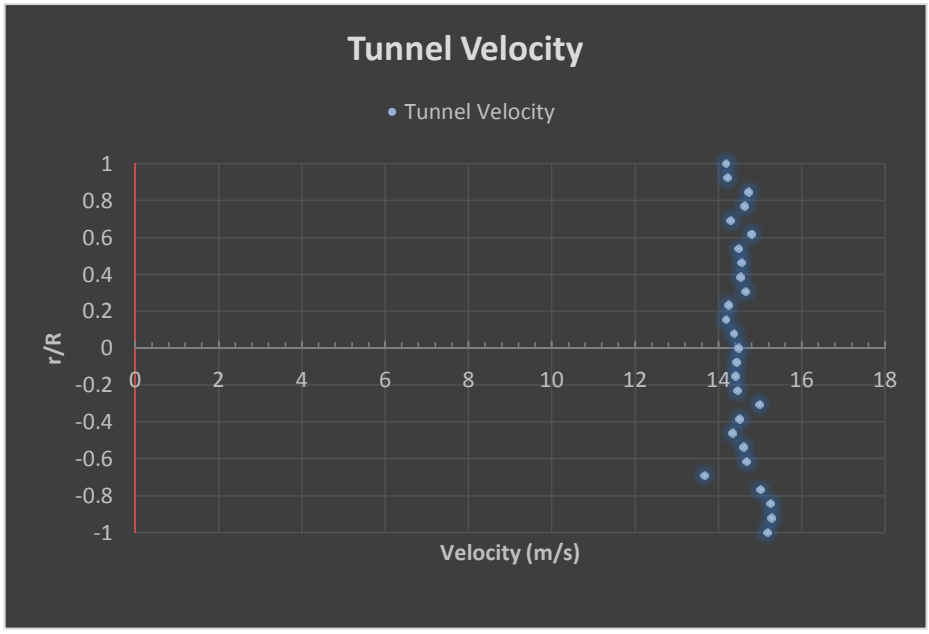

Figure 30. Wind Tunnel Velocity Profile.

Tunnel flow pitch angle was also determined from the 5-hole probe data. The flow straighteners inside the wind tunnel act to minimize the lateral components of velocity. Figure 31 illustrates that the pitch angle in the tunnel was maintained at approximately 2 degrees throughout the tunnel cross section. As with tunnel velocity, the pitch angle was not maintained at this low value in the extreme lower section of the tunnel where it jumped to 13 degrees. As with the wind tunnel velocity, this variation will not have an adverse effect on the findings in this study.

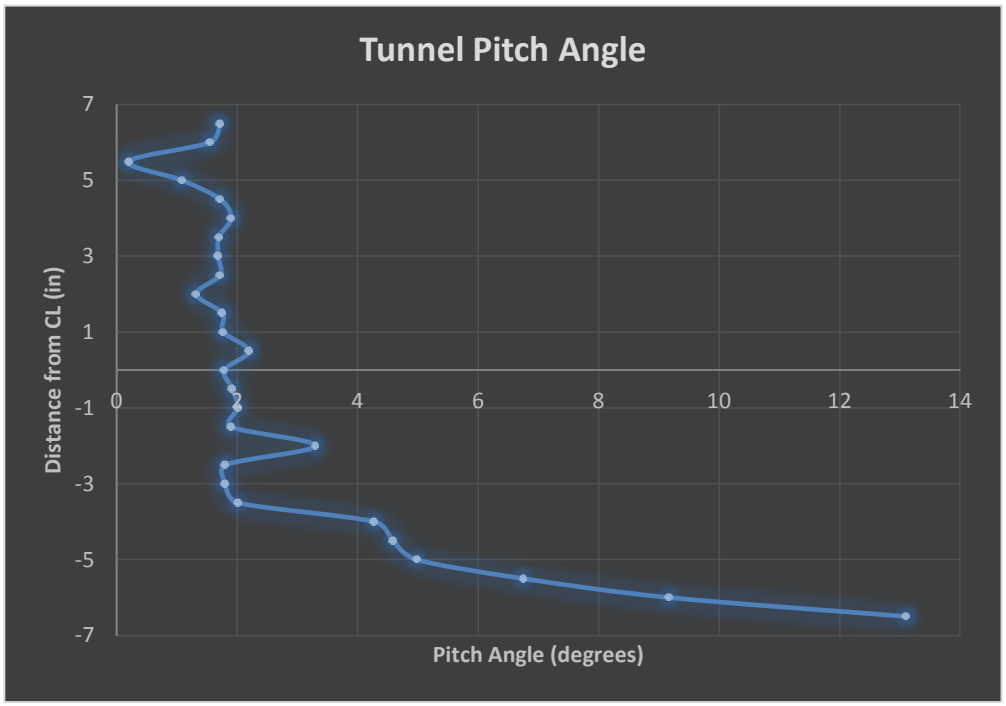

Figure 31. Wind Tunnel Flow Pitch Angle.

B. MODEL 1

1. Model 1 Converging

Model one was first mounted in the wind tunnel in the converging orientation. The presumption with this arrangement was to enlarge the stream tube incident on the duct. Essentially, the duct would work to funnel the air through to the turbine and increase mass flow rate.

As we see in Figure 32, the pressure drops after entering the duct. This is the expected response. However, there is a sharp decrease at station 6 where the duct transitions from converging to straight. This decrease is indicative of flow separation.

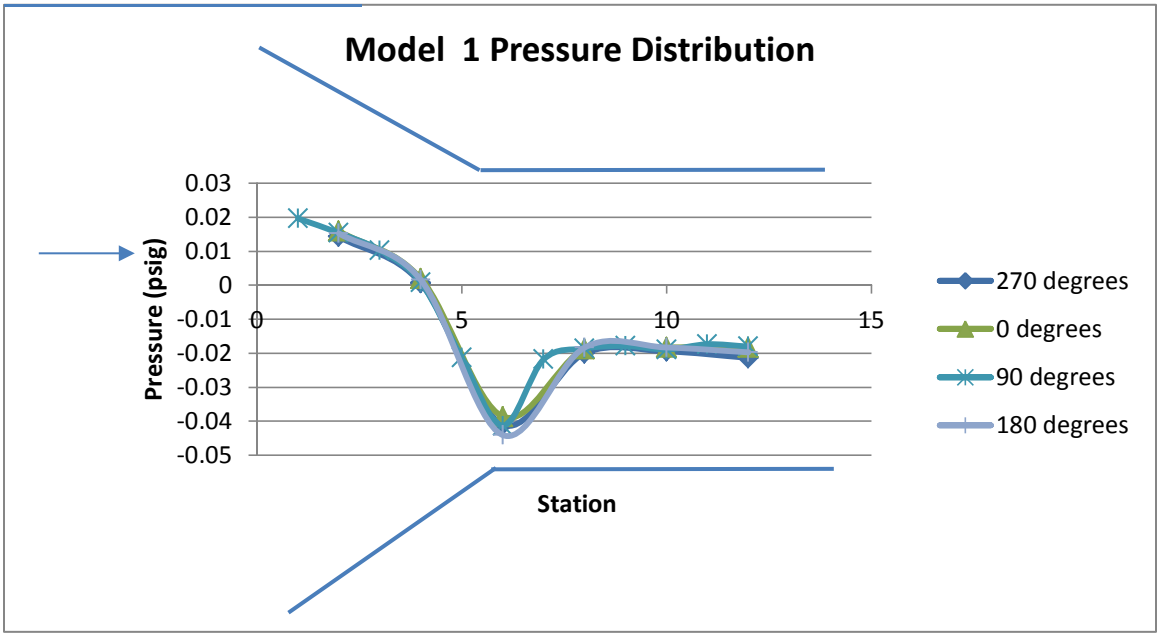

Figure 32. Model One Pressure Distribution.

The velocity was determined using the measured pressures and Bernoulli's equation at each station. The theoretical duct velocity was found by using the measured tunnel velocity and multiplying by the ratio of the square of the diameter at the inlet to the square of the diameter at each station. As seen in Figure 33, the velocity in this case differs from the theoretical velocity. This can be accounted for by the shape of the duct. Without a smooth transition into the duct, such as a bell mouth, there is an initial drop in velocity from the wind tunnel velocity. Additionally, it is shown that there is a jump in velocity at station 6, which is near the point where the duct transitions from converging to straight. The theoretical velocity does not account for possible flow separation, while the actual calculated velocity shows this to be the case.

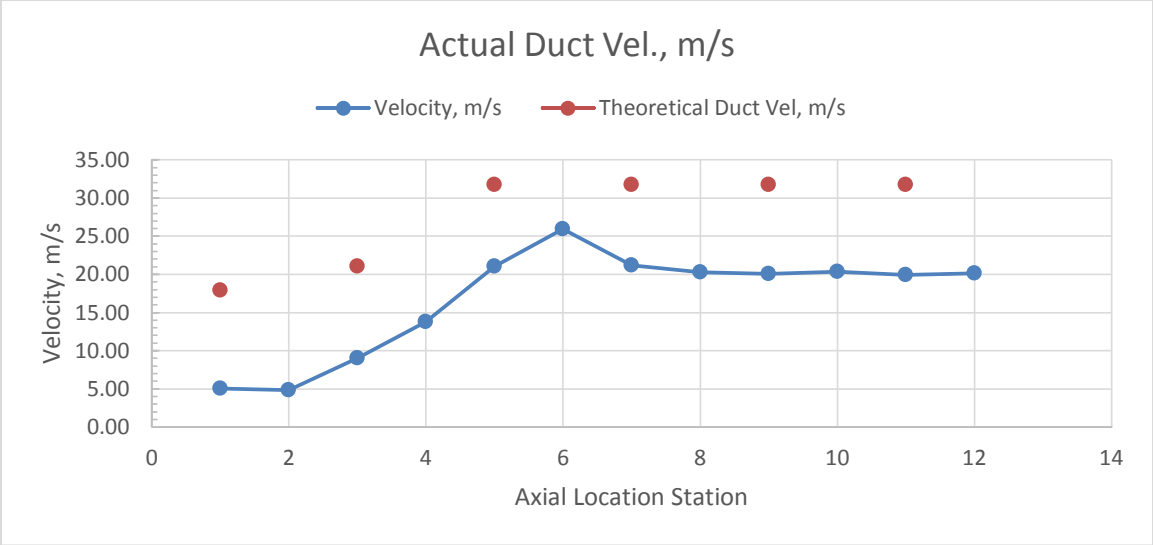

Figure 33. Model One Duct Velocity.

Oil flow visualization was employed in order to verify the flow separation. In Figure 34, the picture on the left shows the oil applied to model prior to the test. On the right, it is clear that the oil travels up the duct where it stalls right after the transition region and begins to pool. This verifies the presumption of flow separation in this region of the duct.

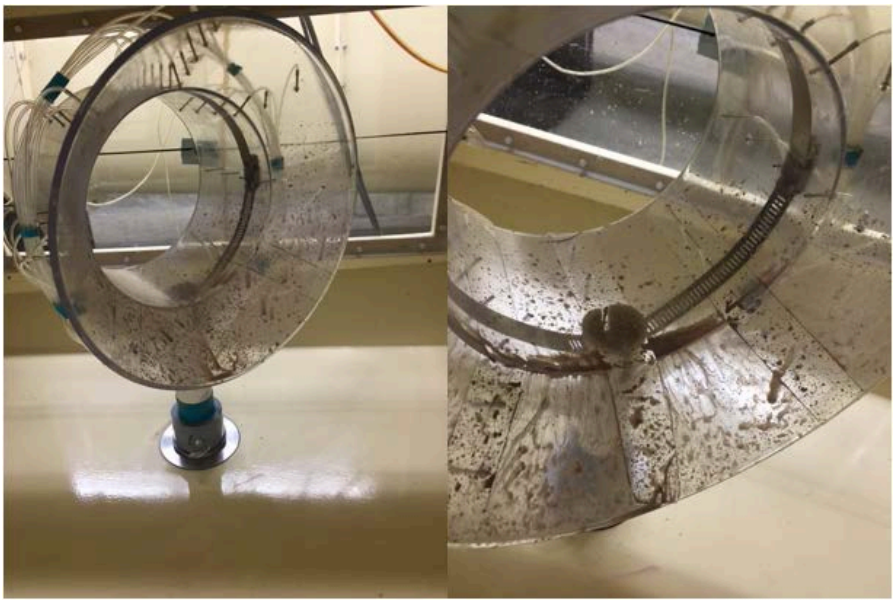

Figure 34. Model One Oil Flow Visualization.

Figure 35 shows the velocity profiles taken with the 5-hole probe. The velocity profile at the transition region shows the flow is turbulent and non-uniform. This is the area where the turbine would be mounted. While the flow does regain uniformity at the exit to the duct, the turbulent region would decrease the efficiency of the turbine.

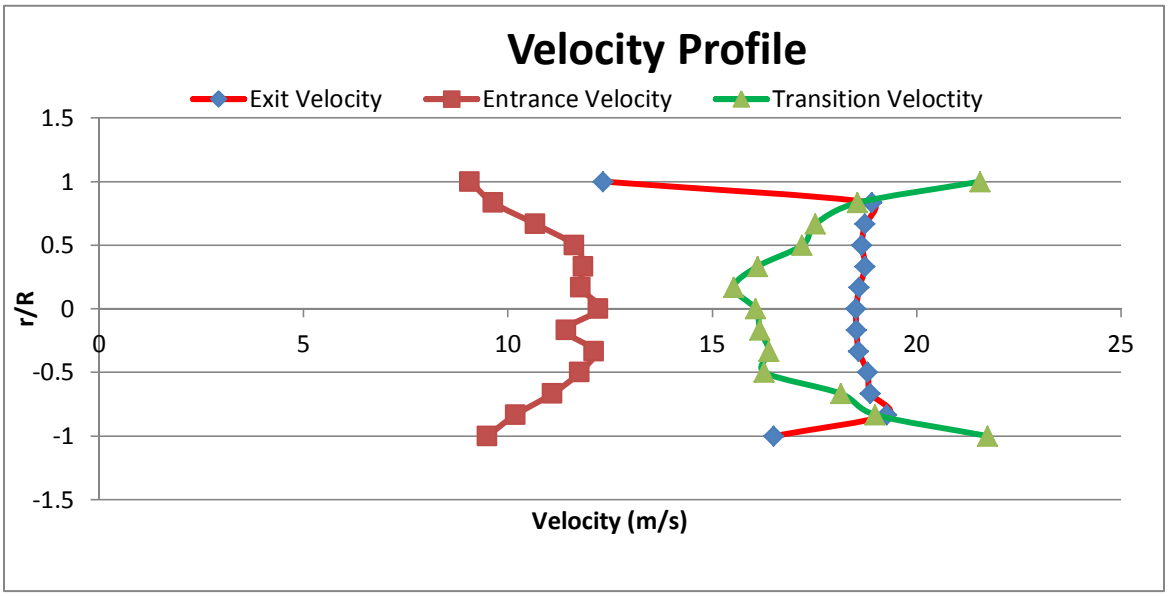

Figure 35. Model One Velocity Profile.

The 5-hole probe is also able to measure pitch angle. Ensuring the duct geometry does not induce any flow swirl is equally as important to determining its ability to increase turbine efficiency. Figure 36 shows model one has minimal effect on flow swirl. In fact, flow pitch angle is decreased from the already low levels measured in the tunnel illustrated in Figure 31.

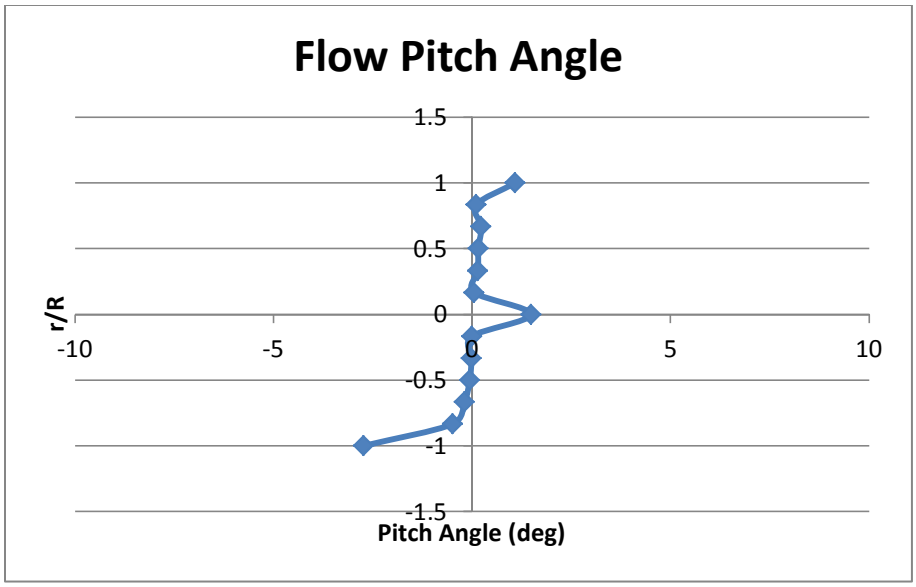

Figure 36. Model One Airflow Pitch Angle.

2. Model 1 Diverging

Model one was then rotated and tested as a diverging duct. The presumption with this arrangement was to create a "Wind Lens" effect at the exit of the duct. Specifically, it was anticipated that the wind passing over the exterior of the diverging section would create a low-pressure area at the exit, which would act to pull more wind through the duct and increase the mass flow rate of air through the turbine.

Figure 37 shows the pressure distribution through model one. The low initial pressure can be accounted for by the sudden entrance to the duct. The addition of a bell mouth might change this parameter by easing the flow of air through the duct. Following the entrance region, the pressure levels out and does not change through the diverging region. I believe that the large angle of the diverging portion of the duct is too extreme and so a two-dimensional stall effect occurs. Essentially, the diameter increases at an excessive rate and the flow does not expand with it. The flow behaves as if the duct ends at the point of divergence.

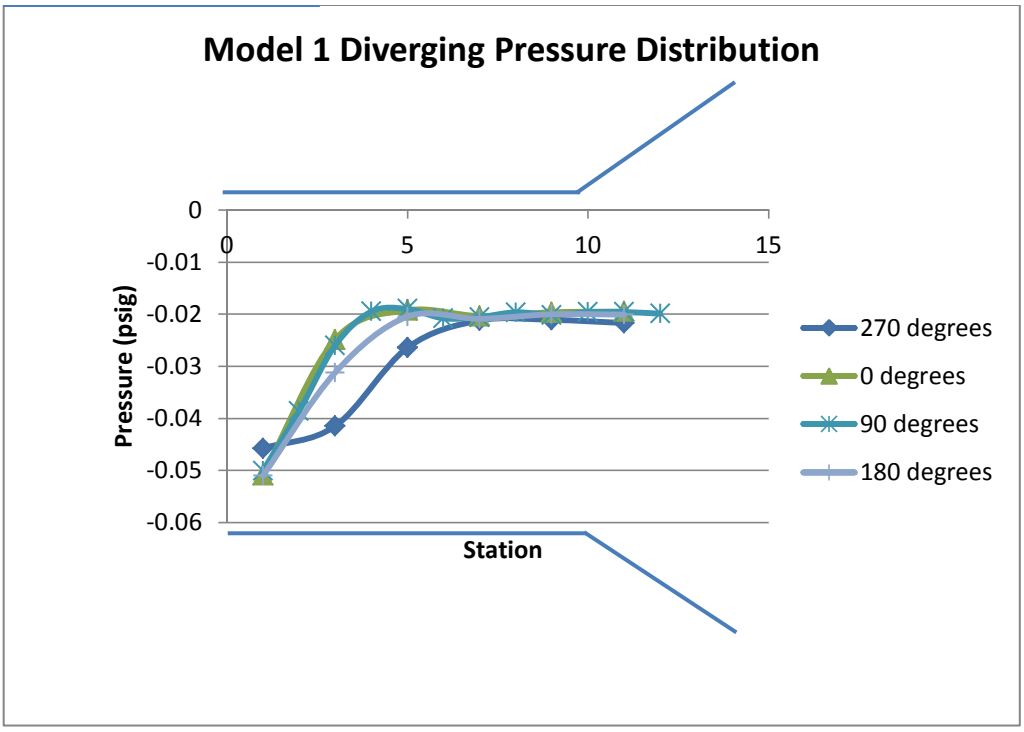

Figure 37. Model One Diverging Pressure Distribution.

The velocity measured is illustrated in Figure 38. After a small initial drop, the velocity remains constant through the duct with the diverging shape of the duct having a negligible effect. The initial velocity is higher than the theoretical value. This can be explained by flow separation close to the inlet. Additionally, the theoretical velocity will drop towards the diverging section due to the same mass flow through a larger cross-sectional area. However, the actual velocity remains constant due to the two-dimensional stall previously noted.

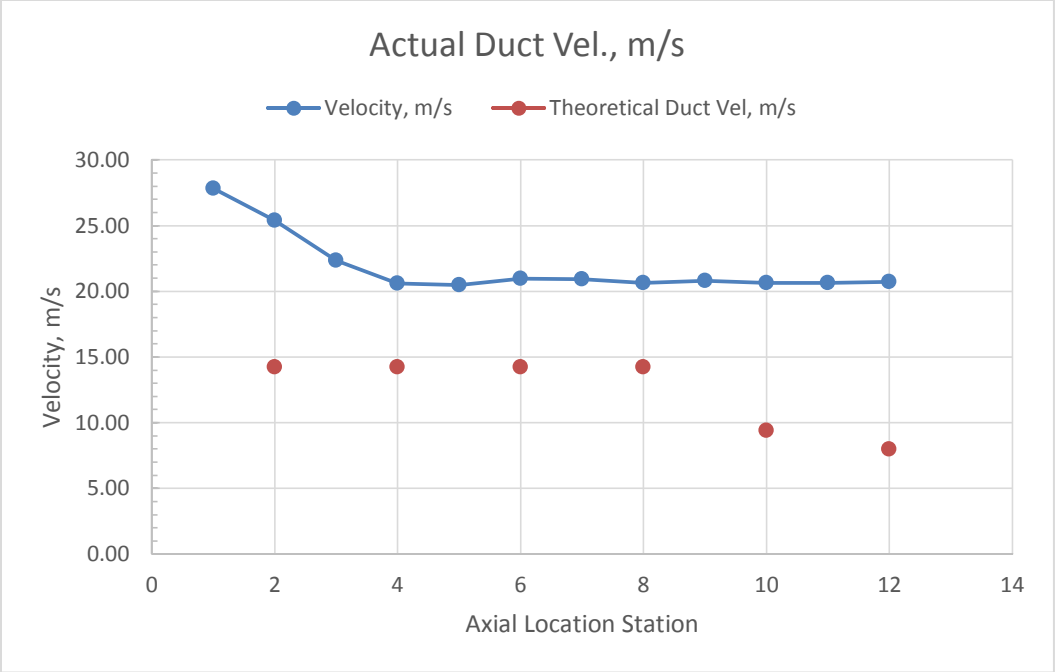

Figure 38. Model One Diverging Duct Velocity

The pressure ports on the model are very limited in demonstrating the full picture due to the fact that the pressure is only being measured on the inside surface of the duct. When the five-hole probe was utilized to measure the velocity profiles, a clearer picture emerged at what was occurring inside the duct. As seen in Figure 39, the exit velocity profile is very similar to the entrance velocity profile. However, where the duct transitions from straight to diverging, the flow is turbulent and the velocity drops significantly. It maintains a higher value at the duct walls, but drops in the center. This is why this is not observable using only the duct pressure ports.

Based on continuity and the conservation of mass, mass flow at each cross section must remain constant. The results in the transition region indicate that instead of the diverging section acting to increase velocity inside the duct, it may conversely act to increase velocity on the exterior of the duct.

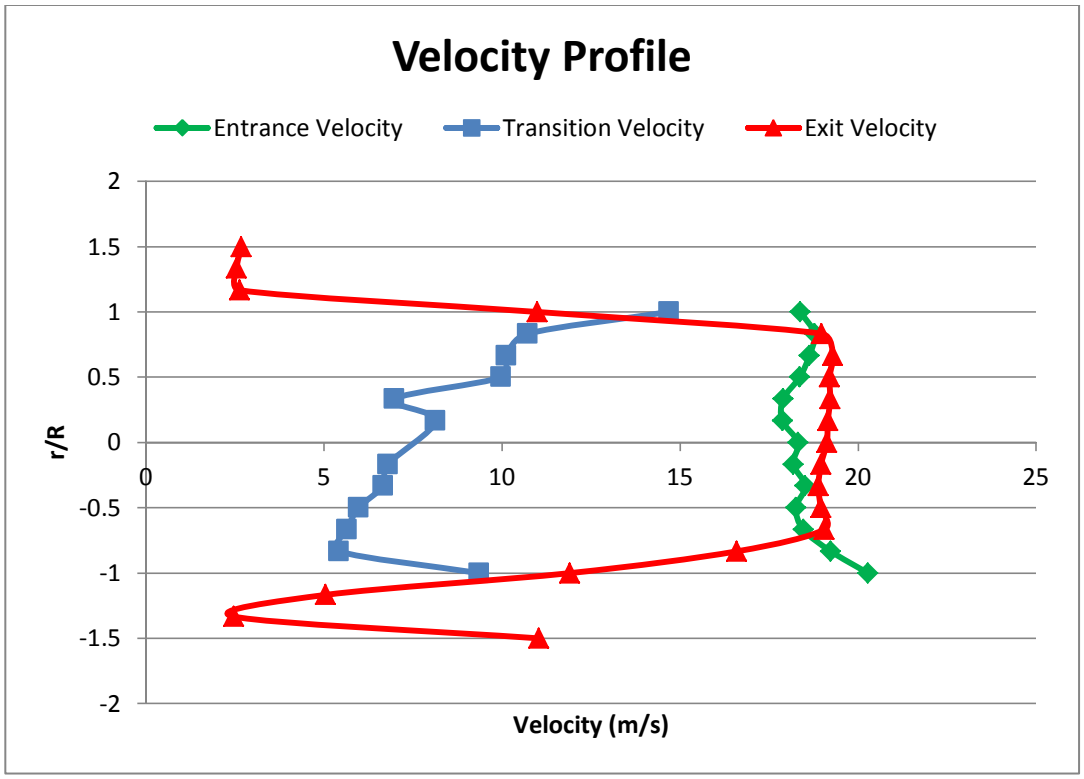

Figure 39. Model One Diverging Velocity Profile.

To verify the two-dimensional stall and flow separation, tuft flow visualization was utilized. Figure 40 shows model one with 2 cm tufts attached linearly along the bottom centerline of the duct. While demonstrated more clearly in video, it can be seen that the tufts attached to the diverging section are unaffected by the wind flowing through the duct.

Figure 40. Model One Tuft Flow Visualization

3. Model 1 Diverging (with Screen)

As previously noted, there have been studies which show that screens can have significant RCS reduction capabilities. Model one was fitted with a screen, as shown in Figure 29. Figure 41 shows that the pressure distribution throughout the duct was relatively constant with only a slight decrease. There is

also a considerable drop in pressure when compared to Figure 36, where no screen was used.

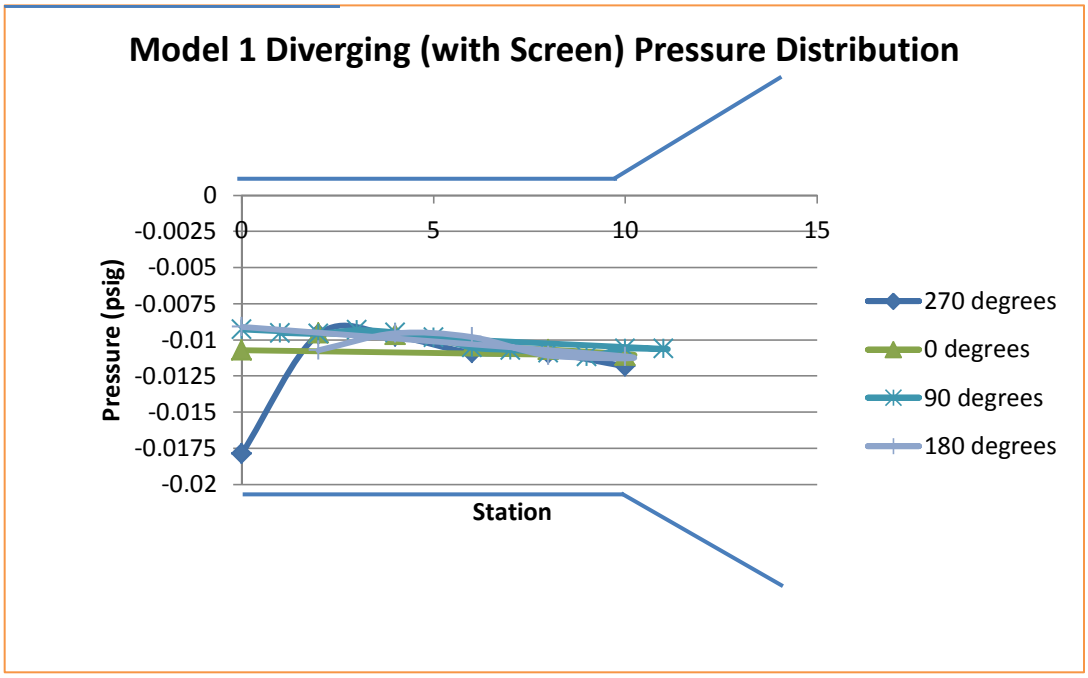

Figure 41. Model One Diverging (with Screen) Pressure Distribution.

Further comparisons using the five-hole probe showed an unacceptable decrease in velocity. Exit velocity from model one changed from approximately 19 m/s without a screen to 6 m/s with a screen. The extreme decrease in velocity warranted repeated tests, and these results were verified with a variation of +/- 1 m/s. While this result does not preclude the integration of a screen with the duct, it does support the need for further research in the optimal OAR of duct screens.

The model and supporting PVC pipe has an approximate cross sectional area of 0.0067 square meters. When compared with the tunnel test section of 0.209 square meters, the model effected a 3.2% blockage of the test section area. This is within acceptable values and precludes the need for corrections.

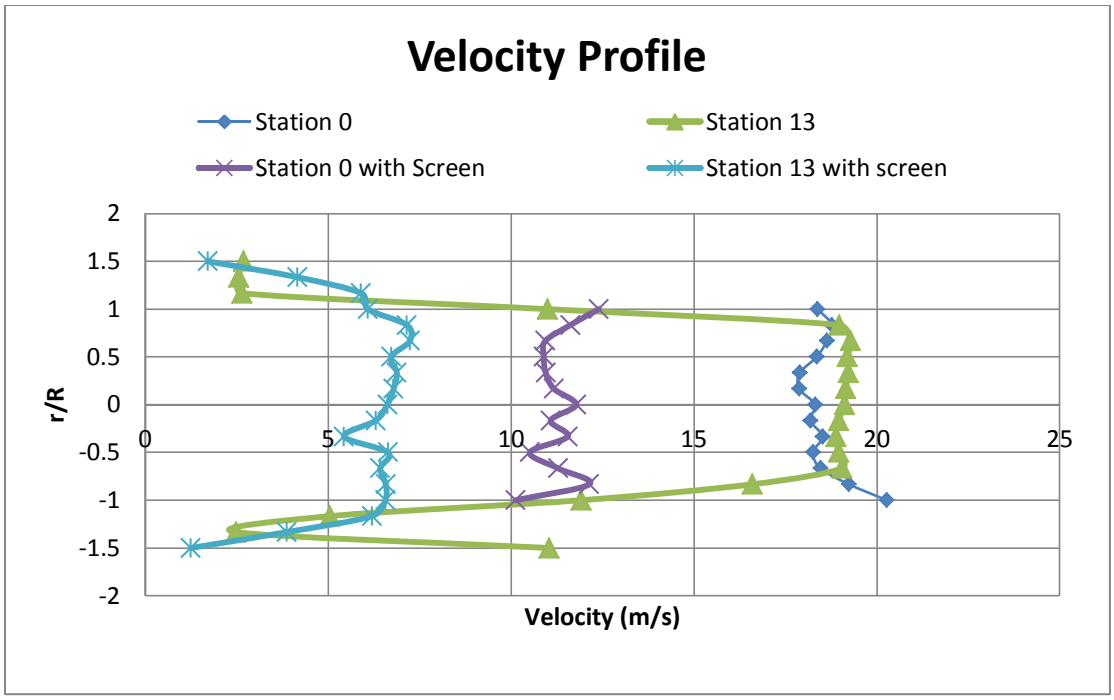

Figure 42. Model One Velocity Profile Screen Comparison

4. Model 1 Diverging (Rotated 5 Degrees)

Wind turbines need to be efficient at varying angles of yaw. An ideal duct would maintain efficiencies with a 5 to 10 degree offset to the direction of the wind to the turbine. To test this, model one was rotated 5 degrees inside the wind tunnel. Figure 43 shows that with just this slight adjustment, the flow inside the duct becomes erratic and unpredictable. The flow varies at each location around the duct and no benefit is gained. The design of this duct is very intolerant of flow angles.

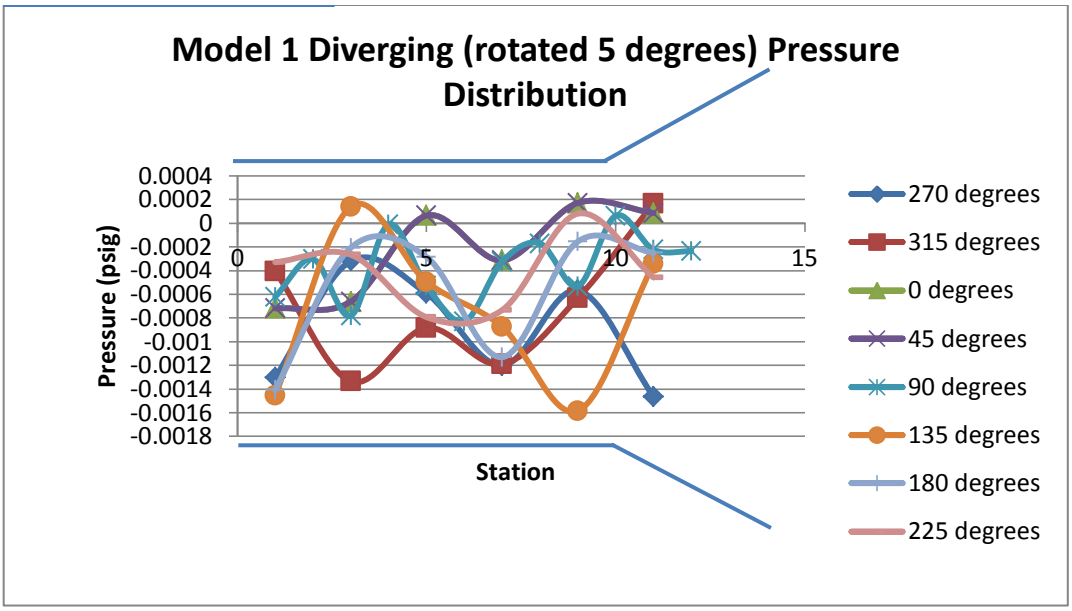

Figure 43. Model One Diverging Pressure Distribution with Five Degree Offset

C. MODEL 2

Model two was studied next. Due to the fact that this was simply a constant diameter duct, the main goal in studying model two was to determine if the flange molded onto the exit of the duct achieved the "Wind Lens" phenomenon that has met success with other designs. The entrance to this duct was identical to model one when mounted in the diverging orientation, therefore the measured pressure distribution was expected to be similar to Figure 37. The flange at the trailing end of the duct is intended to create vortexes downstream which would act to draw more flow through the turbine.

Figure 44 confirms that this model maintains the same pressure behavior at the walls as model one. The pressure drop at the inlet can similarly be attributed to the lack of a smooth transition such as a bell mouth. Following this, as predicted, the pressure reaches and maintains a constant value.

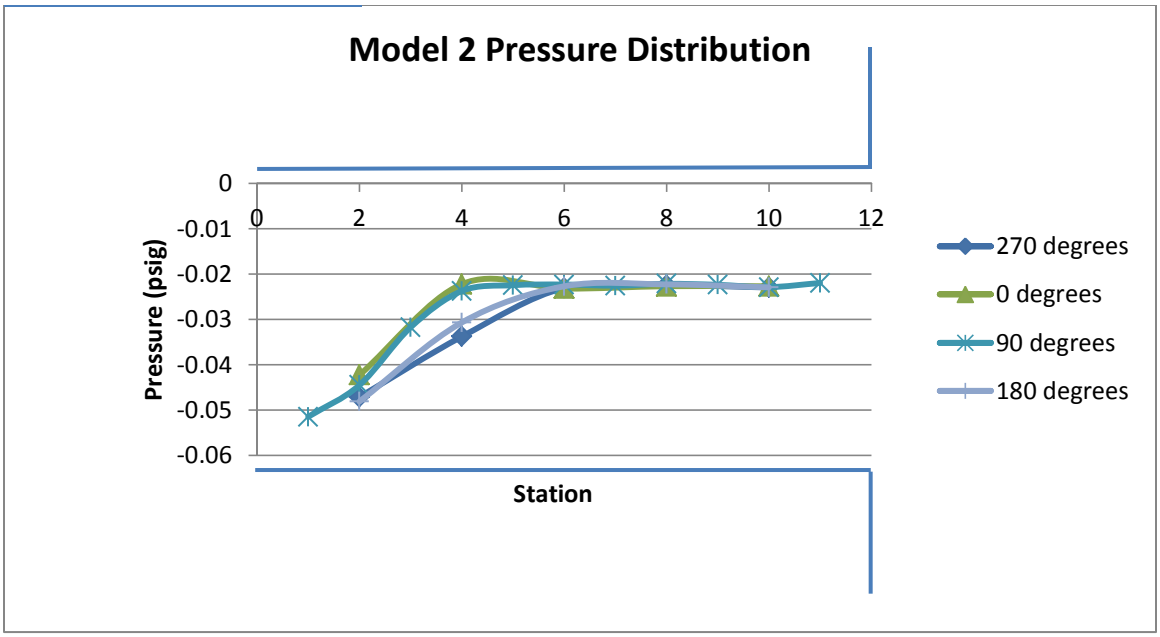

Figure 44. Model Two Pressure Distribution.

When the computed velocity is determined, the duct velocity showed a marked increase from the theoretical value, which in this case was the same as the wind tunnel wind speed itself; see Figure 45. This would support the formation and effectiveness of exit vortices.

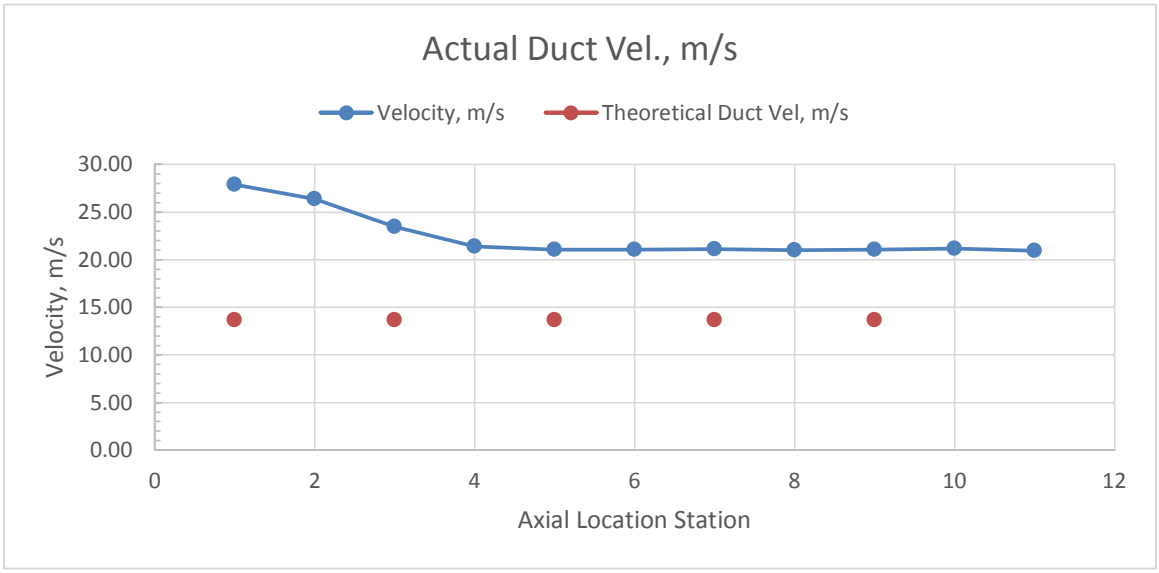

Figure 45. Model Two Duct Velocity.

To confirm these results, the velocity profiles at the inlet and outlet were taken using the 5-hole probe. Figure 46 shows a very significant change from the inlet to the outlet of the duct. Velocity increased from near 11 m/s at the inlet to 18.5 m/s at the outlet. The large difference warranted repeated runs. These runs verified the results within 2 m/s each time. This test thus supports the theory that the “Wind Lens” or exit flange can be very advantageous if employed properly. The low velocities seen at the top and bottom of this chart represent measurements taken when the probe was directly behind the duct flange.

Due to the wide flange that was normal to the flow on this model, the cross-sectional area of .031 square meters represented a 14% blockage of the test section area. This exceeds acceptable limits for blockage.

Multiple runs, however, were performed with the test section windows removed. This enabled flow around the model and negated the blockage. No quantifiable differences were observed, and therefore, it was determined that the high blockage ratio was not a factor in this case.

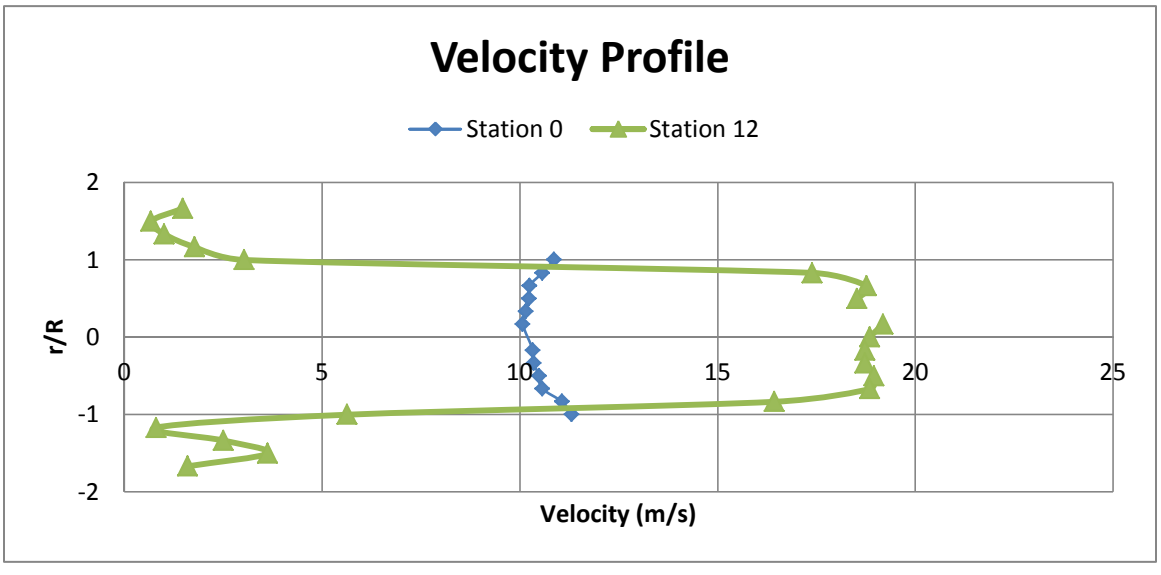

Figure 46. Model Two Velocity Profile

D. MODEL 3

1. Model 3 Unaltered

Model three's hyperbolic profile was expected to solve the issue of the initial pressure drop due to the sudden entrance seen in models one and two. The smooth bell shaped transition into the duct is intended to eliminate the initial pressure drop and gradually accelerate the flow as the diameter decreases towards the center where the turbine would be mounted.

Figure 47 verifies this to be the case. The pressure through the duct decreases to a minimum near station 11 which is where the duct has the smallest diameter. The pressure then increases to station 18 where it appears to even out and remain constant. This is indicative of flow separation at this location. If the angle of the "bell" becomes too large, the flow would separate from the duct and continue with two-dimensional stall as observed in model one.

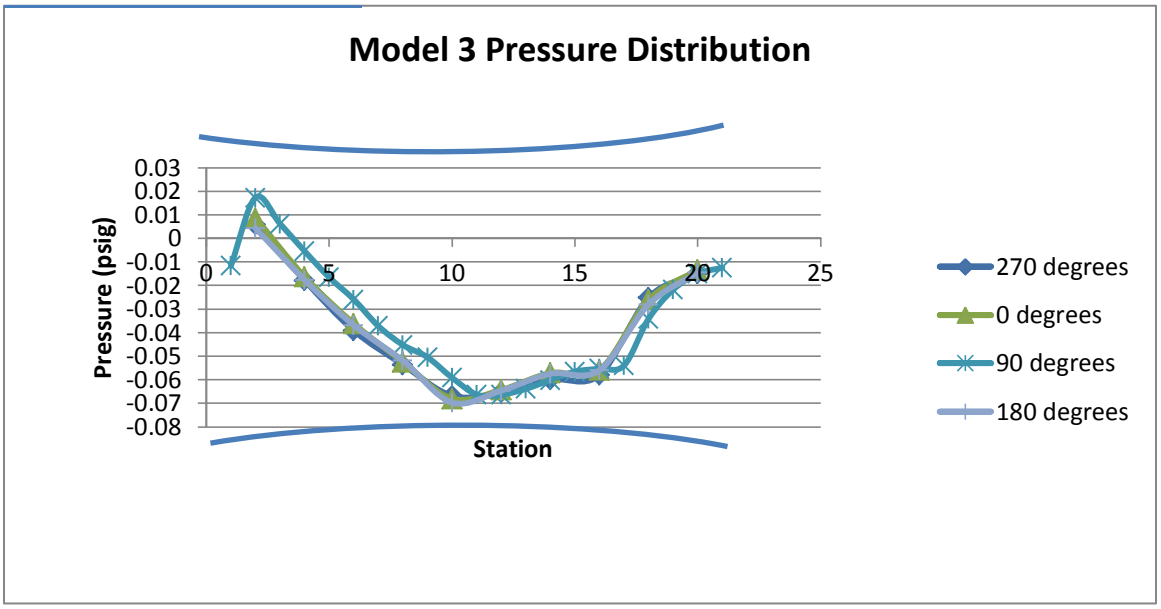

Figure 47. Model Three Pressure Distribution.

When velocity was calculated, the theoretical velocity and the actual velocity matched up almost exactly. This is important, because it signifies that the

speed of the air through the duct behaves in precisely the manner the duct was designed for. Figure 48 shows that while the wind tunnel velocity was 14 m/s, velocity increased to more than 30 m/s in the center section of the duct. With turbine power being proportional to the cube of velocity, this effect is very desirable.

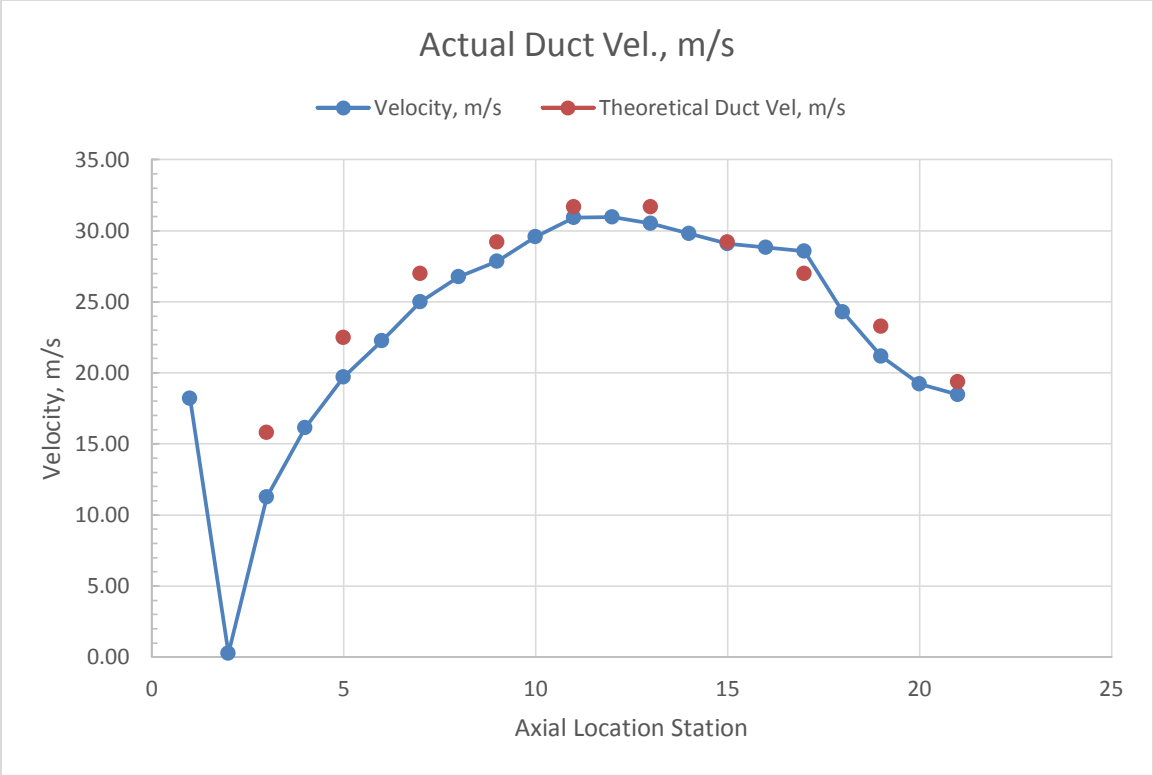

Figure 48. Model Three Duct Velocity.

2. Model 3 with Screen

A wind tunnel screen was fitted on the inlet of model three due to the poor performance of the window screen that was utilized on model 1. While both screens had a similar OAR, the shape of the wire on wind tunnel screens is more aerodynamic and better results were expected. As seen in Figure 49, this was not the case. Both screens had an approximate OAR of 70%. Clearly, the negative effects of a 30% blockage to the duct entrance could not be compensated for by duct geometry.

The measurements shown were obtained using the 5-hole probe. Prior to discussing the screen effects, the results without the screen verify the data obtained with the duct surface pressure taps. Station 11 corresponds to the center of the duct, where the diameter is at a minimum. The measured velocity is less than the value of 31 m/s obtained using pressure and Bernoulli's equation, as seen in Figure 48, however, there is still a marked increase. Additionally, there is a perfectly smooth and uniform velocity profile: a very desirable condition for wind turbines. The measurements at station 16 and subsequently at the exit of the duct show the flow decelerating as the duct diameter increases. Of particular note is the drop off in velocity near the surface of the duct. This is evidence again that the flow separates from the duct at a certain point.

Station 11 was measured again with the wind tunnel screen in place. The decrease in velocity is quite extreme as only 6 m/s was obtained. This test was repeated three times with consistent results.

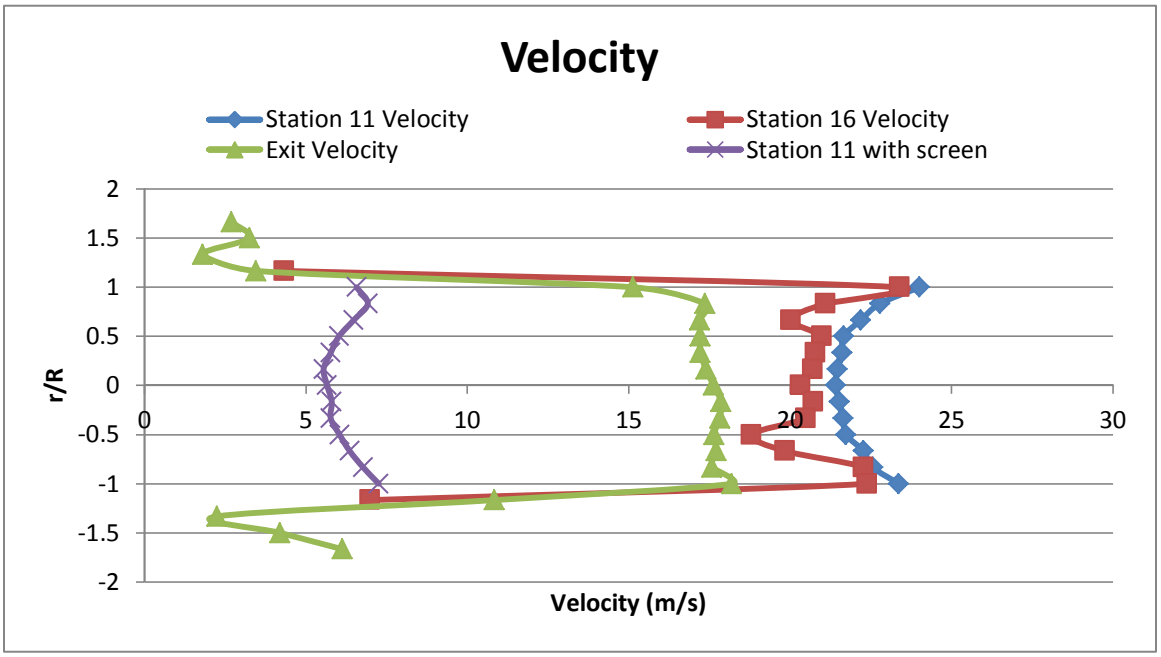

Figure 49. Model Three Velocity Profile Screen Comparison

Oil flow visualization was next utilized to confirm the suspected flow separation. Figure 50 shows that as the wind flows through the expanding portion of the duct, the oil flows with it. At a point that corresponds to station 19, the oil flow stops. This is the point where the duct angle becomes too large and the flow separates from the surface of the duct.

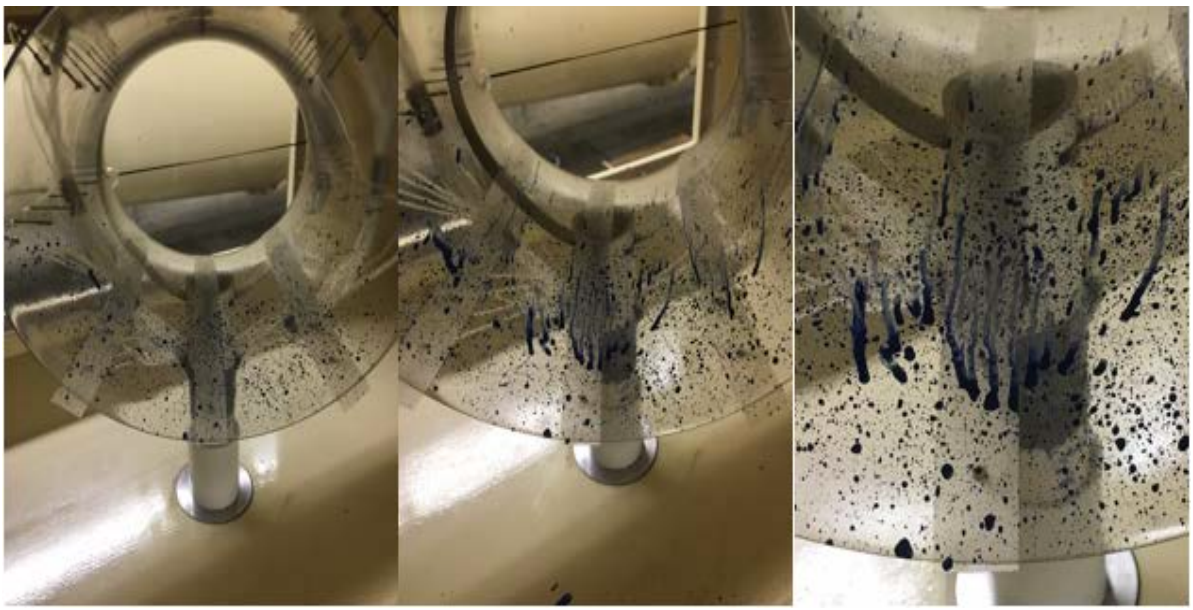

Figure 50. Model Three Oil Flow Visualization.

3. Model 3 Rotated

Model three was first rotated 5 degrees inside the wind tunnel. Figures 51 and 52 show that, with this adjustment, the flow inside the duct is able to maintain the same benefits that were observed when the flow was normal to the duct. Velocity is increased from the wind tunnel speed of 14 m/s to a computed velocity of 28 m/s. Figure 52 shows that there is a drop below the theoretical velocity through the duct. While this represents a slight decrease in efficiency when compared to Figures 47 and 48, a significant velocity increase is still obtained.

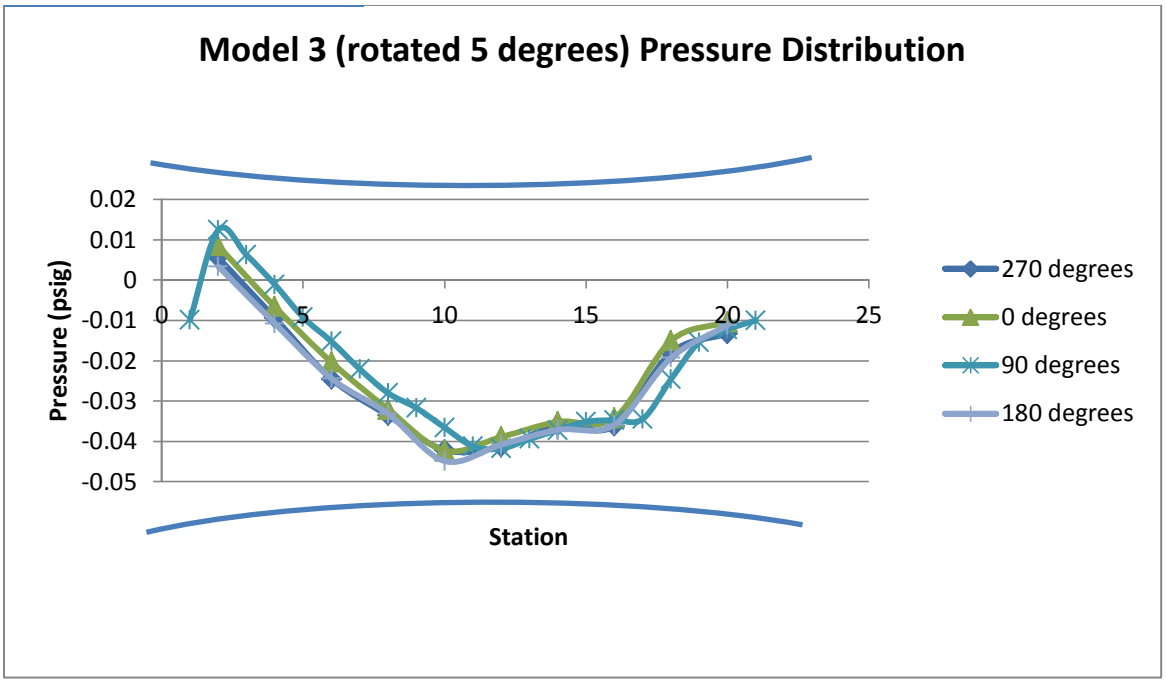

Figure 51. Model Three Pressure Distribution with Five Degree Offset.

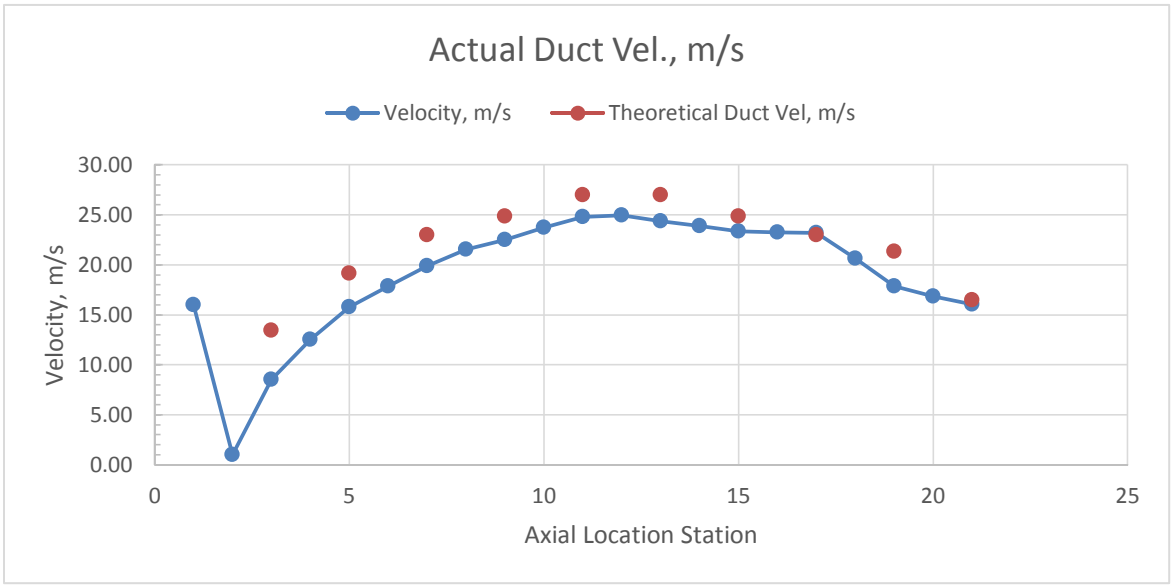

Figure 52. Model Three Duct Velocity with Five Degree Offset.

When model three was rotated 10 degrees, the efficiency could no longer be maintained. Figure 53 compares and contrasts the velocity at station 11 for all three orientations. With the model rotated 5 degrees, the velocity does begin to deviate from a smooth velocity profile, but the benefit of increase velocity through the duct is still achieved at a significantly higher level. When that same velocity profile is measured with a ten-degree rotation, the velocity plummets to an unacceptable level. This shows that while this model is more tolerant of flow angles than model one, it still fails to perform at an acceptable level with a ten degree offset.

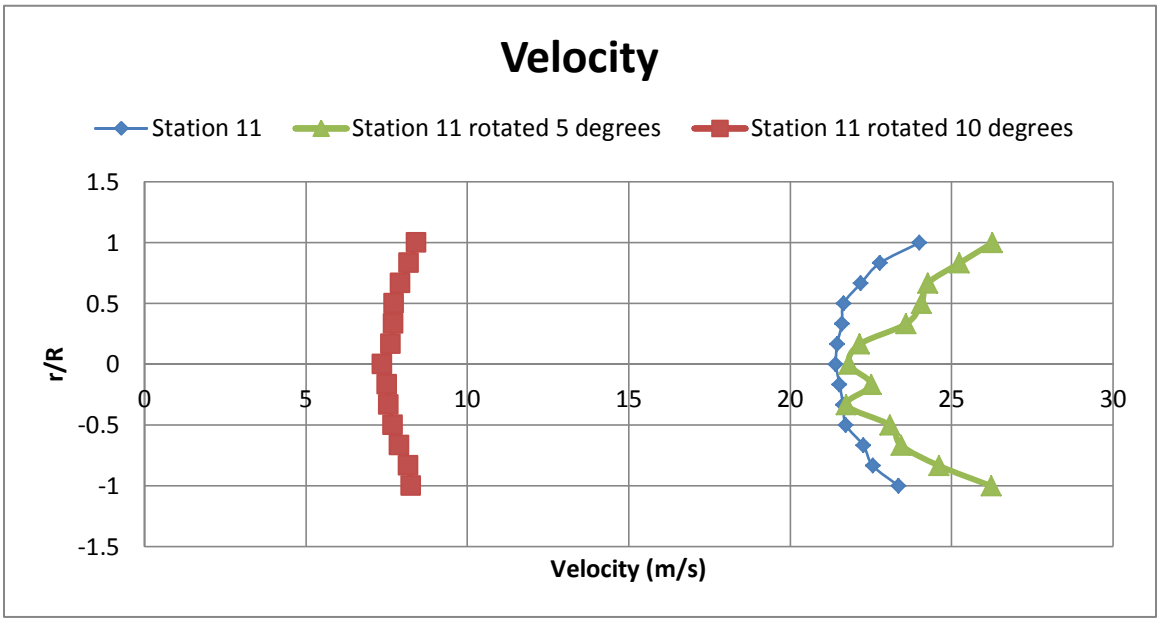

Figure 53. Model Three Velocity Profile with Alternate Flow Angles.

After the success of model three at a flow angle of 5 degrees, the pressure distribution was taken in this orientation with the use of a screen. Figure 54 illustrates that the screen eliminates all the benefits of the changing duct diameter. The measured velocity is maintained at approximately 12 m/s throughout the duct. As seen previously in Figure 49, the velocity is significantly lower in the middle of the duct.

Model 3 and supporting PVC pipe has an approximate cross sectional area of 0.0069 square meters. When compared with the tunnel test section of 0.209 square meters, the model effected a 3.3% blockage of the test section area. This is within acceptable values and precludes the need for corrections.

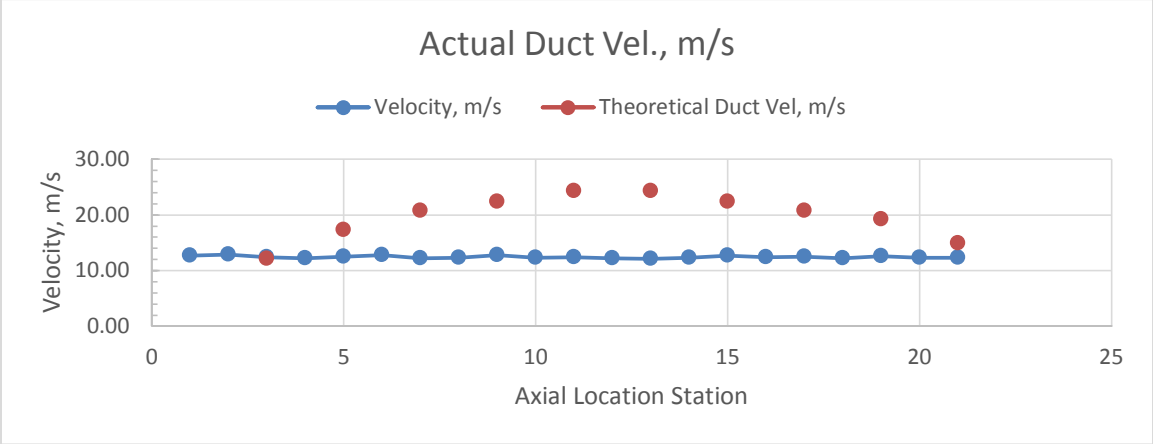

Figure 54. Model Three with Screen Duct Velocity with Five Degree Offset.

E. MODEL 4

As previously discussed, model four is a replication of a design already in production. This model did not have pressure taps and was only tested using the 5-hole probe.

This model was observed under varying conditions. To establish a baseline, the small turbine was removed and the velocity profile was taken on the duct itself. The results in Figure 55 show that in just this 5.08 cm (2 inch) duct, the velocity increased from 14 m/s to an average of 18 m/s. Reiterating that turbine power is proportional to the cube of velocity, this substantial increase could produce incredible power output results.

The turbine was then added to the duct and the velocity profile at the exit was measured. Exit velocity was reduced to an average of 3 m/s. This test was repeated 5 times with similar results. The reduction in velocity when the turbine

was added indicates that the turbine has excellent efficiency in transferring the velocity of the wind into rotational energy.

A screen was then added to the duct and the velocity profile was measured again. The pressure drop across the screen was so great, that the turbine would not spin freely. Wind tunnel velocity was then increased incrementally until the turbine would spin. The wind tunnel speed was increased to 30 m/s without any success. Greater speeds were not attempted due to safety concerned with the fragility of the duct and turbine.

The wind tunnel speed was then reduced back to the baseline 14 m/s and the turbine was started manually by removing the wind tunnel viewing window and engaging it by hand. After attempting this multiple times, efforts were abandoned as the turbine would continually stop on its own. The velocity profile was then taken with the screen installed and the turbine removed. As seen in Figure 55, the velocity profile with the screen is similar to that taken with the turbine engaged explaining why the turbine would not spin.

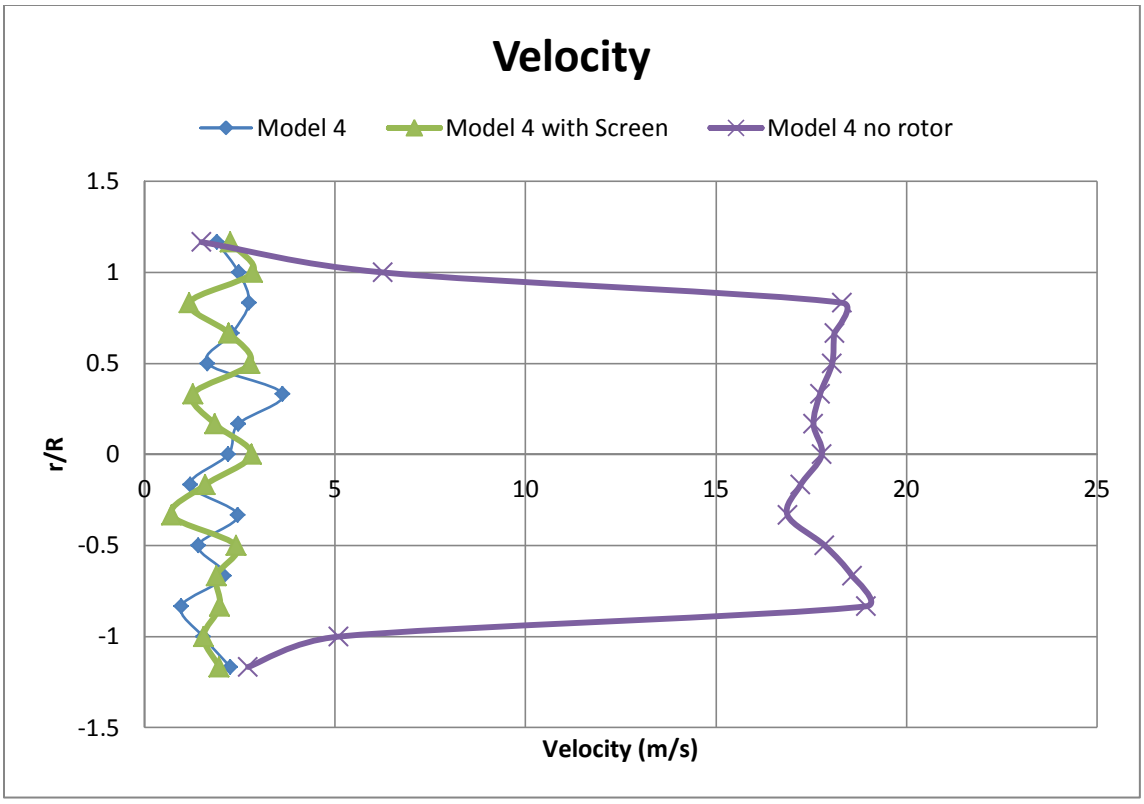

Figure 55. Model 4 Velocity Profiles.

Over 250 sets of data were taken during approximately five cumulative hours of wind tunnel operations. Much of this data was repetitive and offered similar findings. The key results were presented and analyzed in this section. These results will be reiterated and expanded upon in the conclusion and recommendations will be made for future model designs to be tested to include attributes of the current models which can be expanded upon and incorporated into the improved designs.

V. CONCLUSION

This study explored in detail the possible benefits and limitations of various duct shapes in an attempt to solve the problem of radar interference of wind turbines. From an economic perspective, the concept of a shroud which reduces radar cross section can only be beneficial if it also improves wind turbine performance. The main results and interpretations of the efficiency of each design are examined. Each model's surface static pressures were measured in an array of circumstances including flow angle alterations wind tunnel speed and the use of screens. Flow visualization techniques in using both oil and tufts were used to gain a visual verification of measured results. Velocity and flow angle measurements were obtained with an Aeroprobe 5-hole probe to provide a more complete picture of duct effects on air flow

A. MODEL ONE

When model one was mounted in the converging orientation, higher velocities were attained. The design, however, is flawed. The angle at which the duct is constructed does not follow basic fluid dynamic principles. This led to flow separation where the duct abruptly changed from a 36.9-degree angle to a straight duct. This flow separation causes turbulent flow which is very undesirable for wind turbine performance.

The 36.9-degree duct angle also prevented any noticeable gain when model one was mounted in the diverging orientation. The flow experienced a two-dimensional stall and no noticeable advantages were gained from the diverging area of the duct.

B. MODEL TWO

The rear mounted flange showed surprisingly positive effects. This design was very effective in increasing the velocity through the duct. While the formation of downstream vortices is implied by the results, further tests utilizing a water

tunnel would be beneficial in verifying this hypothesis. While blockage could account for an increase in velocity, this theory was ruled out when similar results were obtained with the test section windows removed.

This duct maintains similar flaws to model one. The abrupt entrance has a negative effect on air flow. A modification to this design could employ the use of a bell mouth to eliminate this flaw.

C. MODEL THREE

Model three was the most promising of the ducts. Flow was gradually accelerated through the duct to the centerline by the converging shape. By utilizing a hyperbolic shape as opposed to the straight angle in model one, no flow separation occurred and the centerline maintained laminar flow.

Similarly, on the aft end of the duct, flow was gradually decelerated in the diverging section. However, a similar result to model one was obtained when the angle of the diverging section became too great.

While this model did show promising results, it possesses perhaps the greatest flaw. The size of this duct is unrealistic for any real life application. At 25.4 cm (10 inches) long, the length is 1.66 times the interior diameter and subsequently, the turbine diameter. To put this in perspective, a 1.5 MW GE wind turbine has 35.36 m (116 feet) turbine blades. This would result in a duct that is 117.348 m (385 feet) long. The economics and structural requirements that would be associated with a duct this size is simply not practical.

D. MODEL FOUR

Model four is a recreation of the Wind Lens discussed earlier. The benefits have been documented in previous studies and verified here. The increase in velocity in proportion to the shortness of the duct far exceeds the other models. This duct however, was only designed to increase turbine power output with no thought on RCS reduction.

E. FUTURE STUDIES

Future studies should employ the attributes of the ducts in this study which showed promising results: specifically, the exit flange of model two and the converging-diverging design of model three. Most importantly, to reduce the size of any potential shroud, focus should be mainly placed on screen design. This study very clearly noted the significant drop in performance when an inadequate screen was utilized. However, given the necessary dimensions of a RCS reducing shroud without the use of a screen, I do not believe a practical solution will exist without one.

F. APPLICATION TO THE NAVY

Given the mandate by the Secretary of Defense and follow-on direction from the Secretary of the Navy, the continued employment of renewable energy is in the Navy's best interest and, antecedently, in the country's best interest. The failure to find a solution to this issue will deny the Navy the ability to construct new wind power facilities and harness one of nature's most abundant natural energy resources.

THIS PAGE INTENTIONALLY LEFT BLANK

APPENDIX

Table 1. Model One Converging Station Pressures.

Hole index	station	DP	STD DEV	Hole index	station	DP	STD DEV
P0		0.017407	0.001022	90-1	1	0.019656	0.000867
P		-0.000007	0.001158	90-2	2	0.015387	0.001164
5HP 1		0.020413	0.001192	90-3	3	0.010258	0.000894
5HP 2		-0.003495	0.000901	90-4	4	0.000819	0.001119
5HP 3		-0.001716	0.001305	90-5	5	-0.021276	0.001211
5HP 4		-0.000532	0.000942	90-6	6	-0.041314	0.002934
5HP 5		-0.003012	0.001231	90-7	7	-0.021814	0.001663
270-1	2	0.01429	0.00102	90-8	8	-0.018603	0.001226
270-2	4	0.000628	0.001167	90-9	9	-0.017859	0.001219
270-3	6	-0.040987	0.003255	90-10	10	-0.01887	0.001423
270-4	8	-0.020007	0.001443	90-11	11	-0.017345	0.001259
270-5	10	-0.019464	0.001343	90-12	12	-0.018025	0.001392
270-6	12	-0.021356	0.001718	135-1	2	0.014934	0.001008
315-1	2	0.015203	0.000945	135-2	4	0.000559	0.000839
315-2	4	0.001466	0.001052	135-3	6	-0.043945	0.003641
315-3	6	-0.042498	0.003705	135-4	8	-0.019111	0.001425
315-4	8	-0.019773	0.001373	135-5	10	-0.017812	0.001084
315-5	10	-0.019833	0.001242	135-6	12	-0.01876	0.001415
315-6	12	-0.020483	0.001296	180-1	2	0.015248	0.000902
0-1	2	0.015446	0.001066	180-2	4	0.001593	0.001148
0-2	4	0.001274	0.000864	180-3	6	-0.044063	0.003266
0-3	6	-0.040526	0.004056	180-4	8	-0.018318	0.001763
0-4	8	-0.018842	0.001668	180-5	10	-0.018298	0.00145
0-5	10	-0.018602	0.001378	180-6	12	-0.019723	0.001556
0-6	12	-0.01957	0.001462	225-1	2	0.01492	0.001094
45-1	2	0.015958	0.000889	225-2	4	0.001438	0.00089
45-2	4	0.001935	0.001131	225-3	6	-0.044192	0.003446
45-3	6	-0.038623	0.003467	225-4	8	-0.019588	0.001596
45-4	8	-0.018795	0.001378	225-5	10	-0.018641	0.001676
45-5	10	-0.018267	0.001163	225-6	12	-0.021244	0.001654
45-6	12	-0.018211	0.001326				

Table 2. Model One Converging Exit Profile (5HP).

y	P1	P2	P3	P4	P5
-3	0.006126	-0.00792	-0.0063	-0.0088	-0.00548
-2.5	0.015416	-0.00385	-0.00141	-0.0035	-0.0023
-2	0.015244	-0.003	-0.00139	-0.00308	-0.00177
-1.5	0.015529	-0.00259	-0.00062	-0.00227	-0.00159
-1	0.015422	-0.00224	-0.00051	-0.00178	-0.00158
-0.5	0.015529	-0.00203	-0.00073	-0.00168	-0.00156
0	0.015385	-0.00264	-0.001	-0.00039	-0.00244
0.5	0.015705	-0.00193	-0.00074	-0.00129	-0.00208
1	0.015757	-0.00211	-0.00094	-0.00124	-0.00239
1.5	0.015442	-0.00228	-0.00112	-0.00138	-0.00255
2	0.015566	-0.00226	-0.00113	-0.00166	-0.00279
2.5	0.0155	-0.00272	-0.00151	-0.0016	-0.00274
3	0.001794	-0.00717	-0.00649	-0.00534	-0.00599

Table 3. Model One Converging Transition Profile (5HP).

y	P1	P2	P3	P4	P5
-3	0.010467	-0.01945	-0.01962	-0.02689	0.004878
-2.5	0.01432	-0.00538	-0.00494	-0.01095	0.005421
-2	0.015431	-0.00046	-0.00012	-0.00417	0.004336
-1.5	0.015344	0.001239	0.001727	-0.00087	0.003794
-1	0.01528	0.001853	0.002703	0.000919	0.003454
-0.5	0.015552	0.002216	0.003208	0.002216	0.002366
0	0.01523	0.002344	0.003143	0.003263	0.00153
0.5	0.015408	0.002249	0.002899	0.004195	0.000435
1	0.015026	0.001827	0.002552	0.004734	-0.00052
1.5	0.015376	0.000739	0.001336	0.005572	-0.00262
2	0.015115	-0.0009	-0.00068	0.006287	-0.00589
2.5	0.014168	-0.00525	-0.00536	0.006874	-0.01162
3	0.010753	-0.01877	-0.01955	0.007904	-0.0264

Table 4. Model One Converging Entrance Velocity Profile (5HP).

y	P1	P2	P3	P4	P5
-3.00	0.015118	0.010345	0.011069	0.012545	0.008626
-2.50	0.015173	0.009863	0.010433	0.012143	0.007699
-2.00	0.015349	0.009049	0.009617	0.011175	0.007083
-1.50	0.015313	0.008644	0.009451	0.010216	0.006839
-1.00	0.015113	0.008282	0.009282	0.00957	0.006778
-0.5	0.015081	0.008179	0.008796	0.009173	0.007029
0.00	0.015539	0.008606	0.008656	0.008703	0.007546
0.50	0.015228	0.008122	0.008928	0.008387	0.008201
1.00	0.015213	0.00864	0.009326	0.007861	0.008621
1.50	0.015566	0.008964	0.009545	0.008003	0.00956
2.00	0.015329	0.009727	0.010225	0.008337	0.010691
2.50	0.015234	0.010306	0.011178	0.009008	0.011984
3.00	0.015614	0.01139	0.01196	0.009743	0.012843

Table 5. Model One Diverging Station Pressures.

Hole index	Station	DP	STD DEV	Hole index	Station	DP	STD DEV
P0		0.017621	0.000871	90-1	12	-0.019886	0.001783
P		0.000291	0.001321	90-2	11	-0.019571	0.001787
5HP 1		0.021935	0.000918	90-3	10	-0.019593	0.002297
5HP 2		-0.00506	0.001019	90-4	9	-0.020122	0.002252
5HP 3		0.000122	0.00136	90-5	8	-0.019616	0.002314
5HP 4		-0.0016	0.001148	90-6	7	-0.02053	0.001971
5HP 5		-0.00318	0.001034	90-7	6	-0.020781	0.001981
270-1	11	-0.02168	0.002788	90-8	5	-0.018979	0.002091
270-2	9	-0.02107	0.003442	90-9	4	-0.019487	0.002692
270-3	7	-0.02118	0.004085	90-10	3	-0.025955	0.003264
270-4	5	-0.02642	0.005697	90-11	2	-0.038627	0.003512
270-5	3	-0.04146	0.004658	90-12	1	-0.050041	0.002621
270-6	1	-0.04574	0.002628	135-1	11	-0.020072	0.002006
315-1	11	-0.01969	0.00251	135-2	9	-0.020602	0.002409
315-2	9	-0.01854	0.002755	135-3	7	-0.020891	0.00235
315-3	7	-0.02047	0.002177	135-4	5	-0.019948	0.002046
315-4	5	-0.02192	0.002814	135-5	3	-0.024539	0.002774
315-5	3	-0.03564	0.003718	135-6	1	-0.052251	0.002848
315-6	1	-0.05002	0.002484	180-1	11	-0.02007	0.002134
0-1	11	-0.01963	0.002127	180-2	9	-0.019996	0.002397
0-2	9	-0.02048	0.002405	180-3	7	-0.020869	0.002381
0-3	7	-0.02088	0.002244	180-4	5	-0.020447	0.002965
0-4	5	-0.01975	0.002474	180-5	3	-0.031189	0.004376
0-5	3	-0.02726	0.003812	180-6	1	-0.050996	0.003041
0-6	1	-0.05162	0.003018	225-1	11	-0.019498	0.003351
45-1	11	-0.01948	0.001797	225-2	9	-0.019019	0.003524
45-2	9	-0.01962	0.002695	225-3	7	-0.020254	0.003656
45-3	7	-0.02034	0.00226	225-4	5	-0.023514	0.004303
45-4	5	-0.01924	0.002337	225-5	3	-0.038059	0.003914
45-5	3	-0.02486	0.003899	225-6	1	-0.048514	0.002425
45-6	1	-0.05085	0.002705				

Table 6. Model One Diverging Exit Profile (5HP).

y	P1	P2	P3	P4	P5
-4.5	-0.00877	-0.01617	-0.01513	-0.01339	-0.01613
-4	-0.01707	-0.01649	-0.01553	-0.01684	-0.01645
-3.5	-0.01499	-0.0157	-0.01482	-0.01711	-0.0142
-3	-0.0048	-0.01193	-0.0105	-0.01491	-0.00967
-2.5	0.008841	-0.00689	-0.00416	-0.00799	-0.00427
-2	0.016033	-0.00397	-0.00013	-0.0029	-0.00146
-1.5	0.01637	-0.00336	0.000496	-0.00206	-0.00136
-1	0.01646	-0.00347	0.00075	-0.00136	-0.00139
-0.5	0.016599	-0.00353	0.000858	-0.00103	-0.00194
0	0.01652	-0.00339	0.000488	-0.00076	-0.00274
0.5	0.01661	-0.00337	0.000596	-0.00058	-0.00254
1	0.016682	-0.00343	0.000265	-0.00049	-0.00271
1.5	0.016626	-0.00354	0.000033	-0.00042	-0.00331
2	0.016551	-0.00378	-0.00038	-0.00034	-0.00363
2.5	0.014895	-0.00484	-0.00142	-0.00118	-0.00568
3	-0.0056	-0.0123	-0.01055	-0.00954	-0.01409
3.5	-0.0161	-0.01568	-0.01458	-0.01571	-0.01588
4	-0.01589	-0.01562	-0.01461	-0.0157	-0.01546
4.5	-0.01573	-0.01542	-0.01429	-0.01573	-0.01547

Table 7. Model One Diverging Transition Profile (5HP).

y	P1	P2	P3	P4	P5
-3	-0.0079	-0.01279	-0.01151	-0.01247	-0.01228
-2.5	-0.00636	-0.00762	-0.00421	-0.01104	-0.00414
-2	-0.00575	-0.00431	-4.4E-05	-0.01079	-0.0023
-1.5	-0.0017	-0.00428	-2E-06	-0.00668	-0.00262
-1	-0.00043	-0.00422	0.000267	-0.00582	-0.00272
-0.5	-0.00013	-0.00395	0.000361	-0.00527	-0.0028
0.5	0.001161	-0.00409	0.000251	-0.00448	-0.00335
1	0.000924	-0.0038	0.000384	-0.00457	-0.00333
1.5	0.003021	-0.00387	0.000206	-0.00238	-0.00329
2	0.003193	-0.00388	0.000254	-0.00211	-0.00323
2.5	0.003561	-0.00424	-0.0004	-0.00133	-0.00466
3	0.003573	-0.01018	-0.00728	-0.00104	-0.01224

Table 8. Model One Diverging Entrance Profile (5HP).

y	P1	P2	P3	P4	P5
-3	0.00377	-0.02945	-0.02685	0.013094	-0.03118
-2.5	0.011511	-0.01254	-0.01002	0.009847	-0.01819
-2	0.013524	-0.00598	-0.00425	0.006074	-0.0117
-1.5	0.014245	-0.00365	-0.00217	0.004087	-0.00828
-1	0.014547	-0.00231	-0.00109	0.002594	-0.00631
-0.5	0.014909	-0.00159	-0.00057	0.001598	-0.00434
0	0.015047	-0.00169	-0.00029	0.000639	-0.00305
0.5	0.01484	-0.00095	-0.00029	0.000071	-0.00229
1	0.015165	-0.00106	-0.00051	-0.00115	-0.00139
1.5	0.015219	-0.00137	-0.00129	-0.00284	-0.00016
2	0.015117	-0.00165	-0.00267	-0.00507	0.00096
2.5	0.014722	-0.00365	-0.00586	-0.01084	0.004188
3	0.004434	-0.01871	-0.02655	-0.0242	0.010178

Table 9. Model One Diverging with Screen Station Pressures.

Hole index	Station	DP	STD DEV	Hole index	Station	DP	STD DEV
P0		0.009221	0.001349	90-1	12	-0.01062	0.001267
P		0.000511	0.001064	90-2	11	-0.0106	0.000874
5HP 1		-0.007094	0.000998	90-3	10	-0.011162	0.001132
5HP 2		-0.009577	0.000953	90-4	9	-0.010888	0.001069
5HP 3		-0.00868	0.001256	90-5	8	-0.010698	0.000934
5HP 4		-0.009384	0.000808	90-6	7	-0.010539	0.001137
5HP 5		-0.009808	0.000894	90-7	6	-0.009822	0.000873
270-1	11	-0.011832	0.000954	90-8	5	-0.009483	0.000944
270-2	9	-0.010935	0.001225	90-9	4	-0.009327	0.001151
270-3	7	-0.010881	0.000805	90-10	3	-0.009566	0.001212
270-4	5	-0.009755	0.001105	90-11	2	-0.00952	0.000975
270-5	3	-0.009624	0.00113	90-12	1	-0.008359	0.001126
270-6	1	-0.017881	0.001226	135-1	11	-0.011771	0.000882
315-1	11	-0.010777	0.001186	135-2	9	-0.011462	0.001136
315-2	9	-0.0109	0.001339	135-3	7	-0.01063	0.000996
315-3	7	-0.010703	0.001054	135-4	5	-0.009217	0.000964
315-4	5	-0.010049	0.000832	135-5	3	-0.010165	0.001061
315-5	3	-0.0099	0.000817	135-6	1	-0.0091	0.001118
315-6	1	-0.012241	0.001109	180-1	11	-0.011144	0.001019
0-1	11	-0.011595	0.000941	180-2	9	-0.011092	0.001134
0-2	9	-0.011166	0.000885	180-3	7	-0.009806	0.000671
0-3	7	-0.010212	0.001157	180-4	5	-0.009549	0.001045
0-4	5	-0.010025	0.000974	180-5	3	-0.01072	0.001218
0-5	3	-0.010213	0.001023	180-6	1	-0.010549	0.001226
0-6	1	-0.010715	0.001261	225-1	11	-0.010889	0.000899
45-1	11	-0.011065	0.000973	225-2	9	-0.011199	0.000908
45-2	9	-0.010671	0.001355	225-3	7	-0.010505	0.000987
45-3	7	-0.010376	0.000998	225-4	5	-0.010127	0.001163
45-4	5	-0.009645	0.000876	225-5	3	-0.009994	0.000869
45-5	3	-0.009543	0.001073	225-6	1	-0.014555	0.001651
45-6	1	-0.00928	0.001199				

Table 10. Model One Diverging with Screen Exit Profile (5HP).

y	P1	P2	P3	P4	P5
5.5	0.002679	-0.004571	-0.004322	-0.001935	-0.005981
5	-0.009442	-0.010065	-0.009582	-0.011012	-0.009396
4.5	-0.010473	-0.010346	-0.010468	-0.010128	-0.010562
4	-0.009686	-0.011003	-0.010018	-0.009091	-0.011051
3.5	-0.008473	-0.010809	-0.009529	-0.008541	-0.011254
3	-0.008195	-0.010969	-0.009298	-0.008187	-0.011192
2.5	-0.00749	-0.010505	-0.009243	-0.007699	-0.011524
2	-0.006969	-0.010219	-0.008891	-0.008174	-0.010859
1.5	-0.007048	-0.009813	-0.008814	-0.008547	-0.010198
1	-0.006936	-0.009885	-0.008737	-0.009051	-0.010029
0.5	-0.007541	-0.010063	-0.009169	-0.009248	-0.010188
0	-0.007273	-0.009653	-0.009099	-0.009611	-0.009702
-0.5	-0.006959	-0.009446	-0.008507	-0.009633	-0.009383
-1	-0.007201	-0.009281	-0.008456	-0.010124	-0.00912
-1.5	-0.007255	-0.009338	-0.008971	-0.010419	-0.008587
-2	-0.007713	-0.009432	-0.009329	-0.010784	-0.008612
-2.5	-0.007345	-0.010156	-0.009208	-0.010625	-0.008133
-3	-0.007856	-0.009835	-0.00975	-0.011166	-0.008609
-3.5	-0.007903	-0.010158	-0.009786	-0.011023	-0.007894
-4	-0.009842	-0.010268	-0.010205	-0.010795	-0.009295
-4.5	-0.010653	-0.010489	-0.010244	-0.010725	-0.010518
-5	-0.011552	-0.010931	-0.011106	-0.011026	-0.011529
-5.5	-0.002205	-0.006407	-0.007365	-0.009736	-0.004314

Table 11. Model One Diverging with Screen Entrance Profile (5HP).

y	P1	P2	P3	P4	P5
-3	0.001752	-0.00714	-0.00611	-0.00923	-0.00672
-2.5	-0.00092	-0.00895	-0.00727	-0.00773	-0.00889
-2	-0.00143	-0.00881	-0.00707	-0.00726	-0.00953
-1.5	-0.00243	-0.00886	-0.0072	-0.00738	-0.00912
-1	-0.00047	-0.00786	-0.00682	-0.00646	-0.00861
-0.5	-0.00145	-0.00781	-0.00703	-0.00724	-0.00887
0	-0.00036	-0.00757	-0.00678	-0.00642	-0.00868
0.5	-0.0015	-0.00837	-0.00692	-0.00708	-0.00845
1	-0.00149	-0.00799	-0.00674	-0.00755	-0.00816
1.5	-0.00177	-0.00742	-0.00717	-0.00711	-0.00835
2	-0.00108	-0.00755	-0.00665	-0.00681	-0.00784
2.5	0.000429	-0.0063	-0.00619	-0.00689	-0.00667
3	0.001697	-0.00675	-0.00498	-0.00577	-0.00629

Table 12. Model One Diverging 5 Degree Yaw Station Pressures.

Hole index	Station	DP	STD DEV	Hole index	Station	DP	STD DEV
P0		0.01231	0.000871	90-1	12	-0.000236	0.001783
P		0.000388	0.001321	90-2	11	-0.000222	0.001787
5HP 1		0.014635	0.000918	90-3	10	0.000064	0.002297
5HP 2		0.002366	0.001019	90-4	9	-0.000532	0.002252
5HP 3		-0.007047	0.00136	90-5	8	-0.00017	0.002314
5HP 4		-0.003241	0.001148	90-6	7	-0.000324	0.001971
5HP 5		-0.00398	0.001034	90-7	6	-0.000828	0.001981
270-1	11	-0.001463	0.002788	90-8	5	-0.000529	0.002091
270-2	9	-0.000566	0.003442	90-9	4	-0.000008	0.002692
270-3	7	-0.001202	0.004085	90-10	3	-0.000781	0.003264
270-4	5	-0.000592	0.005697	90-11	2	-0.000302	0.003512
270-5	3	-0.000318	0.004658	90-12	1	-0.000621	0.002621
270-6	1	-0.001303	0.002628	135-1	11	-0.000343	0.002006
315-1	11	0.000167	0.00251	135-2	9	-0.001585	0.002409
315-2	9	-0.000632	0.002755	135-3	7	-0.000874	0.00235
315-3	7	-0.00119	0.002177	135-4	5	-0.000494	0.002046
315-4	5	-0.000883	0.002814	135-5	3	0.00014	0.002774
315-5	3	-0.001335	0.003718	135-6	1	-0.001454	0.002848
315-6	1	-0.000404	0.002484	180-1	11	-0.000249	0.002134
0-1	11	0.000039	0.002127	180-2	9	-0.000154	0.002397
0-2	9	-0.00102	0.002405	180-3	7	-0.001131	0.002381
0-3	7	-0.00053	0.002244	180-4	5	-0.000284	0.002965
0-4	5	0.000095	0.002474	180-5	3	-0.000206	0.004376
0-5	3	-0.000301	0.003812	180-6	1	-0.001407	0.003041
0-6	1	-0.001236	0.003018	225-1	11	-0.000458	0.003351
45-1	11	0.000087	0.001797	225-2	9	0.000082	0.003524
45-2	9	0.000172	0.002695	225-3	7	-0.000733	0.003656
45-3	7	-0.000313	0.00226	225-4	5	-0.000793	0.004303
45-4	5	0.000065	0.002337	225-5	3	-0.000266	0.003914
45-5	3	-0.000661	0.003899	225-6	1	-0.000329	0.002425
45-6	1	-0.000719	0.002705				

Table 13. Model One Diverging 5 Degree Yaw Exit Profile (5HP).

y	P1	P2	P3	P4	P5
3	0.008931	-0.000121	-0.010651	-0.005775	-0.007355
2.5	0.014684	0.001738	-0.007753	-0.00287	-0.004401
2	0.014554	0.001391	-0.007075	-0.003122	-0.004267
1.5	0.014533	0.001959	-0.006666	-0.003352	-0.004182
1	0.014755	0.001215	-0.006857	-0.002598	-0.00424
0.5	0.014816	0.001402	-0.007016	-0.002929	-0.003818
0	0.01458	0.001134	-0.007158	-0.003294	-0.004015
-0.5	0.014966	0.000733	-0.00636	-0.00371	-0.003909
-1	0.014178	0.000603	-0.006376	-0.004006	-0.00341
-1.5	0.01444	0.000358	-0.006726	-0.004379	-0.003288
-2	0.014528	0.001005	-0.007294	-0.005235	-0.002769
-2.5	0.01461	0.001526	-0.008245	-0.006441	-0.002645
-3	0.003676	-0.000519	-0.014403	-0.011541	-0.007149

Table 14. Model Two Station Pressures.

Hole index	Station	DP	STD DEV	Hole index	Station	DP	STD DEV
P0		0.016346	0.000886	90-1	1	-0.051463	0.001219
P		-0.000439	0.00099	90-2	2	-0.044494	0.001528
5HP 1		0.033975	0.000843	90-3	3	-0.031727	0.001768
5HP 2		-0.005396	0.001127	90-4	4	-0.023713	0.00124
5HP 3		-0.007445	0.001184	90-5	5	-0.022434	0.001028
5HP 4		0.031583	0.001225	90-6	6	-0.022283	0.001221
5HP 5		-0.007566	0.001028	90-7	7	-0.022536	0.001054
270-1	2	-0.047132	0.001518	90-8	8	-0.022131	0.001121
270-2	4	-0.033784	0.002077	90-9	9	-0.022348	0.001182
270-3	6	-0.023029	0.001907	90-10	10	-0.022864	0.001137
270-4	8	-0.022443	0.001122	90-11	11	-0.021944	0.001176
270-5	10	-0.022947	0.001241	135-1	2	-0.046933	0.001461
315-1	2	-0.035698	0.001509	135-2	4	-0.027108	0.00152
315-2	4	-0.025654	0.001533	135-3	6	-0.022187	0.001286
315-3	6	-0.02316	0.001378	135-4	8	-0.024594	0.00089
315-4	8	-0.021544	0.001047	135-5	10	-0.023109	0.000965
315-5	10	-0.022944	0.00112	180-1	2	-0.04811	0.001211
0-1	2	-0.042417	0.001727	180-2	4	-0.03067	0.001616
0-2	4	-0.022031	0.000979	180-3	6	-0.022674	0.00146
0-3	6	-0.022142	0.001166	180-4	8	-0.022251	0.001082
0-4	8	-0.022353	0.001261	180-5	10	-0.022909	0.001217
0-5	10	-0.021784	0.000875	225-1	2	-0.0401	0.001316
45-1	2	-0.042273	0.001681	225-2	4	-0.033725	0.001947
45-2	4	-0.022219	0.001266	225-3	6	-0.024317	0.001536
45-3	6	-0.023182	0.001036	225-4	8	-0.022284	0.001324
45-4	8	-0.022659	0.001046	225-5	10	-0.024376	0.001191
45-5	10	-0.022667	0.001109				

Table 15. Model Two Exit Profile (5HP).

y	P1	P2	P3	P4	P5
-5	-0.00996	-0.00796	-0.00955	-0.01183	-0.0072
-3.5	-0.01291	-0.01226	-0.01286	-0.01045	-0.01319
-4	-0.01358	-0.01288	-0.01319	-0.01311	-0.01236
-2.5	-0.00357	-0.00973	-0.00994	-0.01294	-0.00445
-3	0.013528	-0.00236	-0.00202	-0.00616	0.002312
-1.5	0.01409	-0.00173	-0.00106	-0.00464	0.00227
-2	0.014275	-0.00141	-0.0014	-0.00438	0.001959
-0.5	0.01442	-0.00153	-0.00124	-0.00413	0.001274
-1	0.014477	-0.00138	-0.00076	-0.00336	0.000666
0.5	0.014255	-0.00113	-0.00101	-0.00281	-0.00024
0	0.014162	-0.0009	-0.00073	-0.00247	-1.7E-05
-0.5	0.014415	-0.00069	-0.00047	-0.00164	-0.00066
1	0.014317	-0.00057	-0.0003	-0.00113	-0.00124
0.5	0.014498	-0.00019	-0.00038	-0.0003	-0.00126
2	0.013972	-0.00049	0.000163	0.000196	-0.00182
1.5	0.014209	-0.00067	-0.00019	0.000446	-0.00198
3	0.007429	-0.00441	-0.00323	-0.00092	-0.00688
2.5	-0.01015	-0.00998	-0.00967	-0.00941	-0.01086
4	-0.01087	-0.0104	-0.01042	-0.01063	-0.01017
3.5	-0.01085	-0.01038	-0.01045	-0.01132	-0.00986
5	-0.01054	-0.01012	-0.0109	-0.01222	-0.01011

Table 16. Model Two Entrance Profile (5HP).

y	P1	P2	P3	P4	P5
-3	0.056635	-0.01146	-0.01224	-0.01548	-0.01064
-2.5	0.056467	-0.00772	-0.00964	-0.01058	-0.00802
-2	0.054986	-0.00474	-0.00555	-0.00665	-0.00527
-1.5	0.0542	-0.00415	-0.00552	-0.00602	-0.00536
-1	0.052729	-0.00409	-0.00555	-0.00598	-0.00524
-0.5	0.05258	-0.00399	-0.00543	-0.00571	-0.00543
0.5	0.049689	-0.00397	-0.00548	-0.00554	-0.00578
1	0.050475	-0.00396	-0.0055	-0.0053	-0.00578
1.5	0.051384	-0.00414	-0.00552	-0.00536	-0.00587
2	0.051469	-0.00428	-0.00549	-0.00544	-0.00584
2.5	0.052617	-0.00593	-0.00741	-0.00608	-0.00818
3	0.052716	-0.01056	-0.01158	-0.00875	-0.01567

Table 17. Model Three Station Pressures.

Hole index	Station	DP	STD DEV	Hole index	Station	DP	STD DEV
P0		0.01732	0.000773	0-1	2	0.008739	0.000973
P		-0.000337	0.000906	0-2	4	-0.016286	0.001068
5HP 1		0.019936	0.001059	0-3	6	-0.036146	0.001174
5HP 2		-0.014662	0.000973	0-4	8	-0.052383	0.00113
5HP 3		-0.01246	0.001208	0-5	10	-0.067986	0.001163
5HP 4		-0.009234	0.0012	0-6	12	-0.064314	0.001498
5HP 5		-0.017316	0.000821	0-7	14	-0.057119	0.001267
270-1	2	0.005896	0.001136	0-8	16	-0.055901	0.001503
270-2	4	-0.017801	0.000941	0-9	18	-0.026063	0.001387
270-3	6	-0.0391	0.000949	0-10	20	-0.01338	0.001633
270-4	8	-0.053577	0.001241	135-1	2	0.004346	0.001243
270-5	10	-0.066777	0.001259	135-2	4	-0.016555	0.001054
270-6	12	-0.065426	0.001129	135-3	6	-0.036236	0.001035
270-7	14	-0.059893	0.001405	135-4	8	-0.055123	0.001384
270-8	16	-0.057948	0.00152	135-5	10	-0.066639	0.001218
270-9	18	-0.025138	0.002362	135-6	12	-0.063638	0.000905
270-10	20	-0.014986	0.00163	135-7	14	-0.057904	0.001364
225-1	2	0.004863	0.001062	135-8	16	-0.051273	0.002209
225-2	4	-0.018362	0.000962	135-9	18	-0.020038	0.001964
225-3	6	-0.038589	0.001146	135-10	20	-0.012369	0.001313
225-4	8	-0.052742	0.00099	45-1	2	-0.002907	0.00088
225-5	10	-0.067108	0.001257	45-2	4	0.007909	0.00093
225-6	12	-0.065186	0.001264	45-3	6	-0.013565	0.000806
225-7	14	-0.059859	0.001353	45-4	8	-0.036105	0.000927
225-8	16	-0.055617	0.0012	45-5	10	-0.052943	0.001286
225-9	18	-0.031799	0.001795	45-6	12	-0.067445	0.001017
225-10	20	-0.016353	0.00157	45-7	14	-0.062525	0.001215
315-1	2	0.007392	0.001045	45-8	16	-0.057941	0.001308
315-2	4	-0.017048	0.000959	45-9	18	-0.054973	0.001354
315-3	6	-0.040845	0.001056	45-10	20	-0.024379	0.00197
315-4	8	-0.053837	0.001065	90-1	1	-0.011622	0.001339
315-5	10	-0.067966	0.001299	90-2	2	0.017314	0.000897
315-6	12	-0.064646	0.001389	90-3	3	0.006222	0.001163
315-7	14	-0.060062	0.001201	90-4	4	-0.005425	0.001031
315-8	16	-0.056041	0.001198	90-5	5	-0.016531	0.001081
315-9	18	-0.028185	0.001581	90-6	6	-0.025903	0.001218
315-10	20	-0.015375	0.001591	90-7	7	-0.037202	0.001215
180-1	2	0.004325	0.000888	90-8	8	-0.045204	0.001225
180-2	4	-0.01759	0.001101	90-9	9	-0.050438	0.001505
180-3	6	-0.036864	0.001064	90-10	10	-0.059104	0.001267
180-4	8	-0.051896	0.001117	90-11	11	-0.066268	0.001146
180-5	10	-0.069676	0.001287	90-12	12	-0.066355	0.001187
180-6	12	-0.064642	0.001092	90-13	13	-0.063874	0.001214
180-7	14	-0.057425	0.001299	90-14	14	-0.060121	0.001126
180-8	16	-0.055978	0.001342	90-15	15	-0.056508	0.001421
180-9	18	-0.028014	0.001702	90-16	16	-0.055279	0.001263
180-10	20	-0.014491	0.001562	90-17	17	-0.053938	0.001357
				90-18	18	-0.03411	0.002415
				90-19	19	-0.021769	0.002079
				90-20	20	-0.014933	0.001397
				90-21	21	-0.012477	0.001606

Table 18. Model Three Station 11 Profile (5HP).

y	P1	P2	P3	P4	P5
3	0.014544	-0.016037	-0.010921	-0.013858	-0.01529
2.5	0.014301	-0.013729	-0.0085	-0.011203	-0.01278
2	0.014472	-0.012273	-0.007418	-0.009498	-0.011414
1.5	0.014374	-0.010995	-0.006615	-0.008446	-0.010488
1	0.014569	-0.010448	-0.006435	-0.008027	-0.009583
0.5	0.014338	-0.009724	-0.006179	-0.008018	-0.009235
0	0.014462	-0.009777	-0.005741	-0.008417	-0.008792
-0.5	0.014662	-0.01018	-0.005631	-0.008831	-0.008908
-1	0.014183	-0.010502	-0.006145	-0.009205	-0.008668
-1.5	0.014405	-0.010598	-0.00619	-0.010187	-0.009246
-2	0.014549	-0.011457	-0.007025	-0.010721	-0.009396
-2.5	0.01442	-0.012418	-0.008135	-0.011748	-0.010558
-3	0.014538	-0.014651	-0.009625	-0.013062	-0.012084

Table 19. Model three Station 16 Profile (5HP).

y	P1	P2	P3	P4	P5
3.5	-0.026733	-0.025647	-0.025321	-0.025203	-0.022207
3	0.014616	-0.013865	-0.00797	-0.016649	-0.004605
2.5	0.014338	-0.011185	-0.006047	-0.012118	-0.004877
2	0.014493	-0.009898	-0.004895	-0.011095	-0.005932
1.5	0.014338	-0.009274	-0.00459	-0.008904	-0.006297
1	0.014245	-0.008727	-0.004109	-0.008209	-0.006462
0.5	0.014312	-0.008887	-0.004479	-0.007654	-0.007229
0	0.014358	-0.008683	-0.003546	-0.006628	-0.007104
-0.5	0.014792	-0.008001	-0.004398	-0.006098	-0.007254
-1	0.014446	-0.008483	-0.004464	-0.005275	-0.008604
-1.5	0.014333	-0.00857	-0.004562	-0.004298	-0.009963
-2	0.014528	-0.009203	-0.004769	-0.004212	-0.010714
-2.5	0.014303	-0.010688	-0.006407	-0.003276	-0.013785
-3	0.012575	-0.015397	-0.009888	-0.001673	-0.02323
-3.5	-0.026897	-0.025243	-0.02586	-0.018219	-0.026148

Table 20. Model Three Exit Profile (5HP).

y	P1	P2	P3	P4	P5
5	-0.010535	-0.010122	-0.010899	-0.012218	-0.010109
4.5	-0.01085	-0.010379	-0.010445	-0.011315	-0.009857
4	-0.01087	-0.010395	-0.010417	-0.010625	-0.010172
3.5	-0.010153	-0.009975	-0.009669	-0.009406	-0.010858
3	0.007429	-0.004408	-0.003234	-0.000922	-0.006879
2.5	0.014209	-0.000669	-0.000185	0.000446	-0.001976
2	0.013972	-0.000486	0.000163	0.000196	-0.001817
1.5	0.014498	-0.000193	-0.000381	-0.000297	-0.001264
1	0.014317	-0.000566	-0.000303	-0.001128	-0.001243
0.5	0.014415	-0.00069	-0.000472	-0.001642	-0.000656
0	0.014162	-0.000897	-0.000728	-0.002465	-0.000017
-0.5	0.014255	-0.001129	-0.001006	-0.002812	-0.000235
-1	0.014477	-0.00138	-0.00076	-0.003357	0.000666
-1.5	0.01442	-0.001525	-0.001236	-0.004127	0.001274
-2	0.014275	-0.001414	-0.001399	-0.004378	0.001959
-2.5	0.01409	-0.001729	-0.001055	-0.004644	0.00227
-3	0.013528	-0.002362	-0.002016	-0.006163	0.002312
-3.5	-0.003565	-0.009725	-0.009943	-0.012935	-0.004449
-4	-0.01358	-0.012878	-0.013193	-0.013111	-0.012363
-4.5	-0.01291	-0.012259	-0.012855	-0.010448	-0.013187
-5	-0.009964	-0.007964	-0.009549	-0.011833	-0.007197

Table 21. Model Three with Screen Station Pressures.

Hole index	Station	DP	STD DEV	Hole index	Station	DP	STD DEV
P0		0.010467	0.000979	0-1	2	-0.003927	0.001012
P		0.00019	0.001207	0-2	4	-0.002902	0.001103
5HP 1		-0.000821	0.000966	0-3	6	-0.003	0.000974
5HP 2		-0.018052	0.001004	0-4	8	-0.003588	0.000977
5HP 3		-0.01719	0.000913	0-5	10	-0.002836	0.001051
5HP 4		-0.017949	0.001015	0-6	12	-0.003146	0.001095
5HP 5		-0.018109	0.000901	0-7	14	-0.004081	0.000764
270-1	2	-0.004245	0.001086	0-8	16	-0.003101	0.000862
270-2	4	-0.003008	0.000959	0-9	18	-0.003175	0.001136
270-3	6	-0.00381	0.000808	0-10	20	-0.003158	0.000849
270-4	8	-0.002977	0.001151	135-1	2	-0.00325	0.001006
270-5	10	-0.002898	0.001272	135-2	4	-0.002983	0.001216
270-6	12	-0.003625	0.000958	135-3	6	-0.00303	0.001057
270-7	14	-0.00233	0.001154	135-4	8	-0.00255	0.001172
270-8	16	-0.002934	0.001218	135-5	10	-0.003246	0.000983
270-9	18	-0.003745	0.001143	135-6	12	-0.003047	0.001436
270-10	20	-0.003564	0.001106	135-7	14	-0.003139	0.001099
225-1	2	-0.003999	0.000892	135-8	16	-0.004495	0.000966
225-2	4	-0.003284	0.001202	135-9	18	-0.00362	0.001136
225-3	6	-0.003055	0.001012	135-10	20	-0.004095	0.001035
225-4	8	-0.003171	0.00107	45-1	2	-0.003209	0.001058
225-5	10	-0.003926	0.000928	45-2	4	-0.004127	0.000876
225-6	12	-0.003102	0.001031	45-3	6	-0.0033	0.001012
225-7	14	-0.003097	0.001209	45-4	8	-0.004034	0.001036
225-8	16	-0.003967	0.001098	45-5	10	-0.0029	0.000873
225-9	18	-0.002799	0.001235	45-6	12	-0.002851	0.000966
225-10	20	-0.003159	0.000878	45-7	14	-0.003804	0.000967
315-1	2	-0.002976	0.000985	45-8	16	-0.002657	0.001081
315-2	4	-0.002523	0.000813	45-9	18	-0.003174	0.001308
315-3	6	-0.003005	0.001067	45-10	20	-0.003797	0.00125
315-4	8	-0.003351	0.00109	90-1	1	-0.003544	0.00091
315-5	10	-0.00318	0.001005	90-2	2	-0.004136	0.001058
315-6	12	-0.003283	0.000993	90-3	3	-0.003107	0.001143
315-7	14	-0.002907	0.000819	90-4	4	-0.003109	0.000971
315-8	16	-0.003321	0.000794	90-5	5	-0.003351	0.000713
315-9	18	-0.003067	0.001303	90-6	6	-0.00387	0.000952
315-10	20	-0.002965	0.000761	90-7	7	-0.00291	0.001069
180-1	2	-0.002954	0.00137	90-8	8	-0.003272	0.000958
180-2	4	-0.003036	0.000861	90-9	9	-0.003993	0.000869
180-3	6	-0.003617	0.001166	90-10	10	-0.002987	0.00107
180-4	8	-0.003333	0.00122	90-11	11	-0.003191	0.001305
180-5	10	-0.003015	0.001184	90-12	12	-0.003037	0.001223
180-6	12	-0.003132	0.001138	90-13	13	-0.002582	0.001186
180-7	14	-0.003987	0.001286	90-14	14	-0.003163	0.001018
180-8	16	-0.004076	0.001432	90-15	15	-0.003294	0.000966
180-9	18	-0.003509	0.000987	90-16	16	-0.003039	0.001109
180-10	20	-0.002994	0.000963	90-17	17	-0.003326	0.001198
				90-18	18	-0.002846	0.000988
				90-19	19	-0.003559	0.000945
				90-20	20	-0.002992	0.001051
				90-21	21	-0.003016	0.000995

Table 22. Model Three with Screen Station 11 Profile (5HP).

y	P1	P2	P3	P4	P5
3	0.009836	-0.016756	-0.015361	-0.019539	-0.011935
2.5	0.00564	-0.019952	-0.01824	-0.021833	-0.017243
2	0.002913	-0.019176	-0.018207	-0.021238	-0.017211
1.5	0.000842	-0.018828	-0.017657	-0.01979	-0.017446
1	0.00008	-0.018114	-0.017071	-0.019085	-0.017543
0.5	-0.001109	-0.017981	-0.016891	-0.018951	-0.017597
0	-0.000538	-0.018097	-0.016743	-0.01802	-0.017944
-0.5	0.000313	-0.01805	-0.017104	-0.017859	-0.018672
-1	-0.00009	-0.018275	-0.017103	-0.017597	-0.018694
-1.5	0.000903	-0.018619	-0.017054	-0.017395	-0.019337
-2	0.002722	-0.019591	-0.017219	-0.018207	-0.019814
-2.5	0.004646	-0.019956	-0.01889	-0.018298	-0.021489
-3	0.009269	-0.018919	-0.017198	-0.016391	-0.021087

Table 23. Model Three 5 Degree Yaw Station Pressures.

Hole index	Station	DP	STD DEV	Hole index	Station	DP	STD DEV
P0		0.012536	0.001142	0-1	2	0.008465	0.00102
P		-0.000075	0.000823	0-2	4	-0.006615	0.001277
5HP 1		0.014812	0.001135	0-3	6	-0.020354	0.000969
5HP 2		0.000785	0.001114	0-4	8	-0.032028	0.001856
5HP 3		-0.004102	0.001008	0-5	10	-0.042264	0.001732
5HP 4		-0.002358	0.000914	0-6	12	-0.038891	0.001316
5HP 5		-0.002115	0.001374	0-7	14	-0.035127	0.001428
270-1	2	0.005581	0.000933	0-8	16	-0.034225	0.001445
270-2	4	-0.009375	0.001367	0-9	18	-0.01505	0.001871
270-3	6	-0.024505	0.001134	0-10	20	-0.01037	0.001143
270-4	8	-0.033573	0.001004	135-1	2	0.003214	0.0008
270-5	10	-0.042123	0.001314	135-2	4	-0.01024	0.001158
270-6	12	-0.04128	0.001842	135-3	6	-0.023084	0.001088
270-7	14	-0.036044	0.001211	135-4	8	-0.034729	0.001071
270-8	16	-0.036168	0.001314	135-5	10	-0.043047	0.001712
270-9	18	-0.018019	0.001899	135-6	12	-0.040652	0.001267
270-10	20	-0.013255	0.001897	135-7	14	-0.037004	0.00164
225-1	2	0.003645	0.000578	135-8	16	-0.036065	0.001104
225-2	4	-0.011811	0.001606	135-9	18	-0.01697	0.0013
225-3	6	-0.023955	0.000977	135-10	20	-0.011601	0.001583
225-4	8	-0.034144	0.001136	45-1	2	-0.002632	0.001333
225-5	10	-0.043271	0.001178	45-2	4	0.007347	0.001357
225-6	12	-0.040384	0.001481	45-3	6	-0.006097	0.001345
225-7	14	-0.037913	0.00188	45-4	8	-0.02124	0.000869
225-8	16	-0.035469	0.00155	45-5	10	-0.032615	0.00139
225-9	18	-0.021331	0.002014	45-6	12	-0.041388	0.001045
225-10	20	-0.013027	0.001603	45-7	14	-0.03907	0.001089
315-1	2	0.008987	0.000913	45-8	16	-0.034454	0.00075
315-2	4	-0.007144	0.001208	45-9	18	-0.03359	0.001202
315-3	6	-0.023109	0.001294	45-10	20	-0.015185	0.001798
315-4	8	-0.032855	0.00082	90-1	1	-0.009813	0.001368
315-5	10	-0.041578	0.001781	90-2	2	0.01245	0.001039
315-6	12	-0.039718	0.001478	90-3	3	0.00623	0.001091
315-7	14	-0.035609	0.00107	90-4	4	-0.001106	0.000753
315-8	16	-0.034612	0.001274	90-5	5	-0.009243	0.001203
315-9	18	-0.017882	0.002149	90-6	6	-0.015222	0.000998
315-10	20	-0.011733	0.001676	90-7	7	-0.022044	0.00085
180-1	2	0.003397	0.001106	90-8	8	-0.027999	0.001052
180-2	4	-0.010749	0.000863	90-9	9	-0.031687	0.000789
180-3	6	-0.024397	0.001225	90-10	10	-0.036558	0.001214
180-4	8	-0.033146	0.000828	90-11	11	-0.041203	0.001461
180-5	10	-0.044867	0.001111	90-12	12	-0.041776	0.001059
180-6	12	-0.040805	0.001282	90-13	13	-0.0394	0.001214
180-7	14	-0.037118	0.001091	90-14	14	-0.037214	0.001156
180-8	16	-0.035887	0.001491	90-15	15	-0.035112	0.001252
180-9	18	-0.019312	0.002124	90-16	16	-0.034708	0.001101
180-10	20	-0.011191	0.001088	90-17	17	-0.034452	0.001587
				90-18	18	-0.024599	0.002474
				90-19	19	-0.01537	0.001504
				90-20	20	-0.01219	0.001034
				90-21	21	-0.009998	0.001009

Table 24. Model Three 5 Degree Yaw Station 11 Profile (5HP).

y	P1	P2	P3	P4	P5
3	0.015497	-0.011962	-0.025897	-0.022356	-0.01735
2.5	0.014787	-0.010807	-0.022782	-0.019518	-0.017012
2	0.014618	-0.008038	-0.019157	-0.015813	-0.01374
1.5	0.014957	-0.007581	-0.01801	-0.014177	-0.012842
1	0.014723	-0.006798	-0.017082	-0.013365	-0.012696
0.5	0.015075	-0.006534	-0.016764	-0.012594	-0.012911
0	0.01474	-0.006126	-0.015907	-0.011476	-0.012344
-0.5	0.014476	-0.006153	-0.016404	-0.010921	-0.013447
-1	0.014277	-0.00647	-0.015967	-0.01112	-0.013875
-1.5	0.014518	-0.007383	-0.017142	-0.011226	-0.014763
-2	0.014358	-0.008182	-0.017949	-0.011933	-0.016242
-2.5	0.014725	-0.009149	-0.019628	-0.012385	-0.017485
-3	0.014481	-0.012987	-0.025123	-0.01741	-0.023272

Table 25. Model Three 10 Degree Yaw Station Pressures.

Hole index	Station	DP	STD DEV	Hole index	Station	DP	STD DEV
P0		0.011853	0.001573	0-1	2	0.008271	0.001234
P		0.000074	0.00057	0-2	4	-0.00756	0.001099
5HP 1		0.013956	0.000982	0-3	6	-0.024279	0.000991
5HP 2		0.0032	0.001378	0-4	8	-0.038223	0.000931
5HP 3		-0.010516	0.001024	0-5	10	-0.050383	0.001005
5HP 4		-0.00435	0.001009	0-6	12	-0.047547	0.001303
5HP 5		-0.006194	0.000881	0-7	14	-0.042603	0.001055
270-1	2	0.00171	0.001292	0-8	16	-0.041571	0.000993
270-2	4	-0.014909	0.001097	0-9	18	-0.016737	0.001645
270-3	6	-0.031481	0.000909	0-10	20	-0.010982	0.001652
270-4	8	-0.041703	0.000977	135-1	2	-0.002592	0.001785
270-5	10	-0.051934	0.00112	135-2	4	-0.017045	0.000887
270-6	12	-0.049935	0.00126	135-3	6	-0.031208	0.00103
270-7	14	-0.044557	0.000968	135-4	8	-0.044219	0.001235
270-8	16	-0.044601	0.001007	135-5	10	-0.052626	0.001207
270-9	18	-0.020618	0.001922	135-6	12	-0.04959	0.001229
270-10	20	-0.015481	0.001646	135-7	14	-0.045501	0.000795
225-1	2	-0.003814	0.001069	135-8	16	-0.043008	0.001682
225-2	4	-0.019624	0.000904	135-9	18	-0.020026	0.001869
225-3	6	-0.03263	0.001241	135-10	20	-0.015392	0.001156
225-4	8	-0.043522	0.001357	45-1	2	-0.002312	0.000864
225-5	10	-0.052855	0.000918	45-2	4	0.007264	0.000667
225-6	12	-0.049576	0.000849	45-3	6	-0.007848	0.001171
225-7	14	-0.045826	0.00172	45-4	8	-0.02674	0.001022
225-8	16	-0.044088	0.000883	45-5	10	-0.039725	0.000707
225-9	18	-0.024137	0.001806	45-6	12	-0.051005	0.001025
225-10	20	-0.013616	0.001059	45-7	14	-0.049113	0.001296
315-1	2	0.007937	0.000801	45-8	16	-0.04411	0.000785
315-2	4	-0.009364	0.00079	45-9	18	-0.042632	0.000903
315-3	6	-0.028993	0.001223	45-10	20	-0.022945	0.002031
315-4	8	-0.040098	0.001205	90-1	1	-0.014	0.001288
315-5	10	-0.050327	0.00145	90-2	2	0.011327	0.001408
315-6	12	-0.048614	0.000737	90-3	3	0.003617	0.001368
315-7	14	-0.043939	0.000919	90-4	4	-0.004495	0.000924
315-8	16	-0.042013	0.001345	90-5	5	-0.013798	0.000733
315-9	18	-0.020962	0.001161	90-6	6	-0.02104	0.000776
315-10	20	-0.013057	0.001741	90-7	7	-0.028511	0.001106
180-1	2	-0.004839	0.000826	90-8	8	-0.035616	0.000765
180-2	4	-0.019894	0.001308	90-9	9	-0.039886	0.000764
180-3	6	-0.033719	0.001098	90-10	10	-0.045573	0.001207
180-4	8	-0.042615	0.000862	90-11	11	-0.051388	0.001398
180-5	10	-0.055375	0.001289	90-12	12	-0.05206	0.002042
180-6	12	-0.050464	0.001449	90-13	13	-0.049834	0.001213
180-7	14	-0.04605	0.000873	90-14	14	-0.047515	0.001247
180-8	16	-0.044634	0.001292	90-15	15	-0.045968	0.001527
180-9	18	-0.02056	0.001504	90-16	16	-0.043744	0.001446
180-10	20	-0.013521	0.001324	90-17	17	-0.04398	0.001309
				90-18	18	-0.034283	0.002545
				90-19	19	-0.021871	0.002017
				90-20	20	-0.016093	0.00104
				90-21	21	-0.013591	0.001577

Table 26. Model Three 10 Degree Yaw Station 11 Profile (5HP).

y	P1	P2	P3	P4	P5
3	0.013188	-0.007489	-0.040428	-0.031471	-0.024199
2.5	0.013668	-0.00807	-0.036861	-0.027873	-0.025378
2	0.013668	-0.006239	-0.033339	-0.0242	-0.022779
1.5	0.013517	-0.005352	-0.031322	-0.022322	-0.0209
1	0.013915	-0.005282	-0.029568	-0.02056	-0.021088
0.5	0.013911	-0.00451	-0.02928	-0.01955	-0.021275
0	0.013698	-0.004714	-0.028498	-0.018517	-0.020771
-0.5	0.013605	-0.004697	-0.029367	-0.018651	-0.022008
-1	0.013879	-0.005342	-0.029868	-0.01826	-0.022748
-1.5	0.013652	-0.005992	-0.030672	-0.018806	-0.02421
-2	0.013662	-0.006791	-0.032404	-0.019731	-0.026169
-2.5	0.013425	-0.008466	-0.03584	-0.021944	-0.029184
-3	0.013709	-0.008526	-0.037004	-0.022922	-0.03039

Table 27. Model Four with Rotor Exit Profile (5HP).

y	P1	P2	P3	P4	P5
3.5	-0.001883	-0.001584	-0.001803	-0.001907	-0.001406
3	-0.002177	-0.001997	-0.001128	-0.001583	-0.001548
2.5	-0.000717	-0.00159	-0.001139	-0.001326	-0.000768
2	-0.001175	-0.000935	-0.001051	-0.001381	-0.000633
1.5	-0.001128	-0.000967	-0.001292	-0.001679	-0.001141
1	-0.000513	-0.001493	-0.000919	-0.00137	-0.000868
0.5	-0.001113	-0.001693	-0.001165	-0.00145	-0.000596
0	-0.000866	-0.00144	-0.000995	-0.001257	-0.000742
-0.5	-0.000923	-0.000848	-0.000647	-0.001411	-0.001022
-1	-0.001025	-0.00152	-0.00099	-0.001251	-0.001136
-1.5	-0.001129	-0.001392	-0.000838	-0.00106	-0.000917
-2	-0.000775	-0.001021	-0.001077	-0.001423	-0.001232
-2.5	-0.000995	-0.001081	-0.000963	-0.001418	-0.001349
-3	-0.001762	-0.001205	-0.001558	-0.002202	-0.001644
-3.5	-0.002091	-0.002142	-0.001525	-0.002011	-0.001603

Table 28. Model Four with Screen Exit Profile (5HP).

y	P1	P2	P3	P4	P5
3.5	-0.001819	-0.002073	-0.001285	-0.001845	-0.001245
3	-0.001097	-0.001623	-0.000865	-0.001332	-0.00135
2.5	-0.001545	-0.001503	-0.001297	-0.001844	-0.001596
2	-0.00151	-0.001798	-0.001105	-0.001797	-0.001397
1.5	-0.000836	-0.001676	-0.000936	-0.001509	-0.000868
1	-0.001479	-0.001413	-0.001302	-0.001358	-0.001104
0.5	-0.001417	-0.00166	-0.001258	-0.001301	-0.001698
0	-0.001309	-0.00114	-0.001111	-0.001844	-0.000838
-0.5	-0.001391	-0.001343	-0.001345	-0.001562	-0.001141
-1	-0.00149	-0.001258	-0.00118	-0.001641	-0.001457
-1.5	-0.001628	-0.001217	-0.001072	-0.001667	-0.000917
-2	-0.001565	-0.001656	-0.001155	-0.001325	-0.001452
-2.5	-0.00137	-0.001295	-0.001215	-0.00146	-0.000868
-3	-0.001896	-0.001863	-0.001591	-0.002368	-0.00144
-3.5	-0.001824	-0.001793	-0.001188	-0.001823	-0.001725

Table 29. Model 4 No Rotor Exit Profile (5HP).

y	P1	P2	P3	P4	P5
3.5	-0.002148	-0.001623	-0.001247	-0.00169	-0.001436
3	-0.00205	-0.002015	-0.001509	-0.002064	-0.001463
2.5	-0.000779	-0.00123	-0.001192	-0.001278	-0.000794
2	-0.001072	-0.001198	-0.000577	-0.001684	-0.000986
1.5	-0.00083	-0.000866	-0.000865	-0.001753	-0.000585
1	-0.00099	-0.001283	-0.000834	-0.001294	-0.000741
0.5	-0.001175	-0.001291	-0.001012	-0.001663	-0.000848
0	-0.001077	-0.00145	-0.00087	-0.001125	-0.001153
-0.5	-0.000727	-0.000737	-0.000576	-0.001155	-0.001046
-1	-0.001165	-0.001731	-0.000947	-0.001069	-0.001105
-1.5	-0.000984	-0.001331	-0.000975	-0.001625	-0.000603
-2	-0.001138	-0.001616	-0.000951	-0.001497	-0.000575
-2.5	-0.000652	-0.001643	-0.000816	-0.001536	-0.001287
-3	-0.002215	-0.001342	-0.001678	-0.002015	-0.00126
-3.5	-0.002194	-0.001551	-0.001513	-0.00199	-0.001751

Table 30. Model Four with 2 Screens Exit Profile (5HP).

y	P1	P2	P3	P4	P5
3.5	-0.002302	-0.001675	-0.001744	-0.001556	-0.001084
3	-0.001911	-0.000962	-0.001089	-0.001791	-0.001377
2.5	-0.001958	-0.001697	-0.001404	-0.0017	-0.001179
2	-0.001613	-0.001742	-0.001705	-0.002139	-0.001313
1.5	-0.001345	-0.00121	-0.000772	-0.00191	-0.001051
1	-0.002487	-0.001531	-0.000952	-0.001845	-0.001093
0.5	-0.001866	-0.0014	-0.001218	-0.001807	-0.001386
0	-0.001557	-0.001382	-0.001302	-0.001769	-0.001293
-0.5	-0.002055	-0.001664	-0.001438	-0.00154	-0.000501
-1	-0.001649	-0.001135	-0.000778	-0.001459	-0.001104
-1.5	-0.001274	-0.001465	-0.001181	-0.001582	-0.00096
-2	-0.001643	-0.001515	-0.000897	-0.001813	-0.001094
-2.5	-0.001122	-0.001353	-0.000837	-0.0017	-0.001383
-3	-0.00204	-0.001789	-0.001159	-0.002069	-0.001243
-3.5	-0.00204	-0.001945	-0.001366	-0.001817	-0.001344

LIST OF REFERENCES

[1] Office of the Secretary of the Navy. (n.d.). Renewable Energy Program Office. [Online]. Available: http://greenfleet.dodlive.mil/energy/repo-3/.

[2] Office of the Secretary of the Navy. (n.d.). U.S. Navy energy, environment and climate change. [Online]. Available: http://greenfleet.dodlive.mil/energy/shore/renewable/wind.

[3] Saunders, L. (2009). "First large-scale wind turbine at a marine corps facility," America's Navy. [Online]. Available: http://www.navy.mil/submit/display.asp?story_id=44229.

[4] Karlson, B., LeBlanc B., Minster, D., Estill, D., Miller, B., Busse, F., Keck, C., Sullivan, J., Brigada, D., Parker, L., Younger, R., and Biddle, J. (2014). "IFT&E industry report: Wind turbine-radar interference test summary," SAND2014-19003, Sandia National Laboratories, Albuquerque, NM. [Online]. Available: http://energy.gov/sites/prod/files/2014/10/f18/IFTE%20Industry%20Report_FINAL.pdf.

[5] Carter, A. (2015). "Travis tests radar technology," Air Mobility Command. [Online]. Available: http://www.amc.af.mil/News/Article-Display/Article/786244/travis-tests-radar-technology.

[6] "The effect of windmill farms on military readiness," Office of the Director of Defense Research and Engineering, Washington, D.C., 2006.

[7] Isom, B. M., Palmer, R. D., Secrest, G. S., Rhoton, R. D., Saxion, D., Allmon, T. L., Reed, J., Crum, T. and Vogt, R. "Detailed observations of wind turbine clutter with scanning weather radars." *Journal of Atmospheric and Oceanic Technology*, **26**, pp. 894–910, 2009.

[8] Wilcox, B. (2015). Shroud with RF mesh to suppress radar cross-section of small wind turbine. [Online]. Available: http://www.aptep.net/wp-content/uploads/2015/12/ESTEP_NPS_WT-Shroud-RF-Jenn.pdf.

[9] Ohya, Y. "A highly efficient wind and water turbines with wind-lens technology." Available: http://www.japan.ahk.de/fileadmin/ahk_japan/events_2012/5_Kyush_Uni_Prof_Ohya.pdf.

[10] "Wind vision: A new era for wind power in the United States," U.S. Department of Energy, Washington, DC, 2015.

[11] Abea K., Nishidab M., Sakuraia A., “Experimental and numerical investigations of flow fields behind a small wind turbine with a flanged diffuser.” *Journal of Wind Engineering and Industrial Aerodynamics,* vol. 93, no. 12, pp. 951–970, 2005.

[12] Ragheb, M. and Ragheb, A. M. (2011). “Wind turbines theory — The Betz equation and optimal rotor tip speed ratio,” Fundamental and Advanced Topics in Wind Power, Dr. Rupp Carriveau (Ed.), InTech. doi: 10.5772/ 21398. from http://www.intechopen.com/books/fundamental-and-advanced-topics-in-wind-power/wind-turbines-theory-the-betz-equation-and-optimal-rotor-tip-speed-ratio.

[13] Hansen, M. O. L., 2008. *Aerodynamics of Wind Turbines,* Earthscan, UK.

[14] Our technology. (n.d.). Ogin Energy. [Online]. Available: http://oginenergy.com/our-technology.

[15] Schilling, D. R. (2013). “Wind lens: Fluid dynamics concentrated wind energy,” Industry Tap. [Online]. Available: http://www.industrytap.com/ wind-lens-fluid-dynamics-concentrated-wind-energy/523.

[16] “Application of the wind lens to mid to large size wind turbines,” Kyushu University RIAM Division of Renewable Energy Dynamics Wind Engineering Section, Kyushu, Japan. [Online]. Available: http://www.riam.kyushu-u.ac.jp/windeng/en_aboutus_detail04_03.html.

[17] Balleri, A., Al-Armaghany, A., Griffiths, H., Tong, K., Matsuura, T., Karasudani, T. and Ohya, Y., “Measurements and analysis of the radar signature of a new wind turbine at X-band,” *IET Radar, Sonar and Navigation*, vol. 7, no. 2, pp. 170–177, 2013.

[18] Jenn, D., professor at Naval Postgraduate School, USA, private communication, 2016.

[19] Harvey, Scott, “Low-speed wind tunnel flow quality determination,” M.S. thesis, Department of Mechanical and Aerospace Engineering, Naval Postgraduate School, 2011.

[20] *ZOC 33/64Px and ZOC 33/64PxX2 Electronic Pressure Scanning Module Instruction and Service Manual*, Scanivalve, Liberty Lake, WA, 2016.

[21] *Aeroflow 2 product manual*, Aeroprobe Corporation, Blacksburg, VA, 2013.

INITIAL DISTRIBUTION LIST

1. Defense Technical Information Center
   Ft. Belvoir, Virginia

2. Dudley Knox Library
   Naval Postgraduate School
   Monterey, California